



LIBRARY
Michigan State
University

This is to certify that the

dissertation entitled

Modeling Thermomechanical Phase Transformations between Sustenite and A Two Variant Martensite presented by

Xiaochuang Wu

has been accepted towards fulfillment of the requirements for

Doctor of Philosopyregree in Applied Mechanics

Date X April 10, 1997

MSU is an Affirmative Action/Equal Opportunity Institution

0-12771

PLACE IN RETURN BOX to remove this checkout from your record. TO AVOID FINES return on or before date due.

1 on or before date due.	
DATE DUE	DATE DUE
1	
5	
5	
	1

MSU is An Affirmative Action/Equal Opportunity Institution

MODELING THERMOMECHANICAL PHASE TRANSFOR-MATIONS BETWEEN AUSTENITE AND A TWO VARIANT MARTENSITE

By

Xiaochuang Wu

A DISSERTATION

Submitted to
Michigan State University
in partial fulfillment of the requirements
for the degree of

DOCTOR OF PHILOSOPHY

Department of Materials Science and Mechanics

1997

		,

ABSTRACT

MODELING THERMOMECHANICAL PHASE TRANSFOR-MATIONS BETWEEN AUSTENITE AND A TWO VARIANT MARTENSITE

By Xiaochuang Wu

Both austenite/martensite transformations and martensite/martensite variant reorientation are central to shape memory actuation and pseudoelasticity. The approach is to augment conventional continuum mechanical descriptions with internal variables that track fractional partitioning of the material between austenite and the various martensite variants. A three-species model involving austenite and two complementary martensite variants provides sufficient generality to capture the variant distributions that underlie shape memory, and the strain-accommodation associated with pseudoelasticity. Transformations between any of these species can be tracked on the basis of triggering algorithms and kinetic continuation that reflect both transformation hysteresis and the variation of triggering stress and temperature, as given by the Clausius-Clapeyron relation. The particular algorithm that we describe here is for temperature- and stress-dependent response. It requires only the following experimental parameters: the four transformation temperatures M_f , M_s , A_s , A_f , the crystallographic transformation strain, the Young's modulus and the transformation latent heat. The martensite flow and finish stresses are also introduced. As an application of the model, Two Element Thermal Engine (TSTE) is investigated to predict a reciprocal movement upon thermal heating/cooling pulses controlled for example by an electrical signal.

To my parents

ACKNOWLEDGMENTS

It is with heartfelt thankfulness that I here acknowledge my indebtedness to my advisor and friend, Professor Thomas Pence for his instruction and guidance in my doctoral studies, for his patient direction and discussion in the course of my research, and for his constructive suggestion and careful modification which contribute greatly to the completion of this dissertation.

I should also extend my gratitude to Professor David Grummon, who has given me inspiration and advice on physical understanding, whose experimental work and results helped in modifying the mathematics model studied in this approach. I am also grateful to Professor Zhengfang Zhou, who has spent time discussing with me the solution of some difficult mathematics problem, who has been kindly supportive wherever needed. I want to say thanks to Professor Ronald Averill, who has given me advice on numerical simulations. My thanks also go to my friend Rangfu Chen and all others for their help and support.

Last but not the least, I owe my gratitude to my wife Ping Du, who has been taking great care of me during these years of my study here at Michigan State University, who has been understanding and loving, who is always there when help is needed.

TABLE OF CONTENTS

LIST	OFTA	BLES	Viii
LIST	OF FIC	GURES	ix
1	INTE	RODUCTION	1
	1.1	Background to This Work	1
	1.2	Scope of This Work	6
2	FOR	MATION OF A TWO VARIANT PHASE DIAGRAM	11
	2.1	Concept of Nuetrality Curves	11
	2.2	Special Nuetrality Curves and the X-unfolding	15
		2.2.1 Unfolding the Basic Three Species Phase Diagram	15
		2.2.2 Formation of X-unfolding	
		2.2.3 Building Detwinning into the X-unfolding	
		2.2.4 Isothermal Behavior of X-unfolding	
	2.3	Modified Nuetrality Curves and the pY-unfolding	
		Y-unfolding	
		2.3.2 Mathematical Description of pY-unfolding	
	2.4	Refined pY-unfolding Associated with Experiments	35
		2.4.1 Experimental Justification on Detwinning	
		2.4.2 Mathematical Formulation of the Y-unfolding	
		2.4.3 Summary	
	2.5	Analysis of Isothermal Loading/Unloading Processes	
	2.6	Transformation of a Special Variant	
3	TRA	NSITION TYPES FOR THE PHASE FRACTION EVOLUTION	55
	3.1	Transition Types	55
	3.2	Criteria for Determining Transition Type	57
		3.2.1 Algebraic Description	
		3.2.2 Geometric Illustration	59
	3.3	Criteria for Detwinning Transition Types	61
	3.4	Example	
4	THE	HYSTERESIS ALGORITHMS	64

	4.1	Brief Review of the Previous One-variant study	64
		4.1.1 One Variant Algorithm	64
		4.1.2 Envelope Function	66
	4.2	Two Variant Constitutive Functions	68
		4.2.1 Constitutive Function Extension	68
		4.2.2 Possible Extension of the Algorithm to the Two Variant Proble	m 70
	4.3	Analysis on the Algorithm Associated with Transition Types	74
		4.3.1 Unique Algorithm	
		4.3.2 Algorithm Consistency between One and Two Variant Problem	ns.76
5	INT	EGRABILITY AND PATH DEPENDENCE	79
	5.1	Integration of The Hysteresis Equations for The Phase Fractions	79
		5.1.1 Integration of Transition Type (TT1)	
		5.1.2 Integration of Transition Type (TT2)	81
		5.1.3 Integration of Transition Type (TT3)	83
		5.1.4 Integration of Transition Type (TT4)	84
		5.1.5 Integration for Detwinning Process	85
		5.1.6 Path Independence of the depleted Species within a Transition	1 .
		Туре	86
	5.2	Path Dependence and Path Independence within a Transition Type	86
		5.2.1 General Path-Independent Condition	
		5.2.2 Path-dependent Analysis for the case of $A_s > M_s$	
		5.2.3 Path-dependent Analysis for the case of $M_s > A_s$	90
	5.3	Example	92
	5.4	Discussions on the Solutions	96
6	BEH	AVIOR OF THE MODEL	98
	6.1	Isothermal Behavior	98
		6.1.1 Pseudoelastic Behavior	99
		6.1.2 Internal Hysteresis Loops	103
		6.1.3 Shape Memory Effect and Isothermal Behavior below A _f	
		6.1.4 Load Cycling and Saturation	117
	6.2	Differences between Loading-Cooling and Cooling-Loading Paths	120
	6.3	Comparison with Other Models	
7	APP	LICATION OF THE MODEL TO AN ACTUATOR DESIGN	127
	7.1	Analysis on Basic Structure of TSTE	127
	7.2	Deformation Consistency	
	7.3	Heat-Cool Element(I): The First Stroke	
		7.3.1 Heating Process	
		7.3.2 Cooling Process	
		7.3.3 An Uniqueness Point for the Solution of the Equation (7.3.2.4	
		·	,

	7.4	Later Heat-Cool Strokes	142
	7.5	Limit Analysis on Thermal Cycles	144
		7.5.1 Numerical Convergence on Residual Phase Fraction	144
		7.5.2 Stable Response Loops	153
	7.6	Discussion	156
8	CON	CLUSION AND PROPOSED FUTURE WORK	158
9	REF	ERENCE	162
10	APPI	ENDIX	167
	REF	INEMENT OF THE TWO VARIANT PHASE DIAGRAM	167
	10.1	Clausius-Clapeyron Relations	168
		Determination of Strain in Process $A \leftrightarrow M_+$	
		Determination of Strain in Process $A \leftrightarrow M$	
		Determination of Strain in Process $M \rightarrow M_{\perp}$	

LIST OF TABLES

TABLE I	Transformation Possibilities for Isothermal Loading and Unloading.	28
TABLE 2	Simulation Parameters	46
TABLE 3	Temperatures Corresponding to Points a, b, c and d in Figure 13	47
TABLE 4	Transition Types with Their Algorithm	78
TABLE 5	Path-dependent Category for $M_s < A_s$	90
TABLE 6	Path-dependent Category for $M_s > As$	91
TABLE 7	Phase Fractions at the End $(0, M_f)$ of the Three Paths: l_1, l_2, l_3	96
TABLE 8	Phase Fraction Distributions	119
TABLE 9	$\mu_A = 4.0*10^4; \mu_M = 2.0*10^4 \text{ MPa}$	149
TABLE 10	$\mu_A = 4.0*10^4; \mu_M = 2.8*10^4 \text{ MPa}$	150
TABLE 11	$\mu_A = 4.0*10^4; \mu_M = 3.4*10^4 \text{MPa}$	151
TABLE 12	$\mu_A = 3.0*10^4; \mu_M = 3.0*10^4 \text{ MPa}$	152

LIST OF FIGURES

Figure 1	Triple point phase diagram for a transformation that neither admits
	hysteresis nor stable phase mixtures. Values for the phase fraction triple
	$\{\xi_{-}, \xi_{A}, \xi_{+}\}\$ are restricted to the three types shown
Figure 2	The terminal nuetrality curves in the X-unfolding given by (2.2.2.7) and
	(2.2.2.8) for a material with transformation temperatures: $A_f = 42$, $A_s =$
	13, $M_f = -7$, $M_s = 22$ °C; moduli of austenite and martensite:
	$\mu_A = 50,000 \text{MPa}$, $\mu_M = 20,000 \text{MPa}$; transformation strain $\gamma^* = 0.07$;
	entropy difference: $\eta_A^o - \eta_+^o = \eta_A^o - \eta^o = 0.7 \times 10^6$. Since $\mu_A \neq \mu_M$
•	these curves are not linear19
Figure 3	X-unfolding of the triple point for materials obeying $A_s < M_s$. The S-
	regions are stable zones in which transitions do not occur so that the triple
	$\{\xi_{-}, \xi_{A}, \xi_{+}\}\$ is static on these regions. The W-regions allow for changes in
	the phase fraction triple as (τ, T) changes. For example, transitions
	$A \rightarrow M_+$ can occur in that portion of and which is between M_{s+} and
	M_{f+} . Similarly, $M_+ \to A$ can occur in the above two regions between A_{s+}
	and A _{f+} 21
Figure 4	X-unfolding of the triple point for the case of $A_s > M_s$. In contrast to the
-	case described in Figure 3, here the region of Ω_1^+ between M_{s+} and A_{s+}
	does not admit transformations and so is, formally, a stable zone. For
	simplicity the Ω notation is retained and the region is referred to as a dead
	zone. A similar dead zone exists in Ω_1 22

Figure 5	Transition paths are shown in X-unfolding for $A_s < M_s$. Solid lines indicate active transformation while dash or dot lines indicate inactive transformation
Figure 6	Temperature segments for cases $A_s < M_s$ (a) and $A_s > M_s$ (b) in X-unfolding
Figure 7	pY-unfolding is obtained by modifying the X-unfolding with eight specified nuetrality curves: A_{f+} , M_{s+} , A_{s+} , M_{f+} , A_{f-} , M_{s-} , A_{s-} , M_{f-} . The former four are "bent" to vertical positions in $\tau \le 0$ upon encountering M_{f-} and the latter four are similarly "bent" in $\tau \ge 0$ upon encountering M_{f+} . Here $A_s < M_s$; materials with $A_s > M_s$ are treated similarly
Figure 8	Phase transformation active and inactive zones are shown in the pY-unfolding, which is obtained by modifying the X-unfolding below M_{f+} and M_{f-} .
Figure 9	Refined pY-unfolding, say, Y-unfolding, improves upon the pY-unfolding by allowing the detwinning flow stress τ_s and finish stress τ_f to be specified as additional material properties. This diagram is for the case of $A_s < M_s$. In the present development, the terminal nuetrality curves undergo abrupt slope changes upon crossing $\tau = 0$ and upon meeting the nuetrality curves M_{f-} and M_{f+}
Figure 10	Active and inactive zones in Y-unfolding corresponding to Figure 937
Figure 11	Subdomains R_1 , R_2 and R_3 are shown in $\tau > 0$ for materials obeying $A_s < M_s$

Figure 12	Intersecting points of nuetrality curves of detwinning flow and finish for
	$k_f > k_s$ (a) and for $k_f < k_s$ (b)41

Figure 13 Y-unfolding for $\tau > 0$ with $k_2 = 0$. Four intersection points a, b, c and d are shown as: a (τ_{ss}, T_{ss}) , b (τ_{sf}, T_{sf}) , c (τ_{s}, T_{fs}) , d (τ_{f}, T_{ff})48

Figure 14 Loading behavior for initial conditions corresponding to initial conditions of maximum austenite, CFAF (equal amount of martensite two variants). For $T > M_s$ the initial condition is $\{\xi_-, \xi_A, \xi_+\} = \{0, 1, 0\}$ and for $T < M_f$ it is $\{\xi_{-}, \xi_{A}, \xi_{+}\}=\{0.5, 0, 0.5\}$. For $M_f < T < M_s$ the initial condition is a more general $\{\xi_-, \xi_A, \xi_+\}$ with $\xi_- = \xi_+$. The four associated transition paths p_1 , p_2 , p_3 and p_4 go from left to right. On p_1 , so that $T > M_s$, segments 01, 12 and 23 indicate austenite elastic, single transformation $A \rightarrow M_{\perp}$ and pure elastic M_{\perp} deformations respectively. On p₂, so that $T_{fs} < T < M_s$, segment 01, 12, 23, 34 represent single transformation $A \rightarrow M_+$, double transformation $A \rightarrow M_+$ & $M_- \rightarrow A$, detwinning $M_{-} \rightarrow M_{+}$ and elastic M_{+} deformations. On p₃, segments 01, 12, 23 and 34 indicate single transformation $A \rightarrow M_{+}$, two variant martensite elastic, detwinning $M_{-} \rightarrow M_{+}$ and elastic M_{+} deformations. On p₄, segments 01, 12 and 23 represent two variant martensite elastic, detwinning $M_{\perp} \rightarrow M_{+}$ and elastic M_{+} deformations......50

Figure 15 These six transition paths p_1 , p_2 , p_3 , p_4 , p_5 and p_6 associated with maximum martensite initial conditions, HFMF (equal amount of martensite two variants) go from left to right. On p1, segments 01, 12 and 23 indicate two variant martensite elastic, detwinning $M_- \rightarrow M_+$ and right-shear martensite elastic deformations. On p_2 , segments 01, 12, 23 and 34 represent two variant martensite elastic, double transformation $M_- \rightarrow A$ & $A \rightarrow M_+$, detwinning $M_- \rightarrow M_+$ and elastic M_+ deformations. On p_3 , the first two segments 01 and 12 are the same with

	and elastic M_+ deformations. On p_4 , segments 01, 12, 23, 34 and 45 represent two variant martensite elastic, single transformation $M \to A$, double transformation $M \to A$ & $A \to M_+$, single transformation $A \to M_+$ and elastic M_+ deformations. On p_5 , segments 01, 12, 23 and 34 indicate single transformation $M \to A$, austenite and M_+ elastic, single transformation $A \to M_+$ and elastic M_+ deformations. On p_6 , segments 01, 12 and 23 represent austenite elastic, single transformation $A \to M_+$ and elastic M_+ deformations.
Figure 16	These three unloading paths go from the right to left with initial condition of 100% M_+ . All the dashed lines on p_1 , p_2 and p_3 indicate M_+ elastic deformations, except the portion to the left of A_{f+} on p_1 which represents elastic austenite. All the solid lines on p_1 and p_2 indicate single transformation $M_+ \to A$ deformations
Figure 17	For $\tau > 0$, the lowest temperature and largest stress for conducting $M \to A$ are T_{fs} and τ_{fs} and the highest temperature for conducting $M \to M_+$ is T_{ff}
Figure 18	Four open cone areas at a point p in Ω_1 for X- and Y-unfolding show the transition possibilities when a path passes through this point. If the path passing through p proceeds into N (S, W and E), then transition type (TT1) ((TT2), (TT3) and (TT4)) is in progress
Figure 19	This graph shows that how the transition types occur when one follows a counter-clock wise ellipse in the (τ, T) -plane. From point t2 to t3: (TT3) occurs; from t3 to e: (TT2) occurs; from point b to c: (TT5) occurs; in all other parts there is no transformation.

those on p₂, segment 23 and 34 indicate single transformation $A \rightarrow M_+$

Figure 20	For the case $A_s > M_s$, three path-dependent zones d_2 , d_3 and d_4 are separated in Ω_1^+ . ξ_+ and ξ are path-dependent in d_2 if transition type (TT2) occurs (S-paths). ξ_A and ξ are path-dependent in d_3 if transition type (TT3) occurs (W-paths). ξ_A and ξ_+ are path-dependent in d_4 if transition type (TT4) occurs (E-paths).
Figure 21	For the case $A_s < M_s$, six path-dependent zones a_2 , a_3 , a_4 , a_{23} , a_{24} and a_{234} are separated in Ω_1^+ . The situations occurring in a_2 , a_3 and a_4 are the same with those in d_2 , d_3 and d_4 of the case $A_s > M_s$ shown in Figure 20. In a_{23} , if transition type (TT2) is in process then the phase fractions ξ and ξ_+ are path-dependent, while if (TT3) occurs then ξ_A and ξ are path-dependent. In a_{24} , the condition is similar to that in a_{23} under interchange of (TT3) and (TT4) as well as ξ and ξ_+ . In a_{234} , ξ and ξ_+ are path-dependent if (TT2) occurs, ξ_A and ξ are path-dependent if (TT3) occurs, and, ξ_A and ξ_+ are path-dependent if (TT4) is in process
Figure 22	Three paths l_1 , l_2 and l_3 go from $(\tau, \sigma) = (0, M_s)$ to $(0, M_f)$ in the path-dependent zone of transition type (TT2) with initial condition $\{\xi, \xi_A, \xi_+\}=\{0, 1, 0\}$. Transition type (TT2) occurs on all three paths. Path l_2 consists of two straight segments which meet at point $p_2=(\frac{1}{2\Omega k_1}(M_s-M_f), \frac{1}{2}(M_s+M_f))$. Path l_3 is similar. The phase fractions ξ and ξ_+ are path dependent while ξ_A is not. The values of the triple $\{\xi, \xi_A, \xi_+\}$ at the ends of the three paths are listed in TABLE 7
Figure 23	Pseudoelastic behaviors in both tension and compression conditions at test temperature $T_t = 335$. In $\tau > 0$, $A \leftrightarrow M_+$ processes are involved with the loading/unloading, while, in $\tau < 0$, $A \leftrightarrow M$ processes are involved

with the opposite loading/unloading......100

Figure 24	Pseudoelastic behaviors for $M_s < A_s$ at different temperature levels: $T_t =$
	315, 325, 335 °K, all of which are greater than $A_f = 308$ °K100
Figure 25	By Falk's model (1980), austenite transforming to martensite occurs at the
	highest point on the left ascending branch (top dashed line) upon loading.
•	The reverse transformation, martensite to austenite occurs at the lowest
	point on the right ascending branch upon unloading102
Figure 26	By Landau-Devonshire's model, load-deformation diagrams in three
	different temperatures $(T_1 < T_2 < T_3)$ show that the heights of the
	hysteresis loops decrease with the temperature increase102
Figure 27	A dead zone between the top and bottom bands in the stress-strain
	diagram is illustrated. This dead zone corresponds to the portion between
	points 2 and 3 in the phase diagram. Points f and g correspond in stress- strain diagram to points 1 and 4 in the phase diagram. The internal loop
	formation condition is that unloading has to reach the bottom band and
	loading has to reach the top band shown as a-d-b-c-h path104
Figure 28	The stress-strain trajectory approaches a stable internal loop in the stress-
	strain diagram with oscillating scope of stress between points a and b
	(between τ^b and τ^t in stresses) in the phase diagram106
Figure 29	Cycling loads are applied between $\tau = \tau^b < \tau^{MA}$ and $\tau = \tau^t > \tau^{AM}$ at test
	temperature $T > A_f$ to form internal hysteresis loops. It can be seen that
	the top and bottom bands are covered inside the cycling range107
Figure 30	Shape memory effects occur during loading-unloading-heating-cooling
	nmresses 100

Figure 31	Two different procedures recover the residual strain. (a) shows the
	residual strain recovered upon heating, (b) shows that the residual strain
	can be recovered by further unloading. Here the test temperature is 301
	^o K during the loading/unloading process and the original phase fraction is
	$\xi = \{0, 1, 0\}.$

- Figure 32 The residual strains are recovered by further unloading $(a \to b \to c)$. The plateau of the transformation $A \to M_+$ decreases with the test temperature decrease. In the opposite, the yielding plateau of the reverse transformation $M_+ \to A$ increases in the negative direction of the τ -axis as the test temperature decreases.
- Figure 33 Ferroelastic behaviors in both tension and compression conditions at test temperature $T_t = 200$. In $\tau > 0$, $M_- \to M_+$ process is involved with the transformation, while, in $\tau < 0$, $M_+ \to M_-$ process is involved with the transformation.
- Figure 34 Initial conditions are obtained by cooling the temperature from above A_f to the test temperature in a stress free circumstance (CFAF). General features of the transformation process for loading/unloading were described in Figure 14. In (a) the initial condition is $\{0, 1, 0\}$. $1 \rightarrow 2$: austenite elastic deformation; $2 \rightarrow 3$: phase transformation $A \rightarrow M_+$; $3 \rightarrow 4$: M_+ elastic deformation; $4 \rightarrow 5$: M_+ elastic unloading; $5 \rightarrow 6$: partial reverse transformation $M_+ \rightarrow A$ which gives a certain amount of residual strain left at the end of the unloading. In (b) the initial condition is still $\{0, 1, 0\}$ because $270 \, ^{\circ}\text{K} > M_s$ (=263 $^{\circ}\text{K}$). $1 \rightarrow 2 \rightarrow 3 \rightarrow 4$: conduct the same deformation mechanism as those segments in (a) correspondingly; $4 \rightarrow 5$: M_+ elastic unloading. In (c) the initial condition is $\{0.0135, 0.973, 0.0135\}$. $1 \rightarrow 2$: phase transformation $A \rightarrow M_+$; $2 \rightarrow 3$: combined transformations $A \rightarrow M_+$ and $M_- \rightarrow A$; $3 \rightarrow 4$:

Figure 35

Initial conditions are obtained by heating the temperature from below M_f to the test temperature in a zero-stress condition (HFMF). General features of the transformation process for loading/unloading were described in Figure 15. In (a) the initial condition is {0.2801, 0.4397, 0.2801). $1 \rightarrow 2$: phase transformation $M \rightarrow A$; $2 \rightarrow 3$: elasticity of combined austenite and right-shear martensite; $3 \rightarrow 4$: phase transformation $A \rightarrow M_+$; $4 \rightarrow 5$: M_+ elasticity; $5 \rightarrow 6$: elastic M_+ unloading; $6 \rightarrow 7$: partial reverse transformation $M_+ \rightarrow A$ upon continuous unloading which gives a certain amount of residual strain left at the end of the unloading. In (b) the initial condition is {0.5, 0, 0.5} which is also the initial conditions for (c), (d) and (e). $1 \rightarrow 2$: fully twinned martensite elasticity; $2 \rightarrow 3$: phase transformation $M \rightarrow A$; $3 \rightarrow 4$: elasticity of combined austenite and right-shear martensite; $4 \rightarrow 5$: phase transformation $A \rightarrow M_+$; $5 \rightarrow 6$: M_+ elasticity; $6 \rightarrow 7$: elastic M_+ elastic unloading. In (c) $1 \rightarrow 2$: elasticity of twinned martensite; $2 \rightarrow 3$: combined phase transformation $M_{\cdot} \rightarrow A$ and $A \rightarrow M_{+}$; $3 \rightarrow 4$: phase transformation $A \rightarrow M_{+}$; $4 \rightarrow 5$ and $6 \rightarrow 7$ are similar to $5 \rightarrow 6$ and $6 \rightarrow 7$ in (b) respectively. In (d) $1 \rightarrow 2$: elasticity of twinned martensite; $2 \rightarrow 3$: combined phase transformation $M \rightarrow A$ and $A \rightarrow M_{+}$; $3 \rightarrow 4$: detwinning $M_{-} \rightarrow M_{+}$; $4 \rightarrow 5$ and $5 \rightarrow 6$ are similar to the corresponding sections in (c). The only difference of (e) with (d) is that there is only one section to conduct detwinning $M_{-} \rightarrow M_{+}$, which is

	$2 \rightarrow 3$. In (b), (c), (d) and (e) the residual strains left are phase transformation strain γ^*
Figure 36	Isothermal response (b) under cyclic loads (a) at test temperature $T = 270$ °K ($M_s < 270$ °K $< A_s$). The initial condition is from HFMF with $\xi = \{0.5, 0, 0.5\}$. The outside profile is the same with Figure 35 (c). $M_{-} \rightarrow A$ and $A \rightarrow M_{+}$ occur upon loading while elastic relaxations in mixture phase states occur upon unloading. M_{-} phase is roughly consumed out after the fourth cycle. Austenite remains until the tongue-shape stress-strain response reaches the far right lateral straight line of the outside profile. 118
Figure 37	Two groups of driving paths starting at point (0, 325) on T-axis with initial condition {0, 1, 0} go to point (20, 220), (40, 220), (68.9, 220), (110, 220), (150, 220), (160, 220), (170, 220), (180, 220), (190, 220) respectively
Figure 38	Phase fractions of the martensite variant M_+ upon driving paths of loading-cooling (upper point plot) and cooling-loading (lower point plot). Here $\tau^* = 68.9$, $\tau_s = 150$ and $\tau_f = 200$ MPa
Figure 39	Structure of the TSTE confined in a fixed frame129
Figure 40	The path segment ps2 has three possibilities: 1, 2, 3, as shown in the above. Path 3 is the desired situation and approachable for many shape memory alloys, which will be discussed in the following
Figure 41	A physical interpretation for the condition that ensures that detwinning occurs during heating in a stroke

Figure 42	Six (σ , $T_{\rm I}$)-path segments and their connecting points related with the first stroke (heating/cooling element (I)) are schematically presented in the phase diagram for $\sigma > 0$
Figure 43	Temperature pulses applied on the two elements. The maximum temperature in heating must be sufficient to fully austenitize the operating element
Figure 44	(σ , T)-paths for the first stroke for element (I) (a) and for element (II) (b) The operating element here is element (I) with initial temperature $T_0 = M_f$ which is equal to the constant temperature of the response element (II) during this process. Here the material properties come from TABLE 2. It particular the moduli are $\mu_A = \mu_M = 3.0 \times 10^4$ MPa
Figure 45	(σ, T) -curves in the second stroke are presented in (a) for the element (II) and in (b) for the element (I). The operating element is element (II) with initial temperature $T_0 = M_f$, which is equal to the constant temperature of element (I) during this process. In the first part of ps ₂ both $M \to A$ and $M_+ \to A$ are involved in the phase transformation (refer to Figure 42). 154
Figure 46	This graph shows (σ, T) -curves of the operating elements in ten strokes. A stable (σ, T) -loop (the darker one) is reached after the first cycle (the lighter one).
Figure 47	The corresponding displacement against stress (a) and temperature (b) after ten strokes. The lighter dots correspond to the first stroke. The darked dots correspond to the following nine strokes, which are indistinguishabled at this scale. The head down loops correspond to operating element (II

	and (b)
Figure 48	A given phase diagram as might be determined by experimental measurements. R1 is the region above nuetrality curve M_{f+} for $\tau \ge 0$; R2
	is the region between M_{f+} and M_{f-} for $\tau > 0$; R3 is the region between
	M_{f} and T-axis for $\tau \ge 0$. $\overline{R1}$, $\overline{R2}$ and $\overline{R3}$ are corresponding mirror
	images of R1, R2 and R3 about <i>T</i> -axis for $\tau < 0$ 168

1 INTRODUCTION

1.1 Background to This Work

As materials that have many active and interesting properties, shape memory alloys (SMAs) have received more and more attention both theoretically and practically in recent decades. Their many employments in various sensitive areas, which include: the driving force in heat cycle engines (Banks and Weres, 1976), orthopedic devices for securing fractured bones (Wayman, 1980), integrated actuator/sensor fibers in special composite systems for active control of dynamic and structural behavior (Rogers et al., 1989), blood clot filters and displacement sensors (Takeda et al., 1986), and many more all attribute greatly to their enchanting qualities. Although many inventions have been made, potentials of shape memory alloys still hold great chances for more implementation and further development. Shape memory alloys associated with martensitic phase transformation are characterized by first-order solid to solid transformation without atomic diffusion. Their most important properties are the shape memory effect (SME) and pseudoelastic effect which are responsible for many innovative applications. Thus it has become necessary to have an accurate understanding of the thermomechanical behavior of the shape memory alloys.

There are plenty of literature on modeling the behavior of the shape memory alloys, and what we are going to discuss in the following are the most representative approaches that we have reached. Based on Landau-Devonshire's theory, Falk (1980) illustrated the

stable phase transition between austenite and two martensite variants in a single crystals by minimizing non-convex type of Helmholtz free energy, which can either describe stress induced or thermal induced phase transformations strategically. In Falk's model, characterized by the equality of the phase transformation stress and the Maxwell stress, basic features of SMAs, such as pseudoelasticity, lattice softening and shape memory effect (SME) presented, are qualitatively agreeable with experimental works in some sense.

Achenbach et al. (1986) derived rate-dependent types of model, from statistical mechanics and thermodynamics point of views, to rehearse the plane-strain responses of a polycrystalline object under biaxiel loading. In this publication they took the polycrystalline body as a three-phase configuration of austenite and martensite twins, and operated the fractions of the three phases as internal variables which were parametrized by the assumed continuous distribution of orientations of lattice layers for any instant.

By incorporating uses of Helmholtz free energy and dissipation potential, Tanaka (1986) came up with a rate-type constitutive and an evolutionary equations which could represent the pseudoelasticity and shape memory effect again under the condition of one-dimensional tensile only for stress induced martensite transformations in a polycrystal, which the new nucleation and the growth of the martensite may be understood to be fully governed by macroscopic transformation kinetics. The internal variable that depends on stress and temperature is the phase fraction of martensite. Liang and Rogers (1990), based on the integrated form of Tanaka's equation, presented a thermomechanical constitutive model. In their study, a rate-independent type of equation was proposed to fit the martensite fraction and temperature relations in order to predict pseudoelasticity and shape memory behavior. The results from this model had good coincidence with experimental observations made by them.

As far as pseudoelasticity is concerned, Muller and his colleagues made an extensive investigation. For example, with the consideration of non-monotone load-deformation curves generated from non-convex energy forms which are the type deliberate in Falk's model (1980), Muller and Xu (1991) developed Falk's model by taking into account the dissipative effects from interfaces and coherency. They gave a thorough description of pesudoelasticity loops for a single crystal, in which a width of a hysteresis loop of stressstrain relation depends on interfacial energy of phases rather than depends on the temperature, and the hysteresis loop maintains metastable states which loose their stability on a line defining phase equilibrium. Based on the mixture approach of the work done by Muller (1979), and Muller and Xu (1991), Fedelich and Zanzotto (1991) extrapolated the isothermal hypotheses to nonisothermal conditions by contemplating the hardening observation of stress-strain relation with increasing temperature. Only for two-phase situations where the stress and temperature are high enough, they found out, that the elongation rates have a significant influence on phase transformations in a bar, and the slope of the slanted sides of deformation-temperature loops is rate dependent, which was given a reasonable explanation.

In Leo et al's macroscopic descriptions of two phase system (1993), they assumed the austenite to martensite transition stress to be equal to the Maxwell stress plus an additional constant stress equal to half the height of the isothermal hysteresis loop which accounts for dissipative processes associated with the phase transformation. They also incorporated the temperature and stress dependence of energy with heat transfer associated with austenite/martensite single interface. With this model they explained a phenomenon that the hysteretic stress-strain curves depend strongly on the strain rates at which the wire is extended.

Brinson (1993) modified the works by Tanaka & Iwasaki (1985); Tanaka (1986); Liang & Rogers (1990) to describe the SME below a martensite start temperature by splitting the martensite phase fraction into temperature-induced and stress-induced parts. This subdivision is justified by the micromechanical behavior of SMAs and is effected such that the stress-induced martensite fraction represents the extent of transformations of the material into a single martensite variant. This model can well capture the main conducts of either phase transformation between austenite and over all martensite variants in higher temperature ranges (pseudoelasticity), or conversion of all martensite variants in lower temperature ranges (SME), with the suggested equilibrium phase diagram. Latter on, in the study by Bekker and Brinson (1994), more detailed discussions on the this phase diagram were made to generalize the problem.

In all, energy consideration has been the most concentration point in these works mentioned above. From plasticity point of view, Bondaryev and Wayman (1988) combined the plasticity flow theory and the change of Gibbs free energy to narrate phase transformations in the biaxial case. The idea is cast terms of the change of Gibbs free energy of phase transition or detwinning processes to determine the threshold stress for the changes and then using the plastic flow rule to set up the stress-strain relations during the two processes. This model can also recite the phenomena of pseudoelasticity at high temperature and ferroelasticity at low temperature.

The work of Graesser and Cozzarelli (1991) utilized Bonc-Wen type's model of rate independence. It employs the dynamic analysis (Wen, 1976), to generate one-dimensional evolutionary equations of plasticity to modify the macroscopic stress-strain character of SMAs. Later on, they extended the one-dimensional model to three-dimensional cases by means of the agreement of volume preserved between the plastic flow and martensitic

phase transformations. This model was able to offer some helpful theoretical results for different loading conditions with properly choosing parameters to modify the plastic flow theory and then to describe the behavior of SMAs.

All the modeling investigations mentioned above can reflect the most basic characteristics of SMAs to some degree. However, most of them in general are focused on some specific aspects. When more features of SMAs are needed to be described, it follows that the constitutive equations are usually needed to be changed. For instance, Achenbach et al's work (1986) can hardly be used to describe plane stress problems, neither is it easily applicable in engineering; Tanaka and his colleaques's works (or Liang and Rogers's work) are well suitable for the isothermal stress-induced martensitic transformations or reverse transformations, but they are short of enough descriptions of adiabatic, convective, as well as thermal-induced situations of martensite transformations. Muller and other's studies (or Fedelich and Zanzotto's work) have their most concentration on pseudoelasticity but little focus on other properties. Some of the above investigations, such as plastic type of modeling, are in some way or the other in a difficult condition with respect to parameter choosing, physical understanding, or practical engineering. Thus, a more complete model which is easily applied, as well as supported by a accurate theoretical resources, is the motivation of the current study.

Recently, on the basis of the work done by Coleman & Hodgdon (1986 & 1987), Ivshin and Pence furthered the Duhem-Madelung Model for magnetic hysteresis to the constitutive relations of shape memory alloys (Ivshin & Pence, 1994 a,b) to describe the macroscopic behavior of SMAs from the hysteresis, thermodynamics and continuum mechanics point of view. In the study of Ivshin & Pence (1994 a), a model for rate independent hysteresis was examined. The evolution equations for phase fractions of austenite

and one martensite variant was derived by considering temperature as the only driving forces. Several restrictions on the hysteresis envelopes, which are the maximum and minimum values of austenite phase fraction during phase transformations, were given to ensure monotonicity, containment and orientation requirements. Later in the approach made by Ivshin & Pence (1994 b), evolution equations were developed to govern the time history of shape memory alloys under changes in stress, strain and temperature for one martensitic variant problems. In addition to that, Ivshin and Pence also presented simulations of the relations of stress and strain in either isothermal or adiabatic conditions and internal hysteresis transition loops. Comparison, made by Brinson and Huang (Brinson and Huang, 1996), between this model and Tanaka's model, yields nearly identical results if both models are used with the same kinetic law. However, Ivshin and Pence's model gives more flexibility in a variety situations varying from isothermal to adiabatic conditions. To extend one variant model to two variant model, a basic analysis for two variant martensite problems was given in the work by Pence et al. (1994). They began from the discussion of "triple point organizational kernel", and then explored the idea to the mixture of coexistence and hysteresis unfoldings. Lateral pseudoelasticity associated with phase transformations was obtained under cyclic loading in high temperature regions.

1.2 Scope of This Work

The present study will give a relatively complete description to the two variant martensite model by refining and extending the one-dimensional work of Pence et al. (1994). We consider a two-phase material which consists of a high temperature austenite phase A and two symmetric variants of a low temperature martensite phases M_{+} and M_{-} which could

be treated as twin related. The first of these two variants M_{+} is favored in positive stress $(\tau > 0)$ and the second M_{\perp} is favored in negative stress $(\tau < 0)$. We assume that, the forward (austenite to martensite) transition temperatures M_s and M_f , and backward (martensite to austenite) transition temperatures A_s and A_f , could be measured by decreasing and increasing the temperature at zero-load. In the present study we are going to employ a phase fraction triple $\{\xi_{-}, \xi_{A}, \xi_{+}\}$ as internal variables, while temperature T and stress τ are driving forces. Here ξ_A indicates the phase fraction of austenite, while ξ_+ and $\xi_$ indicate the phase fractions of the two martensite variants. We treat the situation in which the temperature and stress vary with time in some prescribed fashion. This generates paths in a (τ, T) -plane, which will be referred to as the state plane. Pairs (τ, T) will be referred to as states, and continuous paths $(\tau(t), T(t))$ in the state plane will be referred to as state paths. The main purpose of this research is to study, refine and apply an algorithm for phase transformations between the three species A, M_{+} and M_{-} as the state of the system varies. Thus we seek to determine the values of ξ_A , ξ_+ and ξ_- on state paths. Hysteresis in these transformations indicate that ξ_A , ξ_+ and ξ_- will not in general be state functions, that is, the instantaneous value of (τ, T) does not determine the values of ξ_A , ξ_+ and ξ_- . Rather we study an algorithm which determine these values on the basis of known initial values for ξ_A , ξ_+ and ξ_- , and knowledge of the subsequent state path. At each instant of time, the three phase fractions satisfy the following balance relation

$$\xi_A(t) + \xi_+(t) + \xi_-(t) = 1$$
 (1.2.0.1)

To achieve the purpose, various kinds of state plane partitions into M_{\star} , A_{\star} , M_{+} regions (X-unfolding, pY-unfolding, Y-unfolding) are developed from a thermodynamic restriction which ensures that Gibbs free energy satisfies the second law of thermodynamics.

These partitions are different unfoldings of a standard triple point phase diagram. Characteristic curves in the state plane are obtained which govern processes $A \leftrightarrow M_+$ and $A \leftrightarrow M_-$ respectively, in a way that is similar to (Pence *et al.* 1994). Descriptions of the $M_+ \leftrightarrow M_-$ process are then developed by modifying the two austenite/martensite processes. The characteristic curves act as nuetrality curves which classify both austenite/martensite phase transformations and detwining processes $(M_+ \leftrightarrow M_-)$ by regions in the (τ, T) -plane. They also enter the evolution equations for the phase fraction triple $\{\xi_-, \xi_A, \xi_+\}$ as an internal variable. Internal variable descriptions for thermodynamic behavior are common, for example, Coleman and Gurtin (1967) employed thermomechanical and internal variables together to generalize dissipation problems.

In section 2, we begin by extending the triple point phase diagram (Pence et al., 1994) to an X-unfolding by taking thermodynamic considerations on the three species M_- , A and M_+ . The nuetrality curves, describing phase transformations between austenite/martensite at high temperature, are modified as detwinning nuetrality curves, when they enter into non-austenite regions. That means the Clausius-Clapeyron relation for austenite/martensite is used to describe the detwinning process, which is not exactly the case. To justify this point, the entropy of austenite is replaced by that of martensite in the Clausius-Clapeyron relation so as to generate constant stress nuetrality curves for detwinning, in which the detwinning flow and finish stresses are predicted as a consequence of this procedure. Experimentally, it is often the case that the detwinning flow and finish stresses are smaller that the ones predicted by the X-unfolding., If the detwinning flow and finish stresses are instead treated as material constants, a Y-unfolding is suggested.

In Section 3, we first define all transition possibilities (transition types) when temperature and stress trigger the transformations. Then criteria for different transition types are

derived based on the nuetrality curves, which are useful for us to determine what kinds of transition types occur at any point on a given path in (τ, T) -plane. These criteria have an explicit geometric illustration. An example of how to use these criteria is given at the end of this section.

Chapter 4 opens with a brief review of one variant model (Ivshin and Pence, 1994, a, b). To extend the model to two martensite variants M_{-} and M_{+} , we introduce a concept of constitutive functions of austenite which is similar to that of the one variant case. We then work on the extension of algorithms from one variant to two variant. Numerous possible algorithms in the two variant case make the problem difficult, but with the symmetry of two martensite variants and the coherence of phase transition possibilities, we arrive at a unique algorithm for each transition possibility. The extension is verified by considering the self-accommodated process in the two models.

In chapter 5, based on the algorithm arrived in the previous section, the solutions of phase fractions for each transition type are calculated. This permits further analysis of the stress-strain relation. The phase fraction evolution depends on the state and the state-path orientation in the (τ, T) -plane. Conditions that would ensure path independent algorithms for the various transition possibilities are derived mathematically. However analysis of the path-independent conditions shows that path independence within a transition type is often not the case.

In chapter 6, several numerical results in stress-strain-temperature relations are given. Pseudoelasticity, shape memory and the features of the associated internal hysteresis loops are thoroughly studied. Some isothermal behaviors between the temperatures A_f and M_f are also conducted for different initial conditions. Finally, comparisons with other models are made at the end of this section.

As an application of this model, a prediction on reciprocal motions of two element devices made of shape memory alloys is analyzed in chapter 7. The analysis focuses on the prediction of phase fraction changes inside the device due to temperature pulses that alternate between the two elements. The result show that a stable cyclic linear motion can be reached after several repititions of the temperature pulses.

Conclusions and possible ideas for future work are presented in Chapter 8.

An appendix is also given for the inverse issue of Chapter 2. In the previous study, it begins with considering the second law of thermodynamics to create the phase diagram. Linear stress-strain relations of each phase are assumed during this process. The prediction for the phase diagram is usually different with experimental observations. Therefore, it naturally arises an inverse problem to determine the stress-strain relation under the same thermodynamic regard and a given phase diagram by experimental measurements. In the appendix, a problem related with the above consideration is well posed. Nonlinear stress-strain relations are obtained corresponding to the given phase diagram. The solution also shows that the two issues are coincident under the same phase diagram.

2 FORMATION OF A TWO VARIANT PHASE DIAGRAM

In this study we begin with assuming that phase transformation triggered by temperature and stress satisfy the second law of thermodynamics. According to this point, characteristics of a differential equation, obtained from increments of Gibbs free energy of the three species system obeying the Maxwell relation, are derived in association with both the process $A \leftrightarrow M_+$ and $A \leftrightarrow M_-$. Those characteristics are interpreted as nuetrality curves in the state plane and govern as a "modifier" transformation between austenite and the martensite variants within the system. At low temperatures they are reinterpreted in terms of a direct $M_- \leftrightarrow M_+$ process. Then considerations of consistency between these new process interpretation and the Gibbs/Maxwell argument, modify the low temperature characteristic. This then adjusts the mathematical treatment of the $M_- \leftrightarrow M_+$ detwining process.

2.1 Concept of Nuetrality Curves

First of all, we recall some thermodynamic views introduced in the work by Pence et al. (1994) to describe the phase transformations. Entropy and strain of the fine mixture of the three species system are extensive variable counterparts to the temperature T and shear stress τ . High temperature and low stress corresponds to a situation of high entropy and low strain (austenite favored); low temperature and high stress is consistent with a condi-

tion of low entropy and high strain (martensite favored). Under a rule of mixtures, these extensive variables are defined by

$$\eta = \xi_A \eta_A + \xi_+ \eta_+ + \xi_- \eta_- , \qquad (2.1.0.1)$$

$$\gamma = \xi_A \gamma_A + \xi_+ \gamma_+ + \xi_- \gamma_-. \tag{2.1.0.2}$$

Here, η_{sub} and γ_{sub} are entropies and strains of pure phases, and are assumed to be state functions of the driving forces (τ, T) . The increments of Gibbs free energy G of the mixture of the three species are required to obey the relation

$$dG = -\eta dT - \gamma d\tau. \tag{2.1.0.3}$$

Here (η, T) and (γ, τ) each form a conjugate pair of thermodynamic variables. The mathematical development is general enough to include both the case where (γ, τ) are regarded as shear variables and are regarded as normal variables. Of course in making contract with experiment, the sense in which (γ, τ) are to be regarded must be specified.

To avoid any violation with the second law of thermodynamics, Gibbs free energy G must be a state function of temperature and stress, so that the overall entropy and strain satisfy the Maxwell relation

$$\frac{\partial \gamma}{\partial T} = \frac{\partial \eta}{\partial \tau} \tag{2.1.0.4}$$

Under the assumption that entropies and strains of pure phases are state functions, which means the Maxwell relation is satisfied in each pure phase, and abides by the law (1.2.0.1) of the balance of the three species, the above relation gives

$$\frac{\partial \xi_{+}}{\partial \tau}(\eta_{+} - \eta_{A}) + \frac{\partial \xi_{-}}{\partial \tau}(\eta_{-} - \eta_{A}) = \frac{\partial \xi_{+}}{\partial T}(\gamma_{+} - \gamma_{A}) + \frac{\partial \xi_{-}}{\partial T}(\gamma_{-} - \gamma_{A}) , \qquad (2.1.0.5)$$

which is a thermomechanical restriction on the system. To interpret the physical meanings of the equation, we are going to consider the phase transformations among the three species.

Changes of temperature and stress in (τ, T) -plane drive transformations between the three phases M_{-} , A and M_{+} . Let us first classify the phase transformations into two courses $A \leftrightarrow M_{+}$ and $A \leftrightarrow M_{-}$. There are two transition directions in each course. The classification remains potentially incomplete until a process is given for describing $M_{+} \leftrightarrow M_{-}$. For the present we only contemplate the first two processes and later on Section 2.2.3 the third course $M_{+} \leftrightarrow M_{-}$ will be introduced in terms of the work by Wasilewski (a,b,c, 1971).

In process $A \leftrightarrow M_+$, beginning at any initial point in the (τ, T) -plane it is assumed that certain paths away from this point will favor the transformation of A to M_+ $(A \to M_+)$. Paths in the opposite direction would then favor the transformation of M_+ into A $(M_+ \to A)$. It is assumed that there exists exactly one neutral direction (including its opposite direction) away from the initial point in which neither an $A \to M_+$ nor an $M_+ \to A$ transformation is favored. The curve traced out as one travels in this neutral direction is an A/M_+ nuetrality curve which will be discussed next.

In the above we assumed that the overall phase transitions obey the Maxwell relation (2.1.0.5). In particular, this equation must hold for $A \leftrightarrow M_+$ process in which the phase fraction ξ_- does not change. For such a virtual process the thermomechanical restriction (2.1.0.5) on the whole system specializes to

$$\frac{\partial \xi_{+}}{\partial \tau}(\eta_{+} - \eta_{A}) = \frac{\partial \xi_{+}}{\partial T}(\gamma_{+} - \gamma_{A}) . \qquad (2.1.0.6)$$

The characteristic equation associated with this differential equation is the following

$$\frac{dT}{d\tau} = -\frac{\gamma_+ - \gamma_A}{\eta_+ - \eta_A},\tag{2.1.0.7}$$

which, in turn, gives the ξ_+ nuetrality curves for the process $A \leftrightarrow M_+$. This is familiar as the Clausius-Clapeyron equation for process $A \leftrightarrow M_+$. Following a similar procedure one finds that the Clausius-Clapeyron equation for process $A \leftrightarrow M_-$ is

$$\frac{dT}{d\tau} = -\frac{\gamma_{-} - \gamma_{A}}{\eta_{-} - \eta_{A}}.$$
 (2.1.0.8)

Integration of the Clausius-Clapeyron equations (2.1.0.7) and (2.1.0.8) yields a parametrization of nuetrality curves in the form of $\beta_o^+(\tau,T)=C^+$ and $\beta_o^-(\tau,T)=C^-$ for the two processes. Here C^+ and C^- are integration constants which locate the individual curves that make up the two families for $A \leftrightarrow M_+$ and $A \leftrightarrow M_-$ respectively. The development so far has made no assumption as to the symmetry of the variants M_+ and M_- . For simplicity we consider a situation in which these two variants are symmetric with respect to stress, that is, the effect of a particular value τ_o in triggering M_+ is identical to the effect of $-\tau_o$ in triggering M_- (all other factors being equal). This requires that $\gamma_+(\tau,T)=-\gamma_-(-\tau,T)$ and $\gamma_+(\tau,T)=\gamma_-(-\tau,T)$. This symmetry assumption implies tension/compression symmetry where (γ,τ) are regarded as normal components. On a finer crystallographic scale where the shear interpretation may be useful, this implies that M_+ and M_- represent variants with equal and opposite lattice shears.

These symmetries give $\beta_o^+(\tau, T) = \beta_o^-(-\tau, T)$ and implies nuetrality curves that are symmetric about $\tau = 0$. It is often convenient to choose this parametrization so that $\beta_o^+(0, T) = T = \beta_o^-(0, T)$ and we shall choose this convention. Then β_o^+ and β_o^- play the role of a generalized temperature. Therefore, we let increasing C^+ and C^- correspond to $M_+ \to A$ and $M_- \to A$ transformations respectively, and decreasing C^+ and C^- correspond to $A \to M_+$ and $A \to M_-$ transformations respectively. Setting $\beta_o^+(\tau, T)$ and $\beta_o^-(\tau, T)$ equal to the four transition temperatures M_f , M_s , A_s and A_f , gives eight canonical nuetrality transition curves. We name these eight curves the *terminal nuetrality curves* in the rest of this study.

2.2 Special Nuetrality Curves and the X-unfolding

2.2.1 Unfolding the Basic Three Species Phase Diagram

Before we find the nuetrality curves it is helpful to recall the unfolding of the standard triple point phase diagram introduced in the approach by Pence *et al.* (1994). Figure 1 is the standard triple point diagram which most simply categorizes the system of the three species of austenite and martensite two variants. In this phase diagram, all phase transformations of austenite/martensite and reorientations of the two variants are abrupt so that either $\{\xi_-, \xi_A, \xi_+\}=\{1, 0, 0\}$, $\{0, 1, 0\}$ or $\{0, 0, 1\}$; these correspond respectively to pure M_- martensite, pure austenite, or pure M_+ martensite (Figure 1). If a continuous path $(\tau(t), T(t))$ is prescribed, then the austenite/martensite phase transformations or the martensite/martensite reorientations take place whenever the path either crosses one of the dual species transformation curves, or else crosses the triple point $(0, T^*)$. The same

transformation curves operate in each process direction, so that these processes are also not hysteretic. To build a natural hysteresis and coexistence of SMAs in the model, we may unfold this triple point phase diagram by the thermodynamic derivations obtained in the last section following Pence *et al.* (1994).

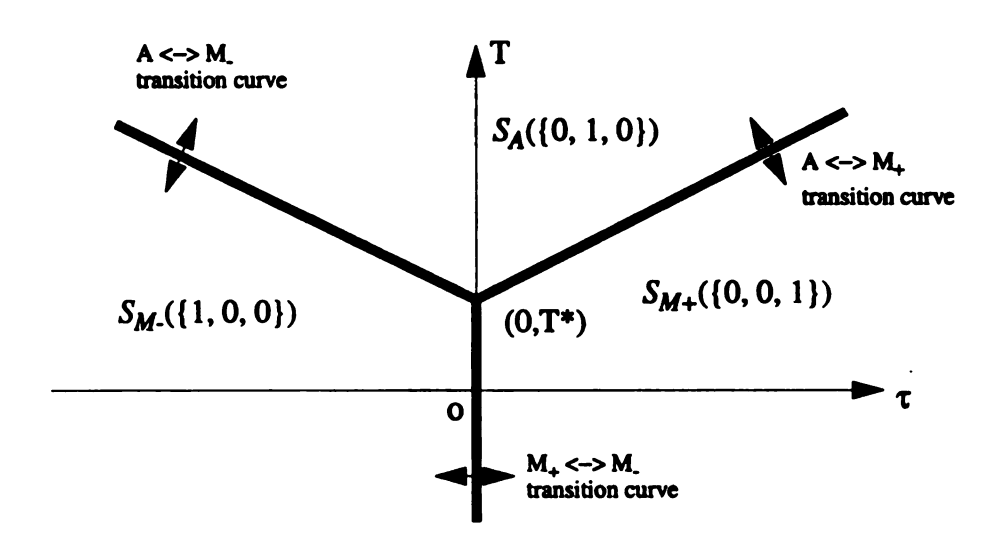


Figure 1. Triple point phase diagram for a transformation that neither admits hysteresis nor stable phase mixtures. Values for the phase fraction triple $\{\xi_-, \xi_A, \xi_+\}$ are restricted to the three types shown.

2.2.2 Formation of X-unfolding

To unfold the triple point phase diagram, it is necessary to determine the form of the characteristics or those nuetrality curves from the Clausius-Clapeyron equations. Integration of equations (2.1.0.7) and (2.1.0.8) gives

$$\beta_o^+(\tau, T) = \frac{1}{\eta_A^o - \eta_{+(0, T_0)}^o} \int_{-\tau_0}^{(\tau, T)} (\eta_A - \eta_+) dT + (\gamma_A - \gamma_+) d\tau$$
 (2.2.2.1)

$$\beta_o^-(\tau, T) = \frac{1}{\eta_A^o - \eta_-^o} \int_{(0, T_0)}^{(\tau, T)} (\eta_A - \eta_-) dT + (\gamma_A - \gamma_-) d\tau$$
 (2.2.2.2)

where, T_o is a fixed reference temperature, $\eta_i^o = \eta_i(0, T_o)$ are zero-stress reference entropies at this temperature for i = -, A, +. In particular if the stress-strain behavior is linearly elastic and temperature independent in each pure phase with moduli μ_i ($\mu_+ = \mu_- = \mu_M$) ie.,

$$\gamma_A = \tau/\mu_A, \ \gamma_+ = \tau/\mu_M + \gamma^*, \ \gamma_- = \tau/\mu_M - \gamma^*,$$
 (2.2.2.3)

and if the entropies of the three species are simply expressed as

$$\eta_i = C \ln(T/T_o) + \eta_i^o,$$
 (2.2.2.4)

where C is a common specific heat for the all three species with $\eta_+^o = \eta_-^o$, then the same results as in the approach by Pence *et al.* (1994) gives

$$\beta_o^+(\tau, T) \equiv T + \frac{1}{\eta_A^o - \eta_A^o} \left(\frac{(\mu_M - \mu_A)\tau^2}{2\mu_A \mu_M} - \gamma^* \tau \right),$$
 (2.2.2.5)

$$\beta_{o}(\tau, T) = T + \frac{1}{\eta_{A}^{o} - \eta_{o}^{o}} \left(\frac{(\mu_{M} - \mu_{A})\tau^{2}}{2\mu_{A}\mu_{M}} + \gamma^{*}\tau \right). \tag{2.2.2.6}$$

Note that, in each phase/species $(M_{\downarrow}, A, M_{+})$ that (2.2.2.3) and (2.2.2.4) are consistent with

the Maxwell relation (2.1.0.4). Here γ^* is the zero-load transformation strain. For example, a system with: moduli of austenite and martensite, $\mu_A = 50,000$, $\mu_M = 20,000$ MPa, the difference of the reference entropies between austenite and martensite, $\eta_A^o - \eta_+^o = \eta_A^o - \eta_-^o = 0.7 \times 10^6$ j/(m³ °K), and transformation strain is assumed $\gamma^* = 0.07$, gives the nuetrality curve parametrization

$$\beta_{c}^{+}(\tau, T) = T - 1 \times 10^{-1} \tau - 2.14 \times 10^{-5} \tau^{2},$$
 (2.2.2.7)

$$\beta_{c}(\tau, T) = T + 1 \times 10^{-1} \tau - 2.14 \times 10^{-5} \tau^{2}. \tag{2.2.2.8}$$

Continuing with this example, suppose $A_f = 42$, $A_s = 13$, $M_f = -7$ and $M_s = 22$ °C. Then, each of equations (2.2.2.7) and (2.2.2.8) gives 4 curves passing through those 4 temperatures, and so that eight terminal nuetrality curves: A_{f+} , A_{s+} , M_{f+} , M_{s+} , A_{f-} , A_{s-} , M_{f-} , M_{s-} , are obtained, which, together, generate an "X-shape" in the (τ, T) -plane (Figure 2). This formally unfolds the triple point phase diagram by separating both the $A \leftrightarrow M_+$ and $A \leftrightarrow M_-$ phase transformation curves. Compared to the triple point phase diagram in Figure 1, this unfolding bifurcates the triple point $(0, T^*)$ into $(0, M_f)$, $(0, A_s)$, $(0, M_s)$ and $(0, A_f)$, and extends $A \leftrightarrow M_+$ and $A \leftrightarrow M_-$ processes into negative and positive stress areas respectively. We temporarily ignore any unfolding of the $M_+ \leftrightarrow M_-$ transformation curve and instead focus on the formal extensions of the terminal nuetrality curves backwards into the low temperature region of phase diagram. This, rather questionable, scheme will be called the X-unfolding. We will discuss this unfolding in its own right, and then show how an additional modification can be used to account for an unfolding of the $M_+ \leftrightarrow M_-$ curve associated with martensite variant reorientation processes.

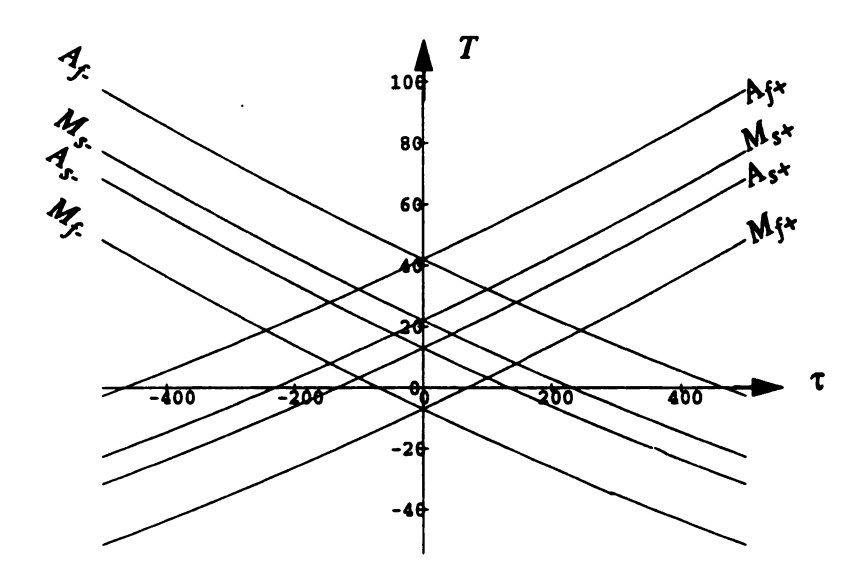


Figure 2. The terminal nuetrality curves in the X-unfolding given by (2.2.2.7) and (2.2.2.8) for a material with transformation temperatures: $A_f = 42$, $A_s = 13$, $M_f = -7$, $M_s = 22$ °C; moduli of austenite and martensite: $\mu_A = 50,000$ MPa, $\mu_M = 20,000$ MPa; transformation strain $\gamma = 0.07$; entropy difference: $\eta_A^o - \eta_+^o = \eta_A^o - \eta_-^o = 0.7 \times 10^6$. Since $\mu_A \neq \mu_M$ these curves are not linear.

2.2.3 Building Detwinning into the X-unfolding

It is convenient to define eleven zones in (τ, T) -plane associated with this X-unfolding, which are indicated in Figure 3 and Figure 4 for the separate cases of material obeying $A_s > M_s$ and $A_s < M_s$ respectively. Formally these regions are given by

$$\begin{split} &\Omega_{1}^{+} = \{(\tau,T) | M_{f} \leq \beta_{o}^{+}(\tau,T) \leq A_{f}, M_{f} \leq \beta_{o}^{-}(\tau,T) \leq A_{f}\}, \\ &\Omega_{1}^{-} = \{(\tau,T) | \beta_{o}^{+}(\tau,T) > A_{f}, M_{f} \leq \beta_{o}^{-}(\tau,T) \leq A_{f}\}, \\ &\Omega_{1}^{+} = \{(\tau,T) | \beta_{o}^{-}(\tau,T) > A_{f}, M_{f} \leq \beta_{o}^{+}(\tau,T) \leq A_{f}\}, \\ &\Omega_{2}^{+} = \{(\tau,T) | \beta_{o}^{+}(\tau,T) < M_{f}, A_{s} \leq \beta_{o}^{-}(\tau,T) \leq A_{f}\}, \\ &\Omega_{2}^{-} = \{(\tau,T) | A_{s} \leq \beta_{o}^{+}(\tau,T) \leq A_{f}, \beta_{o}^{-}(\tau,T) < M_{f}\}, \\ &S_{Mo} = \{(\tau,T) | \beta_{o}^{+}(\tau,T) < M_{f}, \beta_{o}^{-}(\tau,T) < M_{f}\}, \\ &S_{M+} = \{(\tau,T) | \beta_{o}^{+}(\tau,T) < M_{f}, M_{f} \leq \beta_{o}^{+}(\tau,T) < A_{s}\}, \\ &S_{M-+} = \{(\tau,T) | \beta_{o}^{-}(\tau,T) < M_{f}, M_{f} \leq \beta_{o}^{+}(\tau,T) < A_{s}\}, \\ &S_{M} = \{(\tau,T) | \beta_{o}^{+}(\tau,T) > A_{f}, \beta_{o}^{-}(\tau,T) > A_{f}\}, \\ &S_{M+} = \{(\tau,T) | \beta_{o}^{-}(\tau,T) > A_{f}, \beta_{o}^{+}(\tau,T) < M_{f}\}, \\ &S_{M+} = \{(\tau,T) | \beta_{o}^{-}(\tau,T) < M_{f}, \beta_{o}^{+}(\tau,T) < M_{f}\}, \\ &S_{M+} = \{(\tau,T) | \beta_{o}^{-}(\tau,T) < M_{f}, \beta_{o}^{+}(\tau,T) < M_{f}\}. \end{split}$$

Those regions defined in the above way are shown in the following two graphs for materials obeying either $A_s < M_s$ (Figure 3) or $A_s > M_s$ (Figure 4).

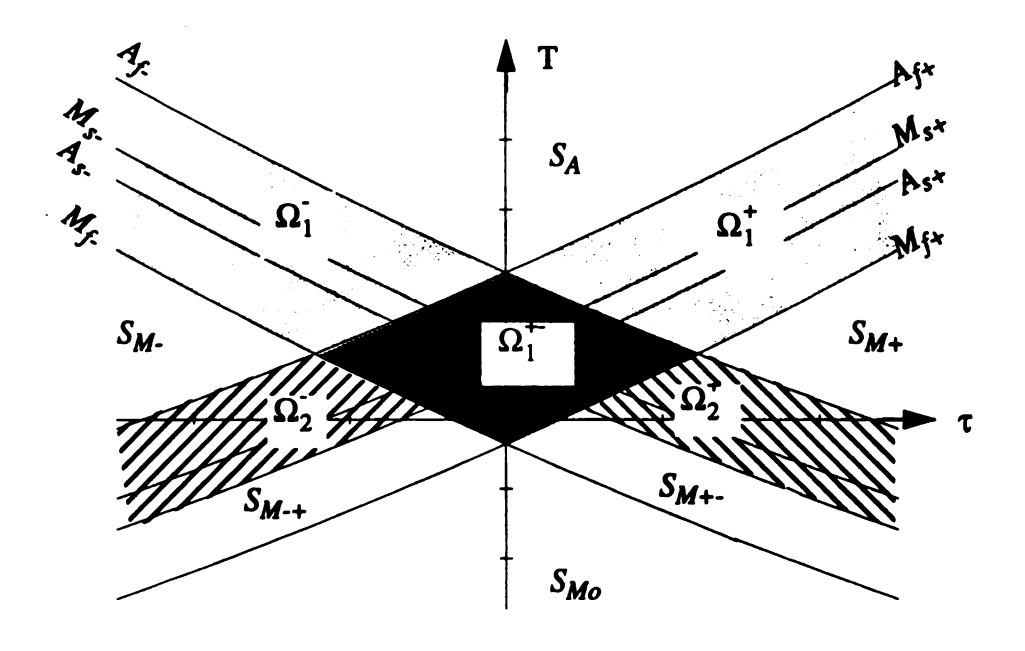


Figure 3. X-unfolding of the triple point for materials obeying $A_s < M_s$. The S-regions are stable zones in which transitions do not occur so that the triple $\{\xi_-, \xi_A, \xi_+\}$ is static on these regions. The Ω -regions allow for changes in the phase fraction triple as (τ, T) changes. For example, transitions $A \to M_+$ can occur in that portion of Ω_1^+ and Ω_1^+ which is between M_{s+} and M_{f+} . Similarly, $M_+ \to A$ can occur in the above two regions between A_{s+} and A_{f+} .

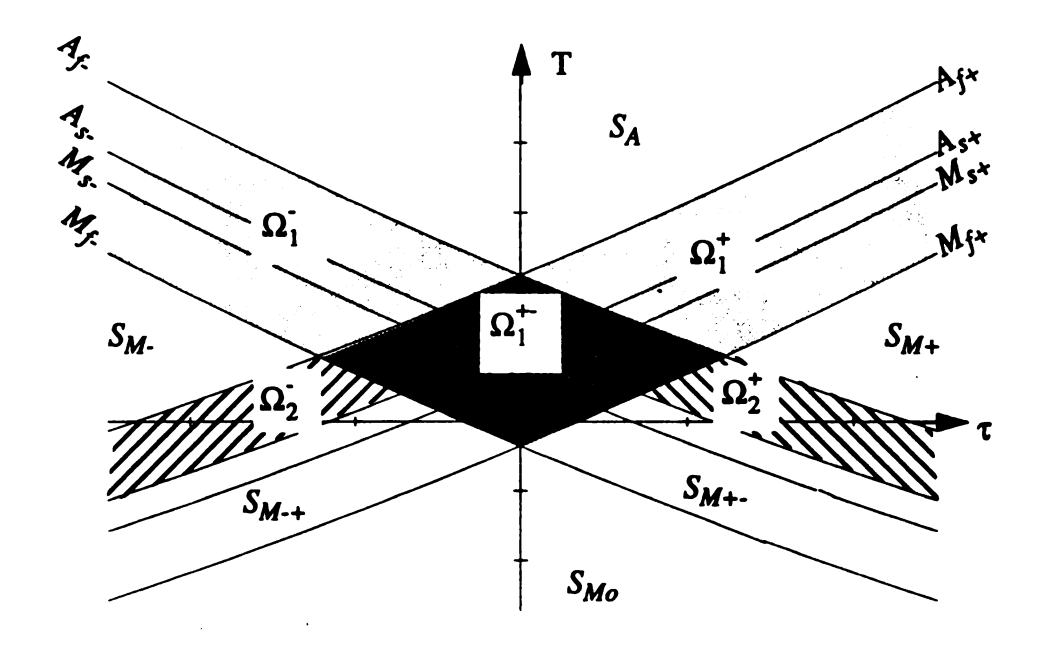


Figure 4. X-unfolding of the triple point for the case of $A_s > M_s$. In contrast to the case described in Figure 3, here the region of Ω_1^+ between M_{s+} and A_{s+} does not admit transformations and so is, formally, a stable zone. For simplicity the Ω notation is retained and the region is referred to as a dead zone. A similar dead zone exists in Ω_1^+ .

The X-unfolding, preserves the three stable phase zones S_A , S_{M+} , and S_{M-} in which the phase fraction triple is $\{0, 1, 0\}$, $\{0, 0, 1\}$ and $\{1, 0, 0\}$ respectively. Since this development treats $A \leftrightarrow M_+$ and $A \leftrightarrow M_-$ nuetrality curves, but neglects a direct $M_+ \leftrightarrow M_-$ process, one identifies the top half of the "X" with the unfolded $A \leftrightarrow M_+$ and $A \leftrightarrow M_-$ transition curves of Figure 1. Actually, $A \leftrightarrow M_+$ and $A \leftrightarrow M_-$ may be active in Ω_1^+ and Ω_1^- respectively while in Ω_1^+ both processes may be active. However the bottom half of the "X" does not, at present, permit an obvious correspondence with the $M_+ \leftrightarrow M_-$ transformation curve of Figure 1. One goal is to naturally develop this correspondence. To do so we identify the region between the two lower branches of the "X" as a region of stable

 M/M_+ mixture, which would likely exist in a crystallographically twinned state. For reasons outlined below, this region naturally extends to the regions S_{M+-} and S_{M+-} . The austenite phase is not present in the zones S_{M+-} , S_{Mo} and S_{M+-} , and so that the phase fraction triple must be of the form $\{\xi_-, 0, \xi_+\}$. The values ξ_+ and ξ_- are determined by how a state path enters into this combined area. The values ξ_+ and ξ_- are then static so long as the driving force path $(\tau(t), T(t))$ does not exit $S_{M+-} \cup S_{Mo} \cup S_{M+-}$. We now consider transformations between the six stable regions: S_A , S_{M+-} , S_{Mo} , S_{M+-} and S_{M-+} , due to driving force paths $(\tau(t), T(t))$ which connect them via the five active regions: Ω_1^- , Ω_1^+ , Ω_1^+ , Ω_2^- , Ω_2^+ .

We first examine connection paths that avoid the central region Ω_1^+ . Consider eight special paths: p_1 , p_2 , p_3 , p_4 , $p_{\overline{1}}$, $p_{\overline{2}}$, $p_{\overline{3}}$, $p_{\overline{4}}$ (Figure 5), which are organized here into pairs of opposite direction (e.g. (p_1, p_2) , ..., $(p_{\overline{3}}, p_{\overline{4}})$). They are also taken to be orthogonal to the various nuetrality curves, and so are referred to as *transformation flux paths*; consequently, they will have the greatest transformation gradient. The general case of an arbitrary path can be approximated by infinitesimal path segments that then alternate between the local nuetrality curve direction and the local transformation flux direction.

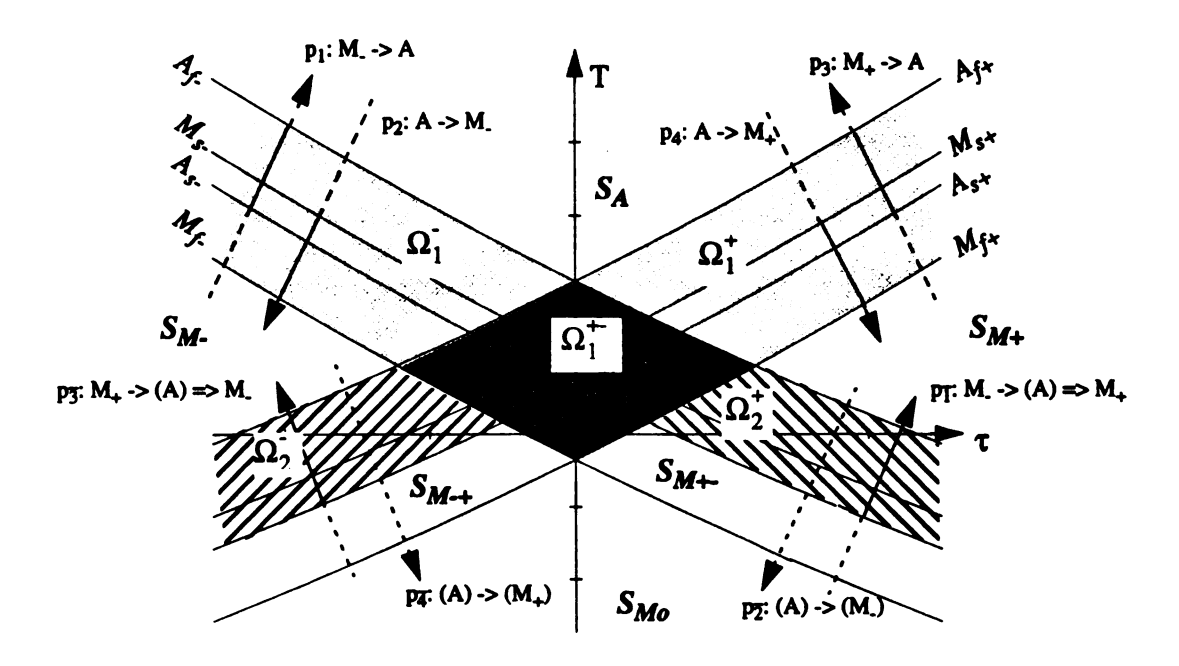


Figure 5. Transition paths are shown in X-unfolding for $A_s < M_s$. Solid lines indicate active transformation while dash or dot lines indicate inactive transformation.

Consider the path p_1 going from S_{M^-} to S_A corresponding to transition direction $M_- \to A$. Note that the portion between nuetrality curves M_{f_-} and A_{s_-} (dash line) is inactive while the portion between A_{s_-} and A_{f_-} is active (solid line). The opposite path p_2 running from S_A to S_{M^-} indicates transition direction $A \to M_-$ in which the portion between A_{f_-} and M_{s_-} (dash line) is inactive while between nuetrality curves M_{s_-} and M_{f_-} (solid line) is active. Both of the two paths could be active in the area between nuetrality curves A_{s_-} and M_{s_-} . Flux paths p_3 and p_4 in Ω_1^+ are similar to that of paths p_1 and p_2 , where now p_4 replaces p_4 . It should be noted that processes p_4 and p_4 and p_4 may operate simultaneously in p_4 , which implies the possibility of phase fraction triples p_4 in p_4 with p_4 with p_4 and p_4 and p_4 in p_4 in p_4 with p_4 and p_4 and p_4 and p_4 in p_4 in p_4 with p_4 and p_4 and

Paths: p_1 , p_2 , p_3 , p_4 , operate above both M_{f+} and M_{f-} . For states (τ, T) underneath either M_{f+} or M_{f-} , the associated transition of the form $A \to M_{+}$ or $A \to M_{-}$ has already gone to completion, so that there is no austenite in the corresponding area. Any austenite that would be predicted by a formal algorithm immediately transforms to M_+ if $\tau > 0$ $(A \Rightarrow M_{+})$ and immediately transforms to M_{-} if $\tau < 0$ $(A \Rightarrow M_{-})$. This will be referred to as an "instability transformation". It is reminiscent of Wasilewski, who introduced assumptions on the reorientation of martensite variants in non-austenite regions (Wasilewski, a, b, c, 1971), such that the austenite state serves as an instantaneously intermediary status to "switch" the reorientations of martensite variants. In the present study this suggests that, transition direction $M_1 \rightarrow A$ indicated by flux path $p_{\overline{1}}$ between A_{s_1} and A_{f_-} (solid line in Figure 5) should be replaced by $M_- \to (A) \Rightarrow M_+$, which is $M_- \to M_+$. We will refer here to direct martensite/martensite reorientation transformations from mixed martensite variant fraction $\{\xi_{-}, 0, \xi_{+}\}\$ to one that involves only one variant as a "detwinning process". Since path $p_{\overline{1}}$ (dot line) was originally inactive between M_{f_-} and A_{s_-} , no transition occurs on $p_{\overline{1}}$ in S_{M+} . On the other hand, path $p_{\overline{2}}$ for transition direction $A \rightarrow M_{\perp}$ (dot line) is completely inactive because of the absence of austenite below M_{f+} . Similarly, the active part of path p_3 (solid line), indicating transition direction $M_+ \to A$ between A_{s+} and A_{f+} , should be replaced by $M_{+} \rightarrow (A) \Rightarrow M_{-}$ or detwinning process $M_+ \rightarrow M_-$, while path $p_{\overline{3}}$ (dot line) is completely inactive between M_{f+} and A_{s+} . Path $p_{\overline{4}}$, like path p₂, is inactive, because of the absence of austenite. Consequently, the terminal nuetrality curves A_{s-} and A_{s+} become detwinning flow curves at sufficiently low temperature. Likewise, the terminal nuetrality curves $A_{f_{-}}$ and $A_{f_{+}}$ become detwinning finish curves at sufficiently low temperature. Thus far, two new transition directions have been set up in low temperature regions Ω_2^+ and Ω_2^- , in which detwinning processes will be triggered by increasing or decreasing the stress and temperature. Further, since paths $p_{\overline{1}}$ is inactive between M_{f_+} and A_{s_-} and path $p_{\overline{3}}$ is inactive between M_{f_+} and A_{s_+} , we verify the earlier claim that the stable mixed martensite variant zone S_{Mo} extends to regions S_{M+-} and S_{M-+} .

In conclusion, in $\Omega_1 = \Omega_1^- \cup \Omega_1^+ \cup \Omega_1^+$, the X-unfolding retains the original features of the previous unfolding by Pence et al. (1994). These include the coexistence of the phase triple $\{\xi_1, \xi_1, \xi_2\}$ away from $\tau = 0$ in Ω_1^+ , and the triggering of the transition direction $M_{\perp} \to A$, for example, by increasing the stress in $\tau > 0$ at a constant temperature. In addition to that, in Ω_2^+ and Ω_2^- , detwinning process $M_+ \leftrightarrow M_-$ is modified by $M_+ \to A$ and $M_- \to A$ austenite/martensite phase transformations, and the two variant martensites would be coexistent in S_M (= $S_{M+} \cup S_{Mo} \cup S_{M+}$), Ω_2^+ and Ω_2^- . In the latter two areas detwining processes are acknowledged to occur. It is obvious that the detwinning process in this X-unfolding come from allowing $M_{\perp} \to A$ and $M_{\perp} \to A$ to extend into the areas where there is no austenite, therefore, the corresponding detwinning flow and finish can be obtained directly from the phase transformation flow and finish in the nonaustenite areas Ω_2^+ and Ω_2^- . However, in Ω_2^+ and Ω_2^- , one should note that the X-unfolding has the property that increasing temperature at a constant stress can trigger the detwinning process. This is caused by the specified driving path crossing what are now detwinning nuetrality curves that continue to depend on both temperatures and stresses inherited from the original austenite/martensite transformation curves. This dubious phenomenon will be amended naturally in following further investigations on the unfoldings at the beginning in section 2.3.

2.2.4 Isothermal Behavior of X-unfolding

At the present stage, strategically, one can contemplate the transformation behavior under the X-unfolding. We here consider only the isothermal behaviors in view of the detwining difficulty mentioned above. Variable temperature and stress paths will be addressed in chapter 6. To see the problem clearly we define the following temperature ranges shown in Figure 6,

$$\begin{split} T_{pd} &= \{T > A_f\}, \\ T_{sh} &= \{T_{ff} \le T \le A_f\}, \\ T_{sm} &= \{T_{fs} \le T < T_{ff}\}, \\ T_{sl} &= \{M_f \le T < T_{fs}\}, \\ T_{se} &= \{T < M_f\}. \end{split}$$

Here, T_{ff} is the intersection temperature for nuetrality curve M_{f+} with nuetrality curve A_{f-} . Similarly T_{fs} is the intersection temperature for nuetrality curve M_{f+} with nuetrality curve A_{s-} . Consider constant temperature loading and unloading paths that increase stress from $\tau=0$ to a stress value in S_{M+} , this ensures complete transformation to M_{+} in the loading process. This is then followed by an unloading process that decreases the stress back to $\tau=0$. It is assumed that all initial conditions are given in status of a general mixture of the three species as allowed by the temperature under consideration. The following isothermal transformation possibilities are arrived for either $M_s>A_s$ or $M_s< A_s$ in TABLE 1.

TABLE 1. Transformation Possibilities for Isothermal Loading and Unloading

TEMPERATURE RANGES	TRANSFORMATION POSSIBILITIES DURING LOADING	TRANSFORMATION POSSIBILITIES DURING UNLOADING	THERMO-MECHANICAL BEHAVIOR			
$T \in T_{pd}$	$A \rightarrow M_{+}$.	$M_+ \to A$.	pseudoelasticity			
$T \in T_{sh}$	*1 $M_{-} \rightarrow A^{1}$, $A \rightarrow M_{+}^{2}$.	*4 $M_+ \rightarrow A^8$, $A \rightarrow M^9$.	if $M_s > A_s$, then shape memory effect with residual strain associated with some more M_+ , and less M left; if $M_s < A_s$, then only with some M_+ left at higher temperatures, 100% M_+ left at lower temperatures.			
$T \in T_{sm}$	*2 $M_{-} \rightarrow A^{3}$, $A \rightarrow M_{+}^{4}$, $M_{-} \rightarrow M_{+}^{5}$.	*5 $M_+ \rightarrow A^{10}$, $A \rightarrow M^{11}$.	if $M_s > A_s$, then shape memory effect with residual strain associated with some M_+ and M left for $T > A_s$ and 100% M_+ left for $T < A_s$; if $M_s < A_s$, then with M_+ 100% left only.			
$T \in T_{sl}$	*3 $A \rightarrow M_{+}^{6}$, $M_{-} \rightarrow M_{+}^{7}$.		shape memory effect with 100% M_{+} left.			
$T \in T_{se}$	$M_{-} \rightarrow M_{+}$.		same with the above.			
NOTES	 *1. If M_s > A_s, then 1 occurs first when T > M_s, and 1, 2 occur simultaneously when T < M_s. If M_s < A_s, then 1 always occurs before 2. *2. If M_s > A_s, then 3 and 4 occur simultaneously when T > A_s, 4 occurs before 3 when T < A_s, and 5 is the last one to occur. If M_s < A_s, then 4 always occurs before 3, and 5 is the last. *3. 6 occurs always before 7. *4. If M_s > A_s, then 8 would not complete, and 9 is active only when T < M_s. If M_s < A_s, then 8 is active only when T > A_s and would not complete. 9 is inactive. For both the two cases, 8 occurs always before 9 in the sense of 8 supports 9 by creating A. *5. If M_s > A_s, then 10 and 11 are active when T > A_s with 10 supporting 11 by creating A. If M_s < A_s, then 10 and 11 are inactive. 					

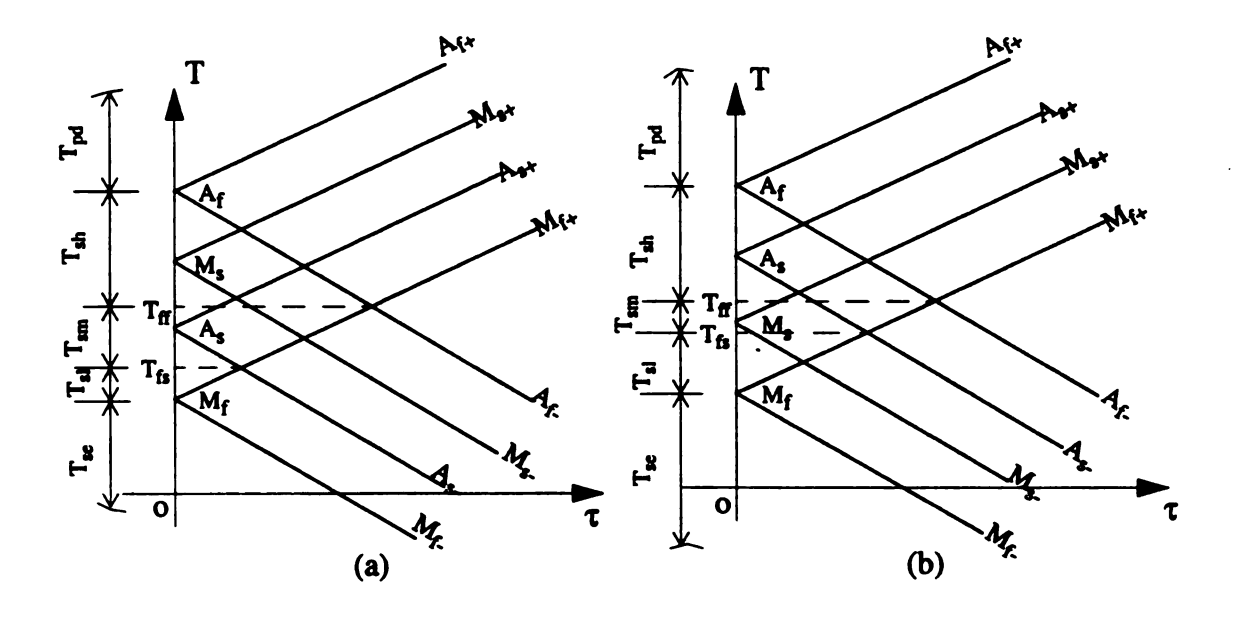


Figure 6. Temperature segments for cases $M_s > A_s$ (a) and $A_s > M_s$ (b) in X-unfolding.

2.3 Modified Nuetrality Curves and the pY-unfolding

2.3.1 Thermodynamic Considerations for Detwinning and a Primitive Y-unfolding

In the approach of the previous section, the X-unfolding naturally gives rise to detwinning process by first allowing martensite/austenite phase transformations to enter non-austenite areas, and second transforming the obtained austenite into martensite variants immediately in terms of Wasilewski's assumptions involving an instability transformation of austenite. An issue that must now be addressed is that the slope of these detwinning process nuetrality curves was determined on the basis of a Clausius-Clapeyron relation for austenite/martensite transformations. However, in Ω_2^+ and Ω_2^- the processes are now associated with martensite detwinning. Thus, the Clausius-Clapeyron argument requires modification. Based on (2.1.0.5), now the Clausius-Clapeyron equation for the detwinning

process in Ω_2^+ and Ω_2^- becomes

$$\frac{dT}{d\tau} = -\frac{\gamma_+ - \gamma_-}{\eta_+ - \eta_-}. (2.3.1.1)$$

In particular, if entropies of martensite variants are assumed identical, so that $\eta_+ - \eta_- = 0$, then the slopes of the nuetrality curves parametrizing detwinning processes lie parallel to the *T*-axis. The condition $\eta_+ - \eta_- = 0$ is met for the example material characterized by (2.2.2.3) and (2.2.2.4) with $\eta_+^o = \eta_-^o$. Note that this condition need not be met for more generalized models, such as those with temperature dependent elastic moduli, since then the individual phase Maxwell relation (2.1.0.4) would in general give a stress dependence on the martensite variant entropy functions η_+ and η_- , which would, in turn, break the relation $\eta_+ = \eta_-$.

For the realistic special case with $\eta_+ = \eta_-$, the above analysis implies that the detwinning flow and finish lines are independent of the temperature, which is agreeable to the approach by Krishnan, et. al (1971) and Brinson (1993). Under this scheme, the detwinning flow stress, say τ_s , could be naturally determined by identifying the stress of the intersection point between nuetrality curves M_{f+} and A_s . In the same manner the detwinning finish stress, named τ_f is naturally resolved by identifying the stress of the intersection point of nuetrality curve M_{f+} and with nuetrality curve A_f . These two special stresses are illustrated in Figure 7. This gives a primitive Y-unfolding, referred to as the pY-unfolding; it is shown in Figure 7 and Figure 8 for the case of a material obeying $M_s > A_s$. In this situation, zones S_A and Ω_1 are the same in the X- and pY-unfoldings, however, zones Ω_2^+ , Ω_2^- , S_{M+} and S_{M-} in the X-unfolding change to zones Ω_2^+ , Ω_2^- , S_{M+} and S_{M-} in the pY-unfolding (Figure 8) respectively while S_M turns to S_M^- . We no longer display the trans-

formation nuetrality curves for $A \to M_+$ and $A \to M_-$ in $\hat{\Omega}_2^+$ and $\hat{\Omega}_2^-$ in view of the previous discussion where it was shown that these two processes are not active in the area below Ω_1 .

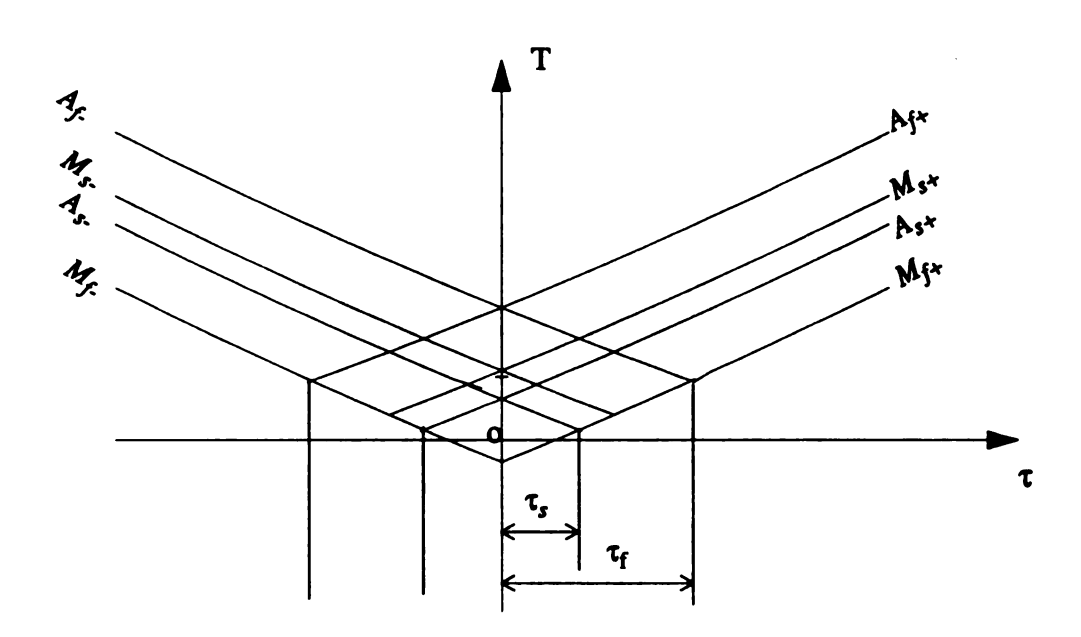


Figure 7 pY-unfolding is obtained by modifying the X-unfolding with eight specified nuetrality curves: A_{f+} , M_{s+} , A_{s+} , M_{f+} , A_{f-} , M_{s-} , A_{s-} , M_{f-} . The former four are "bent" to vertical positions in $\tau \le 0$ upon encountering M_{f-} and the latter four are similarly "bent" in $\tau \ge 0$ upon encountering M_{f+} . Here $A_s < M_s$; materials with $A_s > M_s$ are treated similarly.

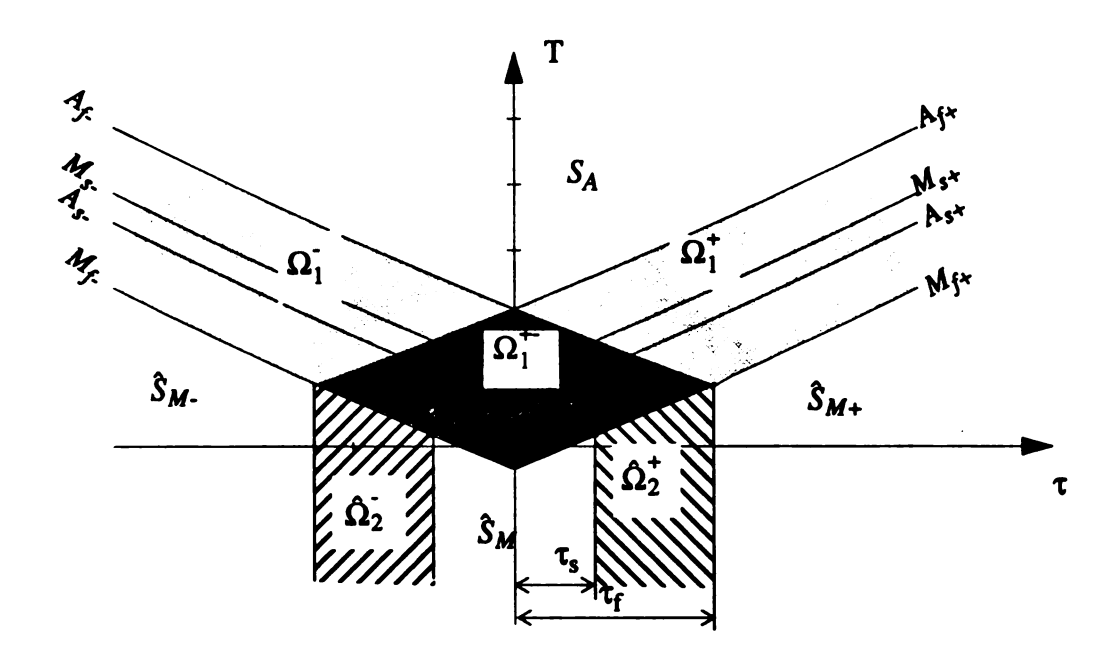


Figure 8. Phase transformation active and inactive zones are shown in the pY-unfolding, which is obtained by modifying the X-unfolding below M_{f+} and M_{f-} .

2.3.2 Mathematical Description of pY-unfolding

With the above discussion we now describe the modified nuetrality curves below M_{f+} and M_{f-} . The primary nuetrality curves $\beta_o^+(\tau,T)$ and $\beta_o^-(\tau,T)$, remain suitable in Ω_1 (above M_{f-} and M_{f+}), Below M_{f-} and M_{f+} these curves are modified so as to be parallel to the T-axis under the thermodynamic assumption $\eta_+ = \eta_-$ taken in the last section. For example, for any temperature C^- obeying $M_f < C^- < A_f$, one can always find the intersection point $(\tau, f(\tau))$ of nuetrality curve $\beta_o^+(\tau, T) = C^+$ with $\beta_o^-(\tau, T) = M_f$. In particular, the intersection point value of τ , corresponding to $C^+ = A_f$, is the detwinning flow $-\tau_s$ in this pY-unfolding. The detwinning finish stress $-\tau_f$ comes from this same procedure with $C^+ = A_f$. The area between the nuetrality curves $\tau = -\tau_s$ and $\tau = -\tau_f$ is renamed $\hat{\Omega}_2^-$. Since

the nuetrality curves are vertically described. Substituting $T = f(\tau)$ into $\beta_o^+(\tau, T)$ gives the modified nuetrality curves $\beta_m^+(\tau, T) = \beta_o^+(\tau, f(\tau))$ below M_{f^-} with $\tau < 0$, which is active only in Ω_2^- . Thus, the nuetrality curves of process $A \leftrightarrow M_+$ in Ω_1 and $M_+ \to M_-$ below M_{f^-} with $\tau < 0$ can be written as

$$\beta^{+}(\tau, T) = \begin{cases} \beta_{o}^{+}(\tau, T) & \text{for } \beta_{o}^{-}(\tau, T) \ge M_{f} \\ \beta_{o}^{+}(\tau, f(\tau)) & \text{for } \beta_{o}^{-}(\tau, T) < M_{f} \end{cases}$$
(2.3.2.1)

Similarly, for process $A \leftrightarrow M_{\perp}$ in Ω_1 and $M_{\perp} \rightarrow M_{+}$ below M_{f+} with $\tau > 0$, the nuetrality curves are found as

$$\beta^{-}(\tau, T) = \begin{cases} \beta_{o}^{-}(\tau, T) & for \ \beta_{o}^{+}(\tau, T) \ge M_{f} \\ \beta_{o}^{-}(\tau, g(\tau)) & for \ \beta_{o}^{+}(\tau, T) < M_{f} \end{cases}$$
(2.3.2.2)

Here $(\tau, g(\tau))$ is the intersection point of nuetrality curves $\beta_o(\tau, T) = C$ with $\beta_o^+(\tau, T) = M_f$.

Let (2.3.2.1) and (2.3.2.2) be equal to the four transition temperatures respectively, eight nuetrality curves are obtained. Four of these are associated with A_s and A_f in $\hat{\Omega}_2^+$ and $\hat{\Omega}_2^-$, and will be naturally interpreted as detwinning flow and finish lines respectively. The other four associated with M_s and M_f below M_{f-} and M_{f+} are not significant for any phase transformation process. The parts of the eight nuetrality curves in Ω_1 remain the same functions with those in the X-unfolding.

Example

Under the material description assumptions given by (2.2.2.3) and (2.2.2.4), the modi-

fied forms of (2.2.2.5) and (2.2.2.6) for this pY-unfolding can be obtained by following the above procedures. This evaluates (2.3.2.1) and (2.3.2.2) into the particular forms

$$\beta^{+}(\tau, T) = \begin{cases} T + \frac{1}{\eta_{A}^{0} - \eta_{+}^{0}} \left(\frac{(\mu_{M} - \mu_{A})\tau^{2}}{2\mu_{A}\mu_{M}} - \gamma^{+}\tau \right) & for \ \beta_{o}^{-}(\tau, T) \ge M_{f} \\ M_{f} - (2\gamma^{+}/(\eta_{A}^{o} - \eta_{+}^{o}))\tau & for \ \beta_{o}^{-}(\tau, T) < M_{f} \end{cases} , \quad (2.3.2.3)$$

$$\beta^{-}(\tau, T) = \begin{cases} T + \frac{1}{\eta_{A}^{0} - \eta_{-}^{0}} \left(\frac{(\mu_{M} - \mu_{A})\tau^{2}}{2\mu_{A}\mu_{M}} + \gamma^{*}\tau \right) & for \ \beta_{o}^{+}(\tau, T) \ge M_{f} \\ M_{f} + (2\gamma^{*}/(\eta_{A}^{o} - \eta_{+}^{o}))\tau & for \ \beta_{o}^{+}(\tau, T) < M_{f} \end{cases}$$
(2.3.2.4)

Especially, in general the detwinning start and finish stresses are naturally determined by

$$\tau_s = \frac{(A_s - M_f)(\eta_A^o - \eta_-^o)}{2\gamma^*},$$
 (2.3.2.5)

and

$$\tau_f = \frac{(A_f - M_f)(\eta_A^o - \eta_{-}^o)}{2\gamma^*}, \qquad (2.3.2.6)$$

respectively for this pY-unfolding.

2.4 Refined pY-unfolding Associated with Experiments

2.4.1 Experimental Justification on Detwinning

An obvious feature of the pY-unfolding as discussed so far is that the detwinning flow stress τ_s and the detwinning finish stress τ_f are a consequence of the nuetrality curve geometry of the original X-unfolding. However, the two stresses determined in this way might not match those found by experiment. For example, the values of τ_s and τ_f given by the formulae ((2.3.2.5), (2.3.2.6)) are larger that those observed in the experiments by Hou and Grummon (1995), and Miyazaki et al. (1991). An improved model would allow these two stresses to be specified as material properties. Here we continue to neglect any temperature influence on both of the flow and finish, which is consistent with the detwinning processes in pY-unfolding. Often the stress of detwinning flow is easily obtained directly from experiments. However, the stress of detwinning finish is more difficult to obtain experimentally. Nevertheless, in $\tau > 0$, we assume that the detwinning flow stress τ_s and finish stress τ_f (both of them are positive) are known for $M_- \to M_+$. Consequently, in $\tau <$ 0, these two are given by $\tilde{\tau}_s = -\tau_s$ and $\tilde{\tau}_f = -\tau_f$ for $M_+ \to M_-$ under the symmetry assumptions of the material, so as to determine the two corresponding nuetrality curves vertically (Figure 9).

Both the active detwinning nuetrality curves and the inactive nuetrality curves will be vertically modified by the flow stress τ_s and the finish stress τ_f to satisfy the condition of the instability transformation of austenite and its associated Clausius-Clapeyron relation (2.3.1.1). Recall also that detwinning process $M_- \to M_+$ is obtained by modifying the process $M_- \to A$ below M_{f+} , this naturally requires that the two corresponding nuetrality curves connect to each other on M_{f+} . A similar requirement is made for processes

 $M_+ \to M_-$ and $M_+ \to A$ on M_{f^-} . We call this kind of requirement a consistency condition, namely that: (1) the nuetrality curve A_{f^+} continues from $\tau > 0$ to the curve $\tau = -\tau_f$ below M_{f^+} ; (2) the nuetrality curve A_{s^+} continues from $\tau > 0$ to the curve $\tau = \tau_s$ below M_{f^+} ; (3) the nuetrality curve A_{f^-} continues from $\tau < 0$ to the curve $\tau = \tau_f$ below M_{f^+} ; (4) the nuetrality curve A_{s^-} continues from $\tau < 0$ to the curve $\tau = \tau_s$ below M_{f^+} . There are many ways to accomplish these procedures, the method taken here is to "bend" each of the nuetrality curves A_{f^+} , A_{s^+} , A_{f^-} and A_{s^-} twice. As an example, A_{f^+} is bent once at point $(0, A_f)$ on the T^- axis, and again at its intersection point with M_{f^-} . This allows A_{f^+} : to remain as it was in the X-unfolding for $\tau > 0$, to be given by $\tau = -\tau_f$ below M_{f^-} , and to have a straight line connection on the resulting boundary of Ω_1^+ . The remaining three nuetrality curves can be modified similarly. Once the above procedures are completed, all the other nuetrality curves must then be modified accordingly. In this refined pY-unfolding, called simply the Y-unfolding in what follows, we still use the notations of the pY-unfolding for a definition of zones (Figure 10).

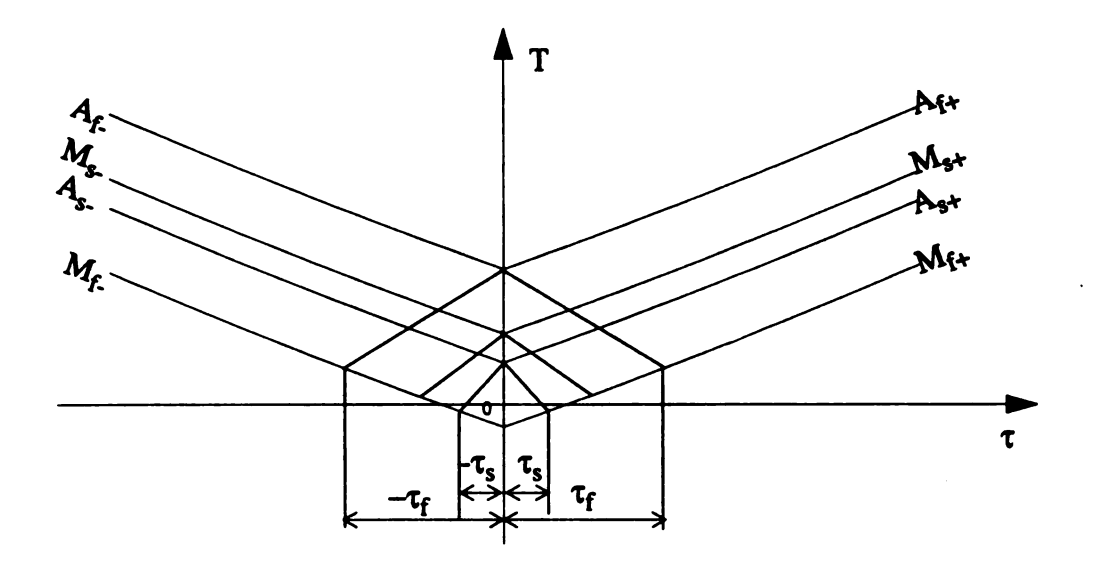


Figure 9. Refined pY-unfolding, say, Y-unfolding, improves upon the pY-unfolding by allowing the detwinning flow stress τ_s and finish stress τ_f to be specified as additional material properties. This diagram is for the case of $M_s > A_s$. In the present development, the terminal nuetrality curves undergo abrupt slope changes upon crossing $\tau = 0$ and upon meeting the nuetrality curves M_{f} and M_{f+} .

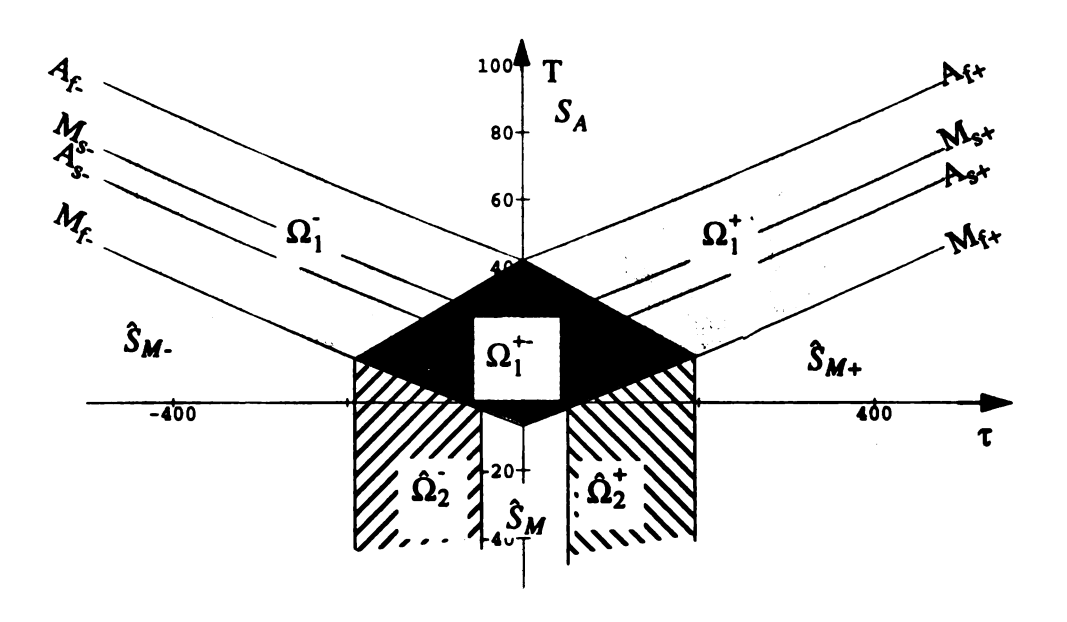


Figure 10. Active and inactive zones in Y-unfolding corresponding to Figure 9.

2.4.2 Mathematical Formulation of the Y-unfolding

In general, for constructing modified nuetrality curves of the Y-unfolding suitable to meet the temperature independent detwinning flow and finish stresses, one must match the two lines $\tau = \tau_s$ and $\tau = \tau_f$ with the two stipulated nuetrality curves $\beta^-(\tau, T) = A_s$ and $\beta^-(\tau, T) = A_f$ on the terminal nuetrality curve M_{f+} . The nuetrality curves inside Ω_2^+ could be simulated by linear interpolation between A_f and A_s associated with the detwinning flow and finish stresses. Nuetrality curves, trivial for $M_- \to M_+$ in \hat{S}_{M+} and \hat{S}_{M-} ($\tau>0$), are all vertical lines corresponding to any temperatures in $T>A_f$ and $M_f < T < A_s$ respectively. Based on the consistency condition introduced in section 2.4.1, each such nuetrality curves should connect with a nuetrality curve of $M_- \leftrightarrow A$ at the point on M_{f+} corresponding the same temperature parameter. This naturally continues $\beta^-(\tau, T)$ beneath the terminal nuetrality curve M_{f+} in $\tau>0$.

As discussed above, since $\beta^-(\tau, T)$ remains unchanged in $\tau \le 0$, the consistency condition restricts the connection between the two nuetrality curve sets of $M_- \leftrightarrow A$ for $\tau \le 0$ and $M_- \to M_+$ for $\tau > 0$ to describe process $M_- \leftrightarrow A$ for $\tau > 0$. At present stage, we ignore the thermodynamic consideration connected with this part, ie. process $M_- \leftrightarrow A$ for $\tau > 0$. Appropriate thermodynamic refines to the problem are discussed in the Appendix. Geometrically, instead, there are many ways to link the two parts. The obvious way mentioned in the previous section involves using straight lines to continue those nuetrality curves with C^0 smooth assumptions (Figure 9, Figure 10), which gives an approximate description for process $M_- \leftrightarrow A$. Note that this modifies the slopes of the nuetrality curves in region Ω_1^+ for $\tau > 0$.

Because of this, it is convenient to decompose the portion of Ω_1^+ in $\tau > 0$ into subre-

gions R_1 and R_2 . The region R_2 is that portion of Ω_1^+ above A_{s_-} and the region R_1 is that portion of Ω_1^+ below A_{s_-} . In addition, let R_3 be the region above A_{f_-} and M_{f_+} in $\tau > 0$. Symmetry determines the corresponding regions in $\tau < 0$. Mathematically, the three regions are expressed as the following shown in Figure 11,

$$R_{1} = \{(\tau, T) | \tau > 0, \beta^{-}(\tau, T) \leq A_{s}, \beta^{+}(\tau, T) \geq M_{f} \},$$

$$R_{2} = \{(\tau, T) | \tau > 0, A_{s} < \beta^{-}(\tau, T) < A_{f}, \beta^{+}(\tau, T) \geq M_{f} \},$$

$$R_{3} = \{(\tau, T) | \tau > 0, \beta^{-}(\tau, T) \geq A_{f}, \beta^{+}(\tau, T) \geq M_{f} \}.$$

We now discuss this particular construction for our standard model involving pure species strains as given by (2.2.2.3) and the pure species entropy as given by (2.2.2.4). The straight line slope of A_{f-} in $\tau > 0$ above M_{f+} , which satisfies the consistency condition, is then found to be

$$k_f = -\frac{A_f - M_f - k_1 \tau_f - k_2 \tau_f^2}{\tau_f}$$
 (< 0). (2.4.2.1)

Here, k_1 and k_2 are given by,

$$k_1 = \gamma^* / (\eta_A^o - \eta_+^o) \ (>0), \quad k_2 = \frac{(\mu_A - \mu_M)}{2\mu_A \mu_M (\eta_A^o - \eta_+^o)} \ (>0).$$
 (2.4.2.2)

The straight line slope of A_{s-} in $\tau > 0$ above M_{f+} , which satisfies the consistency condition, is then found to be

$$k_s = -\frac{A_s - M_f - k_1 \tau_s - k_2 \tau_s^2}{\tau_s}$$
 (< 0), (2.4.2.3)

for the same k_1 and k_2 . Thus, A_f and A_s are given by

$$T - k_f \tau = A_f \text{ for } \tau > 0, \qquad (2.4.2.4)$$

$$T - k_s \tau = A_s \text{ for } \tau > 0, \qquad (2.4.2.5)$$

respectively above M_{f+} .

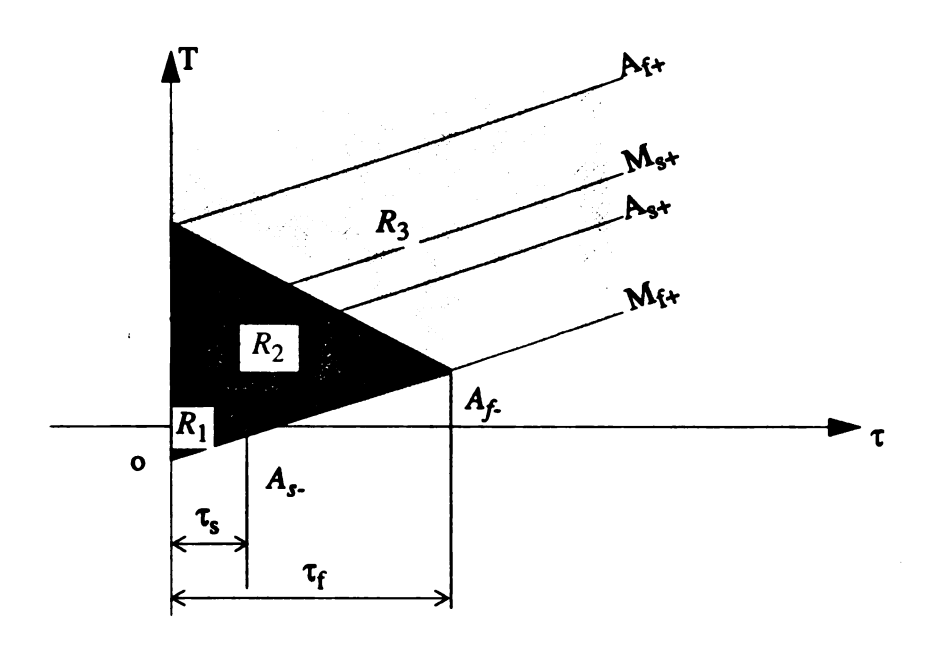


Figure 11. Subdomains R_1 , R_2 and R_3 are shown in $\tau > 0$ for materials obeying $M_s > A_s$.

Since detwinning flow and finish stresses τ_s and τ_f are now regarded as determined by experimental measurements, k_s and k_f are fully settled for this standard model. Three possibilities might be encountered, ie., either $k_f > k_s$, $k_f = k_s$ or $k_f < k_s$. In the first case, the straight line extensions to A_f and A_s that bound R_2 would intersect at a point π_1 obeying $\tau < 0$. In the last case, this intersection would occur at a point π_2 obeying $\tau > 0$

(Figure 12). The coordinates for this intersection point are found to be

$$\tau_{\pi} = \frac{A_f - A_s}{k_s - k_f}, \quad T_{\pi} = \frac{A_f k_s - A_s k_f}{k_s - k_f}.$$
(2.4.2.6)

Note that k_f^- and k_s^- are negative, so that condition $k_f^- > k_s^-$ makes (2.4.2.6) correspond to a point π_1 and condition $k_f^- < k_s^-$ makes (2.4.2.6) correspond to a point π_2 . The intermediate case $k_f^- = k_s^-$ gives parallel lines and so corresponds to an intersection point at infinity.

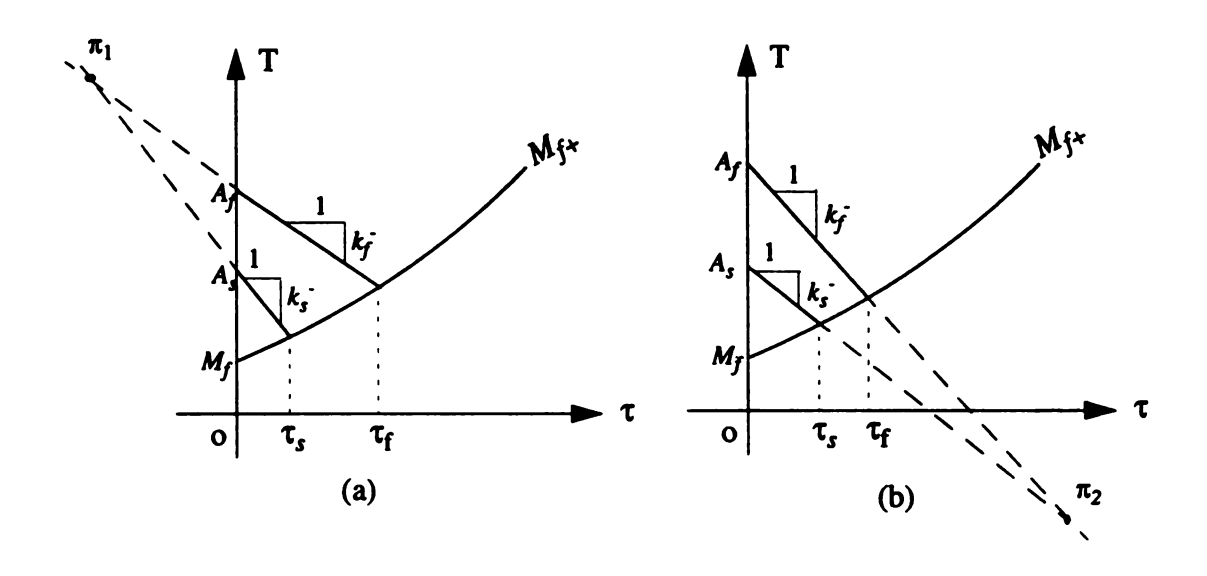


Figure 12. Intersecting points of nuetrality curves of detwinning flow and finish for $k_f > k_s$ (a) and for $k_f < k_s$ (b).

The intersection point π , which is the intersection of the extension of nuetrality curves A_f and A_s , can now be used to organize all the remaining nuetrality curves β in R_1 , R_2 and R_3 corresponding to the process $A \leftrightarrow M$. The nuetrality curves, trivial for $A \leftrightarrow M$ in the region R_3 , are assumed to be straight with slope value k_f . Similarly, the nuetrality curves for $A \to M$ in the region R_1 ($A \to M$ may be active in a part of R_1 if $A_s > M_s$) are

assumed to be straight with slope value k_s . In the intermediate region R_2 , it is natural to assume that the nuetrality curves are determined by linear interpolation between the $M_- \to A$ nuetrality curves A_{f_-} and A_{s_-} .

Therefore, taken together, the nuetrality curves can be expressed as

$$\beta_f(\tau, T) = T - k_f \tau \text{ in } R_3,$$
 (2.4.2.7)

$$\beta_s(\tau, T) = T - k_s \tau \text{ in } R_1,$$
 (2.4.2.8)

respectively. And, the nuetrality curves in R_2 can be obtained as

$$\beta_{sf}(\tau, T) = \frac{T(A_f - A_s) + \tau(A_s k_f^- - A_f k_s^-)}{(A_f - A_s) + \tau(k_f^- - k_s^-)} \text{ in } R_2,$$
(2.4.2.9)

by being assumed to be straight lines with slopes determined by linear interpolation between k_f and k_s . This algebraic construction corresponds geometrically to one in which straight rays are drawn from π_1 if $k_f > k_s$ or π_2 if $k_f < k_s$ which then fill in section R_2 .

Finally, the nuetrality curves for detwinning in $\tau > 0$ below M_{f+} are given as

$$\beta_{dif}(\tau, T) = M_f + (k_1 - k_f)\tau + k_2\tau^2 \text{ in } \hat{S}_{M+},$$
 (2.4.2.10)

$$\beta_{dts}(\tau, T) = M_f + (k_1 - k_s)\tau + k_2\tau^2 \text{ in } \hat{S}_M,$$
 (2.4.2.11)

$$\beta_{disf}(\tau, T) = \frac{(A_f - A_s)(M_f + k_1 \tau + k_2 \tau^2) + (A_s k_f - A_f k_s)\tau}{A_f - A_s + (k_f - k_s)\tau} \text{ in } \hat{\Omega}_2^+.$$
 (2.4.2.12)

Thus, taking together all of the above results, the characteristics for phase transformation $M_{\perp} \leftrightarrow A$ and detwinning process $M_{\perp} \to M_{+}$ are summarized as

$$\beta_{o}^{\cdot}(\tau, T), \qquad \forall \quad \tau \leq 0$$

$$\beta_{f}^{\cdot}(\tau, T), \qquad \forall \quad (\tau, T) \in R_{1}$$

$$\beta_{sf}^{\cdot}(\tau, T), \qquad \forall \quad (\tau, T) \in R_{2}$$

$$\beta_{s}^{\cdot}(\tau, T), \qquad \forall \quad (\tau, T) \in R_{3} \qquad . \qquad (2.4.2.13)$$

$$\beta_{dtf}^{\cdot}(\tau, T), \qquad \forall \quad (\tau, T) \in \hat{S}_{M+}$$

$$\beta_{dtsf}^{\cdot}(\tau, T), \qquad \forall \quad (\tau, T) \in \hat{\Omega}_{2}^{+}$$

$$\beta_{dts}^{\cdot}(\tau, T), \qquad \forall \quad (\tau, T) \in \hat{S}_{M}(\tau > 0)$$

If we use \overline{R}_1 , \overline{R}_2 and \overline{R}_3 to indicate the reflection of the areas of R_1 , R_2 and R_3 with respect to the *T*-axis and follow the same analysis for formulating $\beta^-(\tau, T)$, then the characteristics for phase transformation $M_+ \leftrightarrow A$ and detwinning process $M_+ \to M_-$ can be written as

$$\beta_{o}^{+}(\tau, T), \qquad \forall \quad \tau > 0$$

$$\beta_{f}^{+}(\tau, T), \qquad \forall \quad (\tau, T) \in \overline{R}_{1}$$

$$\beta_{sf}^{+}(\tau, T), \qquad \forall \quad (\tau, T) \in \overline{R}_{2}$$

$$\beta_{s}^{+}(\tau, T), \qquad \forall \quad (\tau, T) \in R_{3} \qquad (2.4.2.14)$$

$$\beta_{dif}^{+}(\tau, T), \qquad \forall \quad (\tau, T) \in \hat{S}_{M+}$$

$$\beta_{disf}^{+}(\tau, T), \qquad \forall \quad (\tau, T) \in \hat{\Omega}_{2}$$

$$\beta_{dis}^{+}(\tau, T), \qquad \forall \quad (\tau, T) \in \hat{S}_{M}(\tau \leq 0)$$

Here, all the components of $\beta^+(\tau, T)$ are decided as the same fashion as those of $\beta^-(\tau, T)$

but associated with equation (2.2.2.6) and the slopes

$$k_f^+ = -k_f^-, \quad k_s^+ = -k_s^-.$$
 (2.4.2.15)

2.4.3 Summary

For sufficiently low temperatures, the pY-unfolding and Y-unfolding involve vertical (temperature independent) detwinning flow and detwinning finish terminal nuetrality curves. These are obtained by assuming $\eta_{\perp}(\tau, T) = \eta_{\perp}(\tau, T)$ for (τ, T) values that trigger detwinning under all circumstances. From the above discussions, this pY-unfolding, being another extension of the triple point phase diagram, not only takes over all the features of X-unfolding in Ω_1 but also reflects the detwinning process between the two martensite variants. In the description of detwinning, since the detwinning nuetrality curves are now all vertical, temperature increase at a constant stress does not traverse nuetrality curves, so that temperature changes no longer trigger reorientation. However, the pY-unfolding completely determines the detwinning flow and finish lines by naturally extending the high temperature phase transformation nuetrality curves. In general, the detwinning flow stress of the pY-unfolding is smaller than that of the X-unfolding, both of which are larger than those determined by experimental measurements (Hou and Grummon, 1995; Miyazaki et al. 1991). This motivated the further modification of the pY-unfolding into the Y-unfolding where the detwinning flow stress and detwinning finish stress are taken as material properties.

It is important to point out that, in general, the detwinning flow stress is found to obey a mild temperature dependence. This phenomenon was, for example, observed in a tension experiment of a bulk (the size of the specimens were 1 mm x 1.5 mm x 15 mm at 50.0, 50.5 51.0, 51.5, and 52.0 at%Ni) by Miyazaki, et al. (1986, 1991), in which the slope of detwinning flow line is -0.385 °K/MPa. This kind of phenomenon was explained in terms of a thermally activated effect (Miyazaki and Otsuka, 1984). Also, in the tension test of NiTi thin film by Hou & Grummon (1995), the slope of detwinning flow line is measured -5.41 °K/MPa. Such a tiny temperature influence on the detwinning flow is also observed in the work by Dye (1990). Furthermore, in two other experimental studies (wire specimens with diameters 0.9 mm and 1.0 mm at Ti₅₀Ni₄₇Fe₃ and Ti-49.8 at. pct Ni (or Ti-50.6 at pct Ni) respectively) by Miyazaki and Otsuka (1984, 1986), they also found that the slopes of detwinning flow lines changed slightly with temperatures. Actually, for most shape memory alloys, the detwinning flow stress may increase when temperature decreases (Miyazaki, Kohiyama and Otsuka, 1991). The explanation in terms of a thermal activation effect is that at lower temperatures the molecules of the material are less active than at higher temperatures, which makes the detwinning process more difficult at lower temperatures.

2.5 Analysis of Isothermal Loading/Unloading Processes

With this Y-unfolding so far, we can illustrate various isothermal behaviors of shape memory alloys, such as pseudoelasticity at high temperatures, shape memory effect at low temperatures, or some properties between the two. Since the phase diagram depends upon parameters: phase transformation temperatures A_f , A_s , M_s and M_f ; detwinning flow stress τ_s and finish stress τ_f shear moduli μ_A and μ_M ; reference entropy difference between austenite and martensite $\Delta \eta^0$, phase transformation strain γ^* and density ρ . Here, these are

determined with reference to work of Hou and Grummon (1995), which are given in the following table.

TABLE 2 Simulation Parameters

Af	Ag	M _s	M_f	μΑ	μМ	Δη	ρ	τ,	ч	γ*
308	295	263	235	3*10 ⁴	3*10 ⁴	414695	6.5*10 ³	150.0	200.0	0.06
°К	°К	°K .	°К	MPa	MPa	J/m ³ °K	Kg/m ³	MPa	MPa	

Here, $\Delta\eta$ is determined by relation $\Delta\eta = \Delta H/T_o$ where $\Delta H = 17.8$ J/g and $T_o = 279$ °K. An Y-unfolding for $\tau > 0$ is obtained as shown in Figure 13. It has straight nuetrality curves for the parameters given above, since the condition $\mu_A = \mu_M$ annihilates the τ^2 terms in the various β -functions (see (2.2.2.5), (2.2.2.6)).

Recall that T_{ff} and T_{fs} were previously defined for the X-unfolding. For convenience, we now define two more special temperatures T_{ss} and T_{sf} This gives four intersection temperatures that distinguish transformation areas in $\tau > 0$, which are expressed in the following,

$$T_{ss} = A_s + k_s^2 \frac{k_s^2 - k_1 + \sqrt{(k_s^2 - k_1)^2 + 4k_2(A_s - M_s)}}{2k_2},$$
 (2.5.0.1)

$$T_{sf} = A_f + k_f^{-1} \frac{k_f^{-1} - k_1 + \sqrt{(k_f^{-1} - k_1)^2 + 4k_2(A_f - M_s)}}{2k_2},$$
 (2.5.0.2)

$$T_{fs} = A_s + k_s \tau_s, \qquad (2.5.0.3)$$

$$T_{ff} = A_f + k_f \tau_f. {(2.5.0.4)}$$

Here, the first subscripts are adopted from the first subscripts of nuetrality curves M_{s+} and M_{f+} and the second are come from the first subscripts of nuetrality curves A_{s-} and A_{f-} . The values k_1 and k_2 were in general defined previously in (2.4.2.2), and, k_f^- and k_s^- are given by (2.4.2.1) and (2.4.2.3) respectively. These four temperatures are in general dependent on the shear moduli of austenite and martensite in virtue of k_2 . The corresponding coordinates on τ -axis are τ_{ss} , τ_{sf} , τ_s and τ_f . In the present situation, the four temperatures are found as in TABLE 3,

TABLE 3. Temperatures Corresponding to Points a, b, c and d in Figure 13

T_{ss}	T_{sf}	T_{fs}	T _{ff}
274.6 °K	280.8 °K	256.7 °K	263.9 °K

Comparing with the four transformation temperatures, shows that

$$A_f > A_s > T_{sf} > T_{ss} > T_{ff} > M_s > T_{fs} > M_f,$$
 (2.5.0.5)

for these particular values of the material parameters.

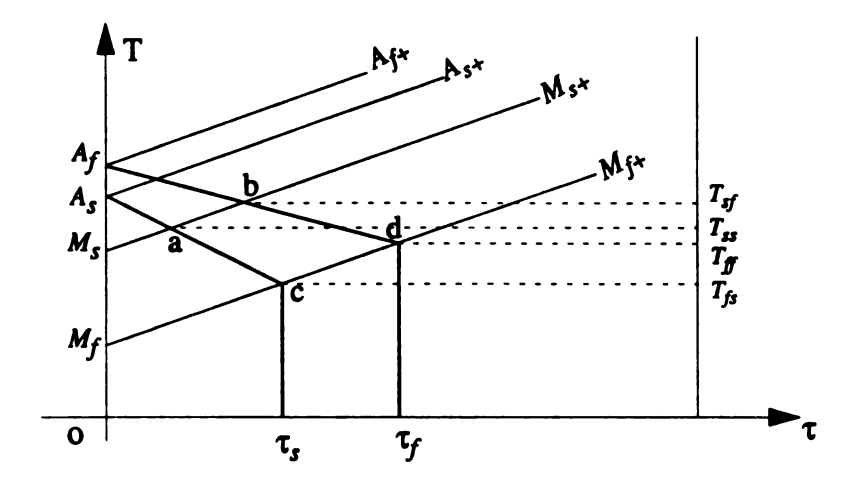


Figure 13. Y-unfolding for $\tau > 0$ with $k_2 = 0$. Four intersection points a, b, c and d are shown as: a (τ_{ss}, T_{ss}) , b (τ_{sf}, T_{sf}) , c (τ_{s}, T_{fs}) , d (τ_{f}, T_{ff}) .

The loading/unloading behaviors strongly depend upon the initial phase fraction. To briefly view the problem, we here consider two type initial conditions which were considered by Wasilewski (1971 d). The first one is that the austenite phase fraction is maximum, which is obtained by cooling the material from a temperature that is above A_f down to the test temperature (CFAF). The second one is that the martensite (with two symmetric variants) phase fraction is maximum, which is obtained by heating the material from a temperature that is below M_f up to the test temperature (HFMF). There are four loading types p_1 , p_2 , p_3 and p_4 (accounted from decreasing temperature direction) in the initial condition case of maximum austenite (CFAF), which are located by the temperature ranges: $T > M_s$, $M_s > T > T_{fs}$, $T_{fs} > T > M_f$, $T < M_f$ respectively, shown in Figure 14. There are six loading types p_1 , p_2 , p_3 , p_4 , p_5 and p_6 (accounted from increasing temperature direction) in the initial condition case of maximum martensite (HFMF), which are located

at temperature ranges: $T < T_{fs}$, $T_{ff} > T > T_{fs}$, $T_{ss} > T > T_{ff}$, $A_s > T > T_{ss}$, $A_f > T > A_s$, $T > A_f$, shown in Figure 15. Conversely, there are three unloading types p_1 , p_2 and p_3 in both of the two initial condition types, which are located at temperature ranges: $T > A_f$, $A_f > T > A_s$, $T < A_s$, shown in Figure 16.

It is noted for both the CFAF and the HFMF conditions that the austenite phase is generated in certain temperature regimes when the stress increases. For CFAF initial condition, if the test temperature is between M_s and T_{fs} , a stress-assisted austenite is formed from process $M_1 \rightarrow A$ (for example, between points 1 and 2 on path p_2 in Figure 14) by increasing the stress. Simultaneously, both the new generated and the original austenite transform into the variant M_+ during the stress increase. Below T_{fs} any stress-assisted austenite is subject to the instability transformation $A \Rightarrow M_{\perp}$ and so immediately experiences a transient phase shift to the variant M_{+} (as used to describe detwinning in section 2.2.3). For HFMF initial condition, (stable) stress-assisted austenite can be generated from $M_{\perp} \rightarrow A$ when stress increases between temperature range A_f and T_{fs} . It is obvious that the temperature range to induce the (stable) stress-assisted austenite of the latter case is wider than that of the former case, ie., the martensite variant M_{\cdot} of HFMF can be initially present up to a temperature $T < A_f$. This kind of transition mechanism, a stable stress-assisted austenite from some special orientations of martensite (special variants), has been suggested by Wasilewski (1971 d). The present model can give detailed predictions about the temperature ranges of the specific transformation upon isothermal loading.

More general loading behaviors occur for other initial conditions, but the limiting cases addressed here give the general flavor of the model. Finally, the example discussed here and shown in Figure 14 to Figure 16 involved a material with $M_s < A_s$. Similar analysis can be carried out for a material with $A_s < M_s$.

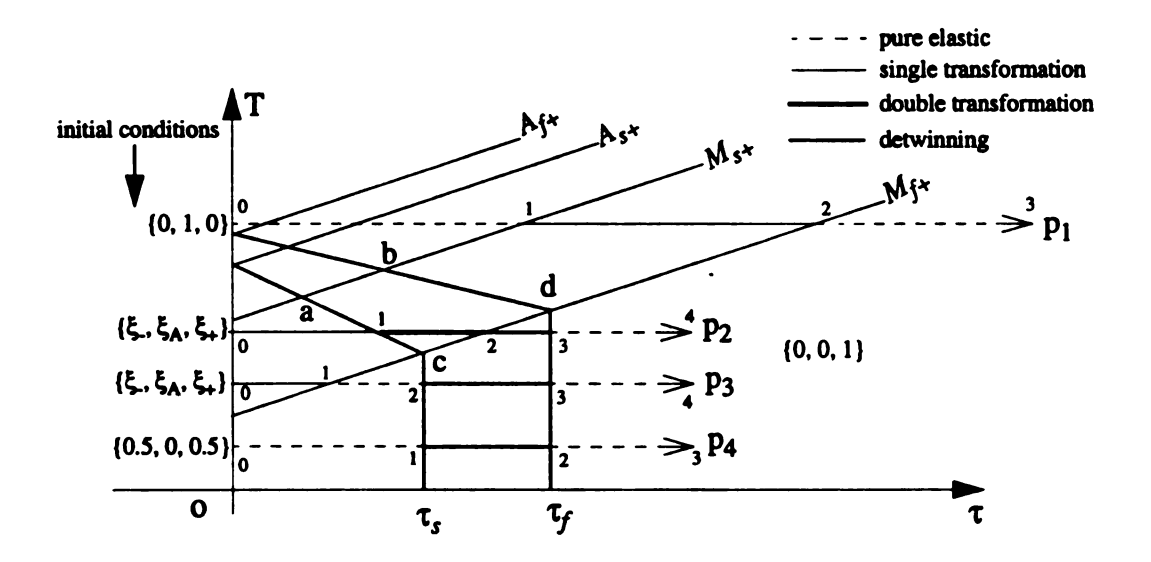


Figure 14. Loading behavior for initial conditions corresponding to initial conditions of maximum austenite, CFAF (equal amount of martensite two variants). For $T > M_s$ the initial condition is $\{\xi_-, \xi_A, \xi_+\} = \{0, 1, 0\}$ and for $T < M_f$ it is $\{\xi_-, \xi_A, \xi_+\} = \{0.5, 0, 0.5\}$. For $M_f < T < M_s$ the initial condition is a more general $\{\xi_-, \xi_A, \xi_+\}$ with $\xi_- = \xi_+$. The four associated transition paths p_1, p_2, p_3 and p_4 go from left to right. On p_1 , so that $T > M_s$, segments 01, 12 and 23 indicate austenite elastic, single transformation $A \to M_+$ and pure elastic M_+ deformations respectively. On p_2 , so that $T_{fs} < T < M_s$, segment 01, 12, 23, 34 represent single transformation $A \to M_+$, double transformation $A \to M_+$ & $M_- \to A$, detwinning $M_- \to M_+$ and elastic M_+ deformations. On p_3 , segments 01, 12, 23 and 34 indicate single transformation $A \to M_+$, two variant martensite elastic, detwinning $M_- \to M_+$ and elastic M_+ deformations. On p_4 , segments 01, 12 and 23 represent two variant martensite elastic, detwinning $M_- \to M_+$ and elastic M_+ deformations.

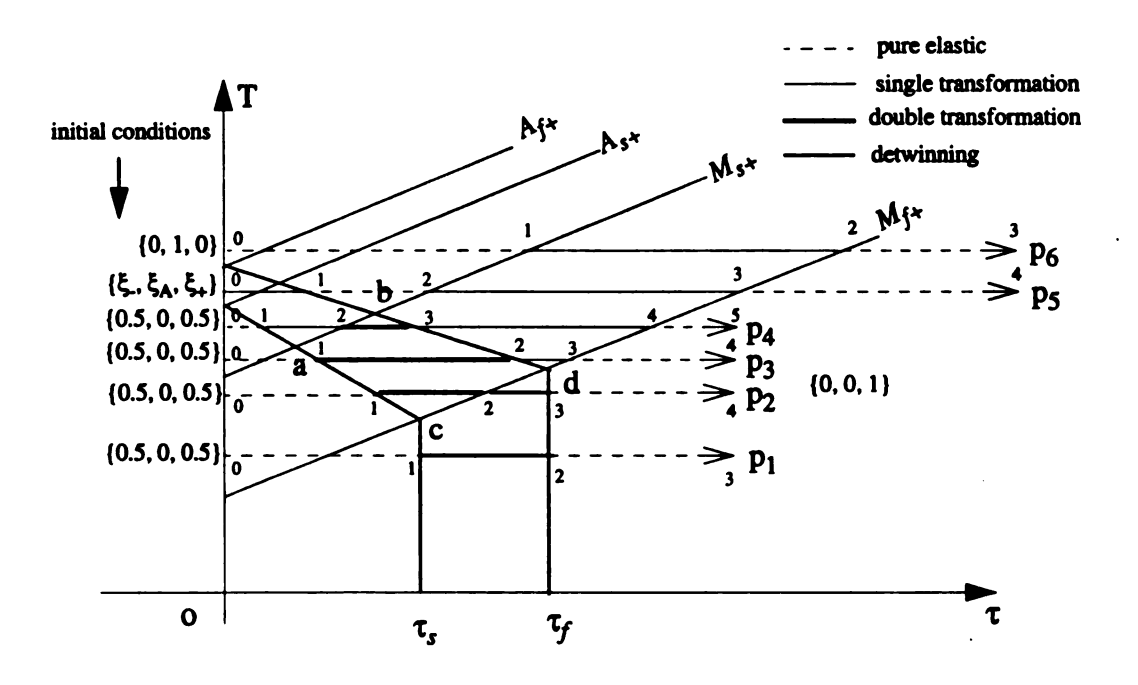


Figure 15. These six transition paths p_1 , p_2 , p_3 , p_4 , p_5 and p_6 associated with maximum martensite initial conditions, HFMF (equal amount of martensite two variants) go from left to right. On p1, segments 01, 12 and 23 indicate two variant martensite elastic, detwinning $M_- \rightarrow M_+$ and right-shear martensite elastic deformations. On p_2 , segments 01, 12, 23 and 34 represent two variant martensite elastic, double transformation $M_- \rightarrow A & A \rightarrow M_+$, detwinning $M_- \rightarrow M_+$ and elastic M_+ deformations. On p_3 , the first two segments 01 and 12 are the same with those on p_2 , segment 23 and 34 indicate single transformation $A \rightarrow M_+$ and elastic M_+ deformations. On p_4 , segments 01, 12, 23, 34 and 45 represent two variant martensite elastic, single transformation $M_- \rightarrow A$, double transformation $M_- \rightarrow A$ double transformation. On p_5 , segments 01, 12, 23 and 34 indicate single transformation $M_- \rightarrow A$, austenite and M_+ elastic, single transformation $A \rightarrow M_+$ and elastic M_+ deformations. On p_6 , segments 01, 12 and 23 represent austenite elastic, single transformation $A \rightarrow M_+$ and elastic M_+ deformations. On p_6 , segments 01, 12 and 23 represent austenite elastic, single transformation $A \rightarrow M_+$ and elastic M_+ deformations.

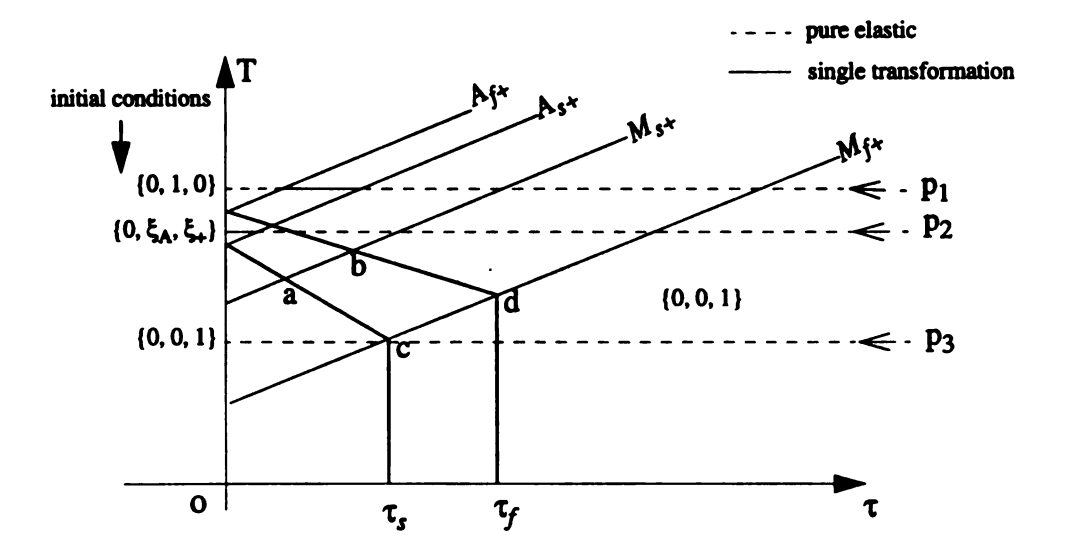


Figure 16. These three unloading paths go from the right to left with initial condition of 100% M_+ . All the dashed lines on p_1 , p_2 and p_3 indicate M_+ elastic deformations, except the portion to the left of A_{f+} on p_1 which represents elastic austenite. All the solid lines on p_1 and p_2 indicate single transformation $M_+ \to A$ deformations.

2.6 Transformation of a Special Variant

Other than the above isothermal features of the Y-unfolding, it is interesting to look at some different characters of this Y-unfolding. Since the observed detwinning flow stress τ_s is, in general, smaller than the extrapolated value from the pY-unfolding (Hou and Grummon, 1995), it follows that the nuetrality curve for the reverse transformation $M_- \to A$ for $\tau > 0$ is below that of the pY-unfolding. Regarding to the continuous assumption between nuetrality curves of $M_- \to A$ and $M_- \to M_+$ on the terminal nuetrality curve M_{f+} (see section 2.4.2), this implies that the start temperature for $M_- \to A$ is lowered. The above extrapolation reflects a transformation mechanism that the martensite variant M_- becomes more unstable in the Y-unfolding for $\tau > 0$. In other words, the energy barrier for $M_- \to A$

is decreased in $\tau > 0$. Phenomenally, this decrease tendency of $M_- \to A$ flow coincides with the postulation made by Wasilewski (1971, c, d). Based on an asymmetric isothermal stress-strain relation of a tension-compression experiment conducted below M_f (Wasilewski, 1971 c), Wasilewski concluded that the yield point for a special martensite variant transforming to a transient austenite phase that shifts to a martensite variant simultaneously is lower than others's yield point in a different stress circumstance. Protracting the above issue to a test temperature range between A_f and M_f , where the transformed austenite is no longer a transient phase but stable, (Wasilewski, 1971 d) deduces a similar phenomenon with that from the present model mentioned above (Delaey, et al., 1974).

Further, since the transformation $M_- \to A$ occurs only in the darker zone R_2 of Figure 17 for $\tau > 0$, one concludes that the lowest temperature and the largest stress for conducting process $M_- \to A$ in $\tau > 0$ are T_{fs} and τ_f respectively at points c and d. Regarding the detwinning process in Ω_2^+ , the highest temperature and lowest stress for conducting detwinning process $M_- \to M_+$ in $\tau > 0$ are T_{ff} and τ_s respectively at points d and c. The two processes $M_- \to A$ and $A \to M_+$ may occur simultaneously inside the zone abcd (which is part of R_2 in Figure 17). Another interesting character is that three processes $M_- \to A$, $A \to M_+$ and $M_- \to M_+$ can be triggered in a same temperature level between T_{ff} and T_{fs} upon loading. First, process $A \to M_+$ proceeds in a small stress range. Second, processes $M_- \to A$ and $A \to M_+$ take place together once the stress increases past the terminal nuetrality curve A_s . The third, detwinning $M_- \to M_+$ occurs once the stress further increases beyond the terminal nuetrality curve M_{f+} . Those are illustrated in Figure 17. Similar results are obtained for $M_+ \to A$ and $M_+ \to M_-$ in $\tau < 0$.

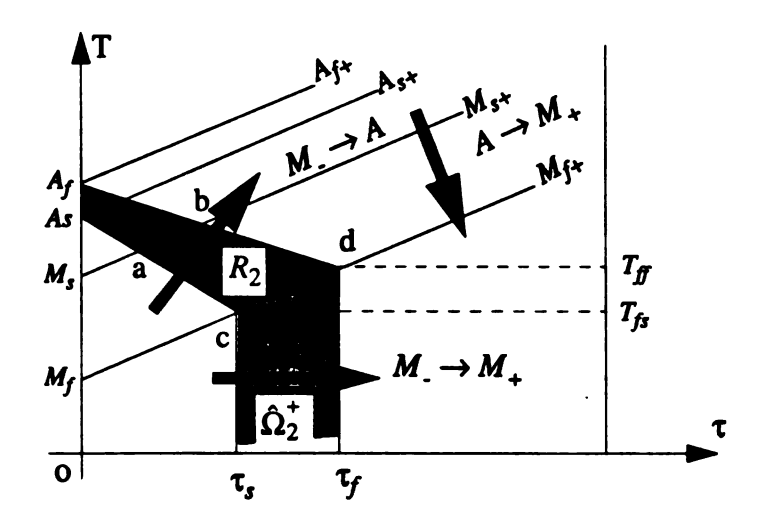


Figure 17. For $\tau > 0$, the lowest temperature and largest stress for conducting $M_{-} \to A$ are T_{fs} and τ_{f} , and the highest temperature for conducting $M_{-} \to M_{+}$ is T_{ff} .

3 TRANSITION TYPES FOR THE PHASE FRACTION EVOLUTION

In chapter 2, phase diagrams were discussed based on certain thermodynamic considerations, which gave rise to different phase transition zones. As shown in figures Figure 14 and Figure 15 for isothermal loading, various double transformations can occur in the region Ω_1^+ corresponding to the unfolded triple point of Figure 1. In this section we are going to investigate different single and double transformation possibilities in the different transition zones, as well as the corresponding criteria for determining the associated transformation possibilities, which will be organized into *transition types* in the following study.

3.1 Transition Types

In general, when temperature and stress trigger the phase transformations in the fine mixture of the three species, austenite and martensite two variants, both of the two transformation processes $A \leftrightarrow M_+$ and $A \leftrightarrow M_-$ might occur simultaneously in Ω_1 . Therefore, at each instant of time, it is assumed that there is either a net transformation from $A \to M_+$ or else a net transformation from $M_+ \to A$. Concurrently, it is assumed at each instant of time that there is either a net transformation from $A \to M_-$ or else a net transformation from $M_- \to A$. Taken together, in Ω_1 , they give the following four combination transition

types:

(TT1):
$$M_{\perp} \rightarrow A, M_{\perp} \rightarrow A;$$

(TT2):
$$A \rightarrow M_{+}, A \rightarrow M_{-}$$
;

(TT3):
$$M_{\perp} \rightarrow A, A \rightarrow M_{\perp}$$
;

(TT4):
$$M_1 \rightarrow A, A \rightarrow M_1$$
.

For relatively high temperatures, transition type (TT1) is that which occurs under pure temperature increase; transition type (TT2) is that which occurs for pure temperature decrease. Transition types (TT3) and (TT4) are those which occur for pure stress decrease and increase respectively. With these four transition types, pseudoelastic behavior can be simulated when the temperature is relatively high (in Ω_1) (see Pence *et al.*, 1995). For combined changes in temperature and stress (processes that are not pure), the particular transition type will depend on the local orientation of the state path in the stress-temperature plane. On the other hand, to complete the model when the temperature is relatively low (below M_{f+} and M_{f-}), the detwinning process $M_+ \leftrightarrow M_-$ must also be accounted for. Recall the discussion in section 2.2 to 2.4, this detwinning process is modified by $M_- \to A \Rightarrow M_+$ and $M_+ \to A \Rightarrow M_-$ in terms of Wasilewski's instability transformations when one formally continues $A \leftrightarrow M_-$ and $A \leftrightarrow M_+$ transformations in the zones where austenite is unstable. Therefore, for X-unfolding in Ω_2^+ , we have transition type

(TT5):
$$M_{\cdot} \rightarrow M_{+}$$
,

and in Ω_2 we have transition type

(TT6):
$$M_{\perp} \rightarrow M_{\perp}$$
.

For the Y-unfolding and the pY-unfolding, the only modification to this X-unfolding description is that transition types (TT5) and (TT6) operate in $\hat{\Omega}_2^+$ and $\hat{\Omega}_2^-$ respectively.

3.2 Criteria for Determining Transition Type

As mentioned above, phase transformation and detwinning are triggered by changes in temperature T and stress τ as the state path is executed in the (τ, T) -plane. The particular transition type that is operating may change at distinct points (τ, T) on the state path. These points occur when the state path is instantaneously aligned with one of the two nuetrality curves that pass though the point. In other words, several transition types may occur successively along a given state path. In Ω_1 , if the local orientation of the state path crosses the A/M_+ nuetrality curves so as to make $d\beta^+ > 0$, then transition $M_+ \to A$ occurs. Conversely if path orientation with respect to the A/M_- nuetrality curves give $d\beta^- \ge 0$, then transition $M_- \to A$ takes place. Thus, the signs of $d\beta^+$ and $d\beta^-$ can be used to determine the operative transition type.

Recall the discussions in the above, there are totally six transition types introduced in the two variant problems. These transition types hold regionally, i.e., transition types (TT1) to (TT4) apply in Ω_1 , and transition types (TT5) and (TT6) hold away from Ω_1 . Thus, the criteria for the different transition types are going to be treated separately in the two regions. In these treatments, it is convenient to introduce the following notations:

$$\beta_T^+ = \frac{\partial \beta^+}{\partial T}, \quad \beta_T^- = \frac{\partial \beta^-}{\partial T}, \quad \beta_\tau^+ = \frac{\partial \beta^+}{\partial \tau}, \quad \beta_\tau^- = \frac{\partial \beta^-}{\partial \tau}.$$
 (3.2.0.1)

3.2.1 Algebraic Description

The criteria for distinguishing between the four transition types are shown as the following based on the nuetrality curves,

(TT1) if
$$d\beta^+ > 0$$
 and $d\beta^- > 0$, (3.2.1.1)

(TT2) if
$$d\beta^+ < 0$$
 and $d\beta^- < 0$, (3.2.1.2)

(TT3) if
$$d\beta^+ > 0$$
 and $d\beta^- < 0$, (3.2.1.3)

(TT4) if
$$d\beta^+ < 0$$
 and $d\beta^- > 0$. (3.2.1.4)

To see more clearly the above conditions, they can be expressed by means of the tangent of the given state path curve. From simple derivations on (3.2.1.1) and (3.2.1.2), we have that the following transition types occur:

(TT1) if
$$\begin{cases} \frac{dT}{d\tau} > max \left\{ -\frac{\beta_{\tau}^{+}}{\beta_{T}^{+}}, -\frac{\beta_{\tau}^{-}}{\beta_{T}^{-}} \right\} & \forall d\tau > 0 \\ \frac{dT}{d\tau} < min \left\{ -\frac{\beta_{\tau}^{+}}{\beta_{T}^{+}}, -\frac{\beta_{\tau}^{-}}{\beta_{T}^{-}} \right\} & \forall d\tau < 0 \end{cases}$$
 (3.2.1.5)

(TT2) if
$$\begin{cases} \frac{dT}{d\tau} < min\left\{-\frac{\beta_{\tau}^{+}}{\beta_{T}^{+}}, -\frac{\beta_{\tau}^{-}}{\beta_{T}^{-}}\right\} & \forall d\tau > 0\\ \\ \frac{dT}{d\tau} > max\left\{-\frac{\beta_{\tau}^{+}}{\beta_{T}^{+}}, -\frac{\beta_{\tau}^{-}}{\beta_{T}^{-}}\right\} & \forall d\tau < 0 \end{cases}$$
(3.2.1.6)

(TT3) if
$$\begin{cases} -\frac{\beta_{\tau}^{+}}{\beta_{T}^{+}} < \frac{dT}{d\tau} < -\frac{\beta_{\tau}^{-}}{\beta_{T}^{-}} & \forall d\tau > 0 \\ -\frac{\beta_{\tau}^{-}}{\beta_{T}^{-}} < \frac{dT}{d\tau} < -\frac{\beta_{\tau}^{+}}{\beta_{T}^{+}} & \forall d\tau < 0 \end{cases}$$
 (3.2.1.7)

(TT4) if
$$\begin{cases} -\frac{\beta_{\tau}^{-}}{\beta_{T}^{-}} < \frac{dT}{d\tau} < -\frac{\beta_{\tau}^{+}}{\beta_{T}^{+}} & \forall d\tau > 0 \\ -\frac{\beta_{\tau}^{+}}{\beta_{T}^{+}} < \frac{dT}{d\tau} < -\frac{\beta_{\tau}^{-}}{\beta_{T}^{-}} & \forall d\tau < 0 \end{cases}$$
(3.2.1.8)

Note:

- (1) If any one of $d\tau$, β_T^+ and β_T^- is equal to zero, then we can check the condition directly from (3.2.1.1) to (3.2.1.4).
- (2) Based on the definitions of $\beta^+(\tau, T)$ and $\beta^-(\tau, T)$ given in (2.2.2.5) and (2.2.2.6) for the X-unfolding, it follows that β_T^+ and β_T^- are positive in the whole plane; however, based on (2.4.2.13) and (2.4.2.14) for Y-unfolding, it follows that β_T^+ and β_T^- are positive in Ω_1 and zero below M_f and M_{f+} respectively.
- (3) In either expression (3.2.1.7) or (3.2.1.8), there is only one criterion that is true because they are mutually exclusive.

3.2.2 Geometric Illustration

To interpret the meanings of those criteria in Ω_1 , let us consider the nuetrality curves defined by (2.3.2.3) and (2.3.2.4) with equality of moduli of austenite and martensite in either the X-unfolding or pY-unfolding. At a point, say p in Ω_1 , of a given path in (τ, T) -plane, the four criteria (3.2.1.5) to (3.2.1.8) define four *open cone zones*: N, S, W and E, which indicate the zones of North, South, West and East. They are formed by the two particular nuetrality curves passing through point p (Figure 18). If the forward direction of the path at point p enters into the open cone zone N in next time increment, then transition

type (TT1) is in progress, and so on.

In this particular equal moduli example, the nuetrality curve slopes do not change with point p so that the four open cone angles remain fixed in Ω_1 . More generally, the cone angles depend upon temperature and stress according to the general forms of $\beta^+(\tau, T)$ and $\beta^-(\tau, T)$ in (2.3.2.3) and (2.3.2.4) involving μ_A and μ_M . For the Y-unfolding, the four open cone areas also loose symmetry in the north-south and west-east directions, because the nuetrality curves for $A \leftrightarrow M_-$ in $\tau > 0$ and for $A \leftrightarrow M_+$ in $\tau < 0$ are modified by the detwinning flow and finish stresses.

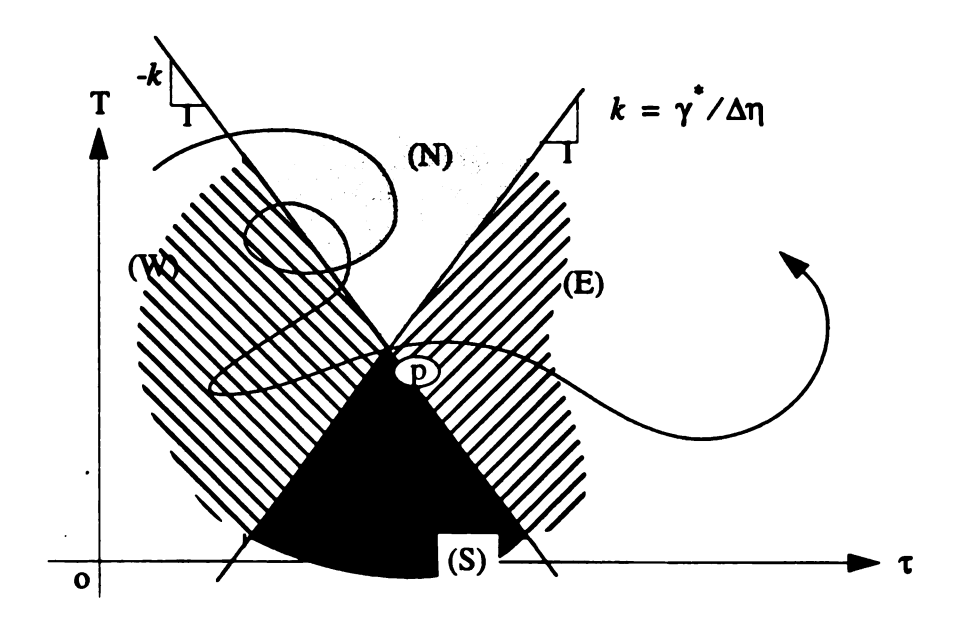


Figure 18. Four open cone areas at a point p in Ω_1 for X- and Y-unfolding show the transition possibilities when a path passes through this point. If the path passing through p proceeds into N (S, W and E), then transition type (TT1) ((TT2), (TT3) and (TT4)) is in progress.

3.3 Criteria for Detwinning Transition Types

Recall the considerations in section 3.1, (TT5) comes from $M_{\perp} \to A$ and is active in Ω_2^+ while (TT6) comes from $M_{\perp} \to A$ and is active in Ω_2^- for X-unfolding. Thus, criteria for (TT5) and (TT6) could be expressed as

(TT5) if
$$d\beta > 0$$
 in Ω_2^+ , (3.3.0.1)

(TT6) if
$$d\beta^+ > 0$$
 in Ω_2^- , (3.3.0.2)

respectively. Furthermore (3.3.0.1) and (3.3.0.2) give

(TT5) if
$$\frac{dT}{d\tau} > \frac{\beta_{\tau}}{\beta_{T}}$$
 $\forall d\tau > 0 \text{ in } \Omega_{2}^{+}$, (3.3.0.3)

(TT6) if
$$\frac{dT}{d\tau} < \frac{\beta_{\tau}^{+}}{\beta_{\tau}^{+}}$$
 $\forall d\tau < 0 \text{ in } \Omega_{2}^{-}$. (3.3.0.4)

One should note in condition (3.3.0.3) that the case $d\tau < 0$ is ignored. Similarly, in (3.3.0.4) the case for $d\tau > 0$ is ignored. The reason is that both (TT5) and (TT6), associated with detwinning, are modified by transition directions $M_- \to A$ amd $M_+ \to A$, which correspond to increasing stress and decreasing stress processes respectively. Therefore, the direction of stress increasing/decreasing should coincide with that of the detwining direction. The other important point that one should note is that criteria (3.3.0.3) and (3.3.0.4) apply only to the X-unfolding. For the pY- and Y-unfoldings, because β_T^+ and β_T^- are equal to zero, one can directly use $\beta_\tau^+ \cdot d\tau \ge 0$ to check (TT5) in Ω_2^+ and $\beta_\tau^+ \cdot d\tau \ge 0$ to check (TT6) in Ω_2^+ . This gives

(TT5)
$$\beta_{\tau} > 0 \quad \forall d\tau > 0 \text{ in } \hat{\Omega}_{2}^{+},$$
 (3.3.0.5)

(TT6)
$$\beta_{\tau}^+ < 0 \qquad \forall \ d\tau < 0 \text{ in } \hat{\Omega}_2^-.$$
 (3.3.0.6)

In the Y-unfolding, all of the nuetrality curves in $\hat{\Omega}_2^+$ and $\hat{\Omega}_2^-$ become perpendicular to the τ -axis. Hence temperature changes at constant stress does not cause detwinning. This contrasts with the X-unfolding, where temperature increase at constant stress causes detwining processes to occur in Ω_2^- and Ω_2^+ .

3.4 Example

Assume that $\beta^+(\tau, T)$ and $\beta^-(\tau, T)$ are given as (2.3.2.3) and (2.3.2.4) with equality of moduli of austenite and martensite for pY-unfolding. Here k_1 (>0) is given (2.4.2.2). If the state-path is an ellipse in the (τ, T) -plane in Figure 19, we can then determine the transition types on the different parts of the ellipse state-path as follows.

With (3.2.0.1), we find $-\beta_{\tau}^{+}/\beta_{T}^{+} = k_{1}$, $-\beta_{\tau}^{-}/\beta_{T}^{-} = -k_{1}$ in Ω_{1} , and $\beta_{T}^{+} = 0$, $\beta_{T}^{-} = 0$ $\beta_{\tau}^{+} = -2k_{1}$ and $\beta_{\tau}^{-} = 2k_{1}$ in Ω_{2}^{-} and Ω_{2}^{+} . t1, t2, t3 and t4 indicate the tangent points where the path is tangent to the nuetrality lines respectively. Based on (3.2.1.5) to (3.2.1.8) and the discussions on (TT5) and (TT6) for pY-unfolding, it follows that: from point t2 to t3 the transition type (TT3) occurs in Ω_{1} ; from t3 to e the transition type (TT2) occurs in Ω_{1} ; in Ω_{2}^{-} , \hat{S}_{M} , \hat{S}_{M-} and \hat{S}_{M+} there is no phase transformation; from point b to c the transition type (TT5) occurs in Ω_{2}^{+} .

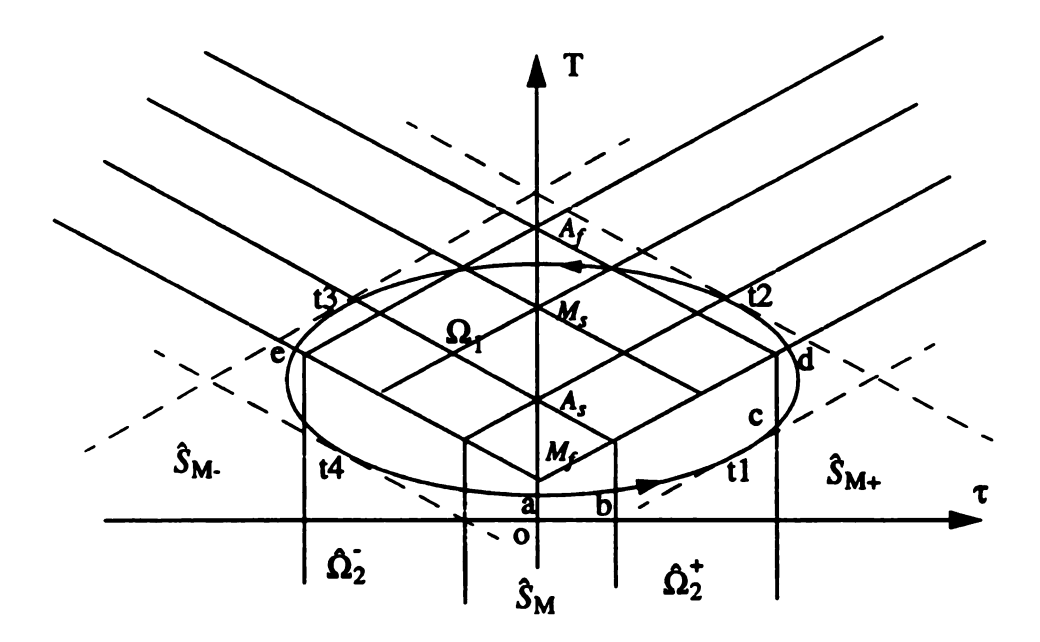


Figure 19. This graph shows that how the transition types occur when one follows a counterclock wise ellipse in the (τ, T) -plane. From point t2 to t3: (TT3) occurs; from t3 to e: (TT2) occurs; from point b to c: (TT5) occurs; in all other parts there is no transformation.

4 THE HYSTERESIS ALGORITHMS

This chapter will extend the hysteresis algorithm of the one-variant martensite case given in the work by Ivshin and Pence (1994 b) to a two-variant martensite case on the basis of the two-variant analysis (Pence et al., 1994). For this reason it is useful to briefly summarize the one-variant model (Ivshin and Pence, 1994 b). The extending work begins from the analysis of the envelope functions and the algorithms presented in (Pence et al., 1994). If only one transition is active then the extension of the algorithm can be expressed by different equivalent forms. However if two transitions are active, then these different forms are no longer equivalent. Thus an examination on combinations of various transition directions from different transformation processes becomes necessary for determining the proper extension of the one-variant model into the two-variant regime.

4.1 Brief Review of the Previous One-variant study

4.1.1 One Variant Algorithm

The one-variant model studied in the work (Ivshin and Pence 1994 b) involves transition between a high-temperature/low-stress austenite phase A-and a low temperature/high-stress martensite phase M. In the present three species model, this is as if two martensite variants are treated together as one martensite species ($\xi_M = \xi_+ + \xi_-$) and only $A \leftrightarrow M$

takes place on each state path. At any instant, either there is a net transformation tendency for $A \to M$ (so that $\dot{\xi}_A \le 0$) or else a net transformation tendency for $M \to A$ (so that $\dot{\xi}_A \ge 0$). Note that the nuetral tendency $\dot{\xi}_A = 0$ can be regarded as either a trivial $A \to M$ tendency or else a trivial $M \to A$ tendency. Thus the state path $(\tau(t), T(t))$ is partitioned into segments on which either the $A \to M$ or the $M \to A$ transformation tendency occurs. If this partitioning is known, the transformation is governed by the following equations (see equations (30) and (32) of the work by Ivshin and Pence (1994 b):

$$\frac{d\xi_M}{dt} = -\frac{\xi_A}{\alpha_{A \to M}(\tau, T)} \cdot \frac{d}{dt} \alpha_{A \to M}(\tau, T) \text{ for } A \to M, \qquad (4.1.1.1)$$

$$\frac{d\xi_M}{dt} = -\frac{\xi_M}{1 - \alpha_{M \to A}(\tau, T)} \cdot \frac{d}{dt} \alpha_{M \to A}(\tau, T) \text{ for } M \to A. \tag{4.1.1.2}$$

Here $\xi_A = 1 - \xi_M$ is phase fractions of austenite, $\alpha_{A \to M}(\tau, T)$ and $\alpha_{M \to A}(\tau, T)$ are constitutive functions; they were given the respective symbols $\alpha_{max}(\tau, T)$ and $\alpha_{min}(\tau, T)$ in (Ivshin and Pence, 1994 b), but the symbols used in (4.1.1.1) and (4.1.1.2) will be more convenient for the present discussion. The equations (4.1.1.1) and (4.1.1.2) ensure that the transformation proceeds at a pace that is proportional to the phase that is transforming (A in (4.1.1.1) and M in (4.1.1.2)) and is independent of the phase that is experiencing a net increase. In the event that the $A \to M$ transformation begins from pure austenite $(\xi_A = 1)$, then the transformation governed by (4.1.1.1) gives an $\xi_A(t)$ that coincides with $\alpha_{A \to M}(\tau(t), T(t))$. Similarly $\xi_A(t) = \alpha_{M \to A}(\tau(t), T(t))$ for $M \to A$ transformations that start with pure martensite $\xi_A = 0$.

4.1.2 Envelope Function

As discussed in the approach by Ivshin and Pence, (1994 b), equations (4.1.1.1) and (4.1.1.2) give immediate integrals. There are however practical advantages to operate with the differential equations (4.1.1.1) and (4.1.1.2). The constitutive functions are required to obey $\alpha_{A \to M}(\tau, T) \ge \alpha_{M \to A}(\tau, T)$. Both $A \to M$ transformations that start at some initial time t_o with $\xi_A \le \alpha_{A \to M}(\tau(t_o), T(t_o)) \le 1$, and $M \to A$ transformations that start with $\xi_A \ge \alpha_{M \to A}(\tau(t_o), T(t_o)) \ge 0$, are required to generate phase fraction trajectories $\xi_A(t)$ obeying $\alpha_{M \to A}(\tau(t), T(t)) \le \xi_A(t) \le \alpha_{A \to M}(\tau(t), T(t))$. In fact, as shown in (Ivshin and Pence, 1994 b), the above containment requirement are not ensured by (4.1.1.1) and (4.1.1.2) alone, but are guaranteed if the constitutive functions $\alpha_{A \to M}$ and $\alpha_{M \to A}$ obey certain additional containment restrictions. This justifies the terminology envelope functions for $\alpha_{A \to M}$ and $\alpha_{M \to A}$. The special situation involving equality of the envelope functions ensures that $\xi_A(t)$ coincides with the new single "envelope function" so that $\xi_A(t)$ is a state function of (τ, T) ; hysteresis is not present in this special situation $(A_s =$ M_f , $M_s = A_f$). Envelope functions that are step functions between 0 and 1 give abrupt transformations at the locus (τ, T) where the step takes place $(A_s = A_f, M_s = M_f)$. Thus, in combination, identical envelope functions that involve only a step between 0 and 1 on some (τ, T) curve gives the standard notion of abrupt nonhysteretic phase transitions $(M_f = M_s =$ $A_s = A_f$). However, unequal envelope functions that smoothly vary between 0 and 1 generate the hysteretic mixtures which were the focus of the work by Ivshin and Pence (1994 b). Finally it is to be pointed out that the issue of determining whether an $A \rightarrow M$ or an $M \rightarrow A$ transformation tendency operates is resolved by requiring algorithmic consistency in (4.1.1.1) and (4.1.1.2). Namely at each instant of time (4.1.1.1) and (4.1.1.2) should both give that either $\dot{\xi}_A < 0$ or $\dot{\xi}_A > 0$. In the former event then ξ_A (or ξ_M) is to be determined from (4.1.1.1) and in the latter event then ξ_A (or ξ_M) is to be determined from (4.1.1.2). As shown in (Ivshin and Pence, 1994 b), this requires that $\alpha_{A \to M}(\tau, T)$ and $\alpha_{M \to A}(\tau, T)$ display dependence on (τ, T) by means of a characteristic function $\beta(\tau, T)$ in the following fashion:

$$\alpha_{A \to M}(\tau, T) = \hat{\alpha}_{max}(\beta(\tau, T)) \text{ and } \alpha_{M \to A}(\tau, T) = \hat{\alpha}_{min}(\beta(\tau, T)).$$
 (4.1.2.1)

Therefore characteristic functions that describe nuetrality arise naturally in models of the type presently under study. If the state path $(\tau(t), T(t))$ ever coincides with the curves $\beta(\tau, T) = C$ (constant), then $\xi_A(t)$ is constant as long as the coincidence is maintained. Here it is to be emphasized that $\hat{\alpha}_{max}$ and $\hat{\alpha}_{min}$ are functions of a single argument which can be determined by experimental measurements at free-stress circumstance. Thus they obey

$$0 \le \hat{\alpha}_{min}(\beta) \le \hat{\alpha}_{max}(\beta) \le 1$$

$$\hat{\alpha}_{min}(\beta) = \begin{cases} 1 & \text{if } \beta \ge A_f \\ 0 & \text{if } \beta \le A_s \end{cases}$$

$$\hat{\alpha}_{max}(\beta) = \begin{cases} 1 & \text{if } \beta \ge M_s \\ 0 & \text{if } \beta \le M_f \end{cases}$$

$$(4.1.2.2)$$

$$\hat{\alpha}'_{max}(\beta) \geq 0$$

 $\hat{\alpha}'_{min}(\beta) \geq 0$

Additional conditions on $\hat{\alpha}_{min}(\beta)$ and $\hat{\alpha}_{max}(\beta)$ which ensure trajectory containment

and trajectory orientation requirements can be found in the work by Ivshin and Pence (1994 a). Normalization $\beta(0, T) = T$ gives

$$\alpha_{A \to M}(0, T) = \hat{\alpha}_{max}(T) \text{ and } \alpha_{M \to A}(0, T) = \hat{\alpha}_{min}(T).$$
 (4.1.2.3)

4.2 Two Variant Constitutive Functions

To develop the two variant model on the basis of one variant model by Ivshin and Pence (1994 b), there are two things important to be considered, one of them is the extension of the constitutive functions while the other is the extension of the algorithms for phase fraction evolution during transformation.

4.2.1 Constitutive Function Extension

In the high temperature two variant study (Pence, et. al., 1994), $\alpha_{A+}(\tau, T)$ and $\alpha_{+A}(\tau, T)$ are used as constitutive functions to describe $A \to M_+$ and $M_+ \to A$ phase transformations, respectively; while $\alpha_{A-}(\tau, T)$ and $\alpha_{-A}(\tau, T)$ are used to as constitutive functions to describe $A \to M_-$ and $M_- \to A$ phase transformations respectively. When the A/M_+ neutrality curves are parametrized by the nuetrality function $\beta^+(\tau, T)$ introduced in (2.4.2.14) for the Y-unfolding, then the $A \leftrightarrow M_+$ constitutive functions are of the form:

$$\alpha_{A+}(\tau, T) \equiv \alpha_{A \to M}(\tau, T) = \hat{\alpha}_{max}(\beta^{+}(\tau, T)), \qquad (4.2.1.1)$$

$$\alpha_{+A}(\tau, T) \equiv \alpha_{M_{-} \to A}(\tau, T) = \hat{\alpha}_{min}(\beta^{+}(\tau, T)), \qquad (4.2.1.2)$$

for constitutive functions $\hat{\alpha}_{max}(x)$, $\hat{\alpha}_{min}(x)$ of a single variable. More than this, since

detwinning process $M_+ \to M_-$ is considered, $\alpha_{+A}(\tau, T)$ is also the $M_+ \to M_-$ constitutive function below M_f . Based on the symmetry of the two martensite variants, when the A/M_- nuetrality curves are parametrized by the nuetrality function $\beta^-(\tau, T)$ introduced in (2.4.2.13) for the Y-unfolding. The constitutive functions for $A \leftrightarrow M_-$ are defined as

$$\alpha_{A}(\tau, T) \equiv \alpha_{A \to M}(\tau, T) = \hat{\alpha}_{max}(\beta(\tau, T)), \tag{4.2.1.3}$$

$$\alpha_{-A}(\tau, T) \equiv \alpha_{M \rightarrow A}(\tau, T) = \hat{\alpha}_{min}(\beta^{\dagger}(\tau, T)). \tag{4.2.1.4}$$

Similarly, $\alpha_{-A}(\tau, T)$ is also the $M_{-} \to M_{+}$ constitutive function below M_{f+} . Under normalization $\beta^{+}(0, T) = \beta^{-}(0, T) = T$, we have the following relations,

$$\alpha_{AA}(0, T) \equiv \alpha_{AB}(0, T) = \hat{\alpha}_{max}(T) \text{ and } \alpha_{AA}(0, T) \equiv \alpha_{AA}(0, T) = \hat{\alpha}_{min}(T).$$
 (4.2.1.5)

The relations corresponding to (4.1.2.2) in the two variant case are

$$0 \le \alpha_{A}(\tau, T) \le \alpha_{A}(\tau, T) \le 1, \quad 0 \le \alpha_{A}(\tau, T) \le \alpha_{A}(\tau, T) \le 1$$

$$\alpha_{-\mathbf{A}}(\tau, T) = \begin{cases} 1 & \text{if } \beta^{-} \geq A_{f} \\ & , & \alpha_{\mathbf{A}}(\tau, T) = \begin{cases} 1 & \text{if } \beta^{-} \geq M_{s} \\ 0 & \text{if } \beta^{-} \leq A_{s} \end{cases}$$

$$0 & \text{if } \beta^{-} \leq M_{f} . \quad (4.2.1.6)$$

$$\alpha_{+A}(\tau, T) = \begin{cases} 1 & \text{if } \beta^+ \ge A_f \\ & , & \alpha_{A+}(\tau, T) = \begin{cases} 1 & \text{if } \beta^+ \ge M_s \\ 0 & \text{if } \beta^+ \le A_s \end{cases}$$

4.2.2 Possible Extension of the Algorithm to the Two Variant Problem

After the analysis about the characteristics and constitutive functions, it is necessary to introduce a calculation system into the two variant model, which is a group of algorithms to determine the phase fractions associated with different transition directions in two variant problems.

For purposes of developing the appropriate extensions of the algorithms, the discussion is initially confined to phase transformations $A \leftrightarrow M_{+}$ and $A \leftrightarrow M_{-}$ without the detwinning. Since $\hat{\alpha}_{max}(x)$ can be interpreted as the maximum value of austenite phase fraction during phase transformations from 100% austenite to overall martensite, and, $\beta^+(\tau, T)$ and $\beta^-(\tau, T)$ parametrize the phase transformation families of $A \leftrightarrow M_+$ and $A \leftrightarrow M$ respectively, constitutive functions $\alpha_{A+}(\tau, T)$ and $\alpha_{A-}(\tau, T)$ would be deciphered as state functions of austenite narrating phase transformations from 100% austenite to individual martensite variants respectively. In a similar fashion, since $\hat{\alpha}_{min}(x)$ is the minimum value of austenite phase fraction during phase transformations from 100% overall martensite to austenite, constitutive functions $\alpha_{+A}(\tau, T)$ and $\alpha_{-A}(\tau, T)$ indicate state functions of austenite phase fraction describing the transformation from 100% individual martensite variant to austenite. Before extending the one variant algorithms (4.1.1.1) and (4.1.1.2), we consider in what follows the observation that each of (4.1.1.1) and (4.1.1.2)can be rewritten in three extra forms with ξ_{A} and ξ_{M} . These four equations are equivalent for either $A \to M$ or $M \to A$ in the one variant case, but extensions to the two-variant case are sensitive to the form of the one-variant equations that are used before the extension.

To get insight into this problem, note since $\xi_A + \xi_M = 1$, that all of the following

forms are equivalent to (4.1.1.1) for governing an $A \rightarrow M$ transition direction:

$$\frac{d\xi_A}{dt} = \frac{\xi_A}{\alpha_{A \to M}(\tau, T)} \cdot \frac{d}{dt} \alpha_{A \to M}(\tau, T), \qquad (4.1.1.1)a$$

$$\frac{d\xi_M}{dt} = -\frac{1 - \xi_M}{\alpha_{A \to M}(\tau, T)} \cdot \frac{d}{dt} \alpha_{A \to M}(\tau, T), \qquad (4.1.1.1)b$$

$$\frac{d\xi_A}{dt} = \frac{1 - \xi_M}{\alpha_{A \to M}(\tau, T)} \cdot \frac{d}{dt} \alpha_{A \to M}(\tau, T). \tag{4.1.1.1}c$$

A similar four way equivalence holds for (4.1.1.2) with respect to $M \rightarrow A$ transition direction. The extra three are expressed as

$$\frac{d\xi_A}{dt} = \frac{\xi_M}{1 - \alpha_{M \to A}(\tau, T)} \cdot \frac{d}{dt} \alpha_{M \to A}(\tau, T), \qquad (4.1.1.2)a$$

$$\frac{d\xi_M}{dt} = -\frac{1 - \xi_A}{1 - \alpha_{M \to A}(\tau, T)} \cdot \frac{d}{dt} \alpha_{M \to A}(\tau, T), \qquad (4.1.1.2)b$$

$$\frac{d\xi_A}{dt} = \frac{1 - \xi_A}{1 - \alpha_{M \to A}(\tau, T)} \cdot \frac{d}{dt} \alpha_{M \to A}(\tau, T). \tag{4.1.1.2}$$

When multiple martensite species (only two in this study) are present, this kind of equivalence no longer holds. For example, suppose that an $A \to M_+$ transformation occurs in concert with either an $A \to M_-$ transformation (TT2) or an $M_- \to A$ transformation (TT4). Then $\xi_- + \xi_A + \xi_+ = 1$ and the $A \to M_+$ transition might arguably be governed by any one of the four possibilities (see (4.1.1.1)):

$$\frac{d\xi_{+}}{dt} = -\frac{\xi_{A}}{\alpha_{A+}(\tau, T)} \cdot \frac{d}{dt} \alpha_{A+}(\tau, T), \qquad (4.2.2.1)$$

$$\frac{d\xi_A}{dt} = \frac{\xi_A}{\alpha_{A+}(\tau, T)} \cdot \frac{d}{dt} \alpha_{A+}(\tau, T), \qquad (4.2.2.1)a$$

$$\frac{d\xi_{+}}{dt} = -\frac{1 - \xi_{+}}{\alpha_{A+}(\tau, T)} \cdot \frac{d}{dt} \alpha_{A+}(\tau, T), \qquad (4.2.2.1)b$$

$$\frac{d\xi_A}{dt} = \frac{1 - \xi_+}{\alpha_{A+}(\tau, T)} \cdot \frac{d}{dt} \alpha_{A+}(\tau, T). \tag{4.2.2.1}$$

Since in the two variant approach, coefficient $1-\xi_+$ no longer indicates ξ_A in process $A \to M_+$, the last two equations (4.2.2.1)b and (4.2.2.1)c in the set of (4.2.2.1) are not consistent with the viewpoint that this coefficient should give the phase fraction of the precursor phase and so will not be considered in the further study.

In a similar fashion, an $A \rightarrow M_{\perp}$ transition in (TT2) and (TT3) might similarly be governed by any one of four equations, only two of which are reasonable,

$$\frac{d\xi_{-}}{dt} = -\frac{\xi_{A}}{\alpha_{A}(\tau, T)} \cdot \frac{d}{dt} \alpha_{A}(\tau, T), \qquad (4.2.2.2)$$

$$\frac{d\xi_A}{dt} = \frac{\xi_A}{\alpha_A(\tau, T)} \cdot \frac{d}{dt} \alpha_{A}(\tau, T). \tag{4.2.2.2}$$

The martensite to austenite transformation admit to similar interpretation. For transition direction $M_+ \to A$ the possible algorithms for use in (TT1) and (TT3) are (see (4.1.1.2)):

$$\frac{d\xi_{+}}{dt} = -\frac{\xi_{+}}{1 - \alpha_{+A}(\tau, T)} \cdot \frac{d}{dt} \alpha_{+A}(\tau, T), \qquad (4.2.2.3)$$

$$\frac{d\xi_A}{dt} = \frac{\xi_+}{1 - \alpha_{+A}(\tau, T)} \cdot \frac{d}{dt} \alpha_{+A}(\tau, T) , \qquad (4.2.2.3)a$$

$$\frac{d\xi_{+}}{dt} = -\frac{1 - \xi_{A}}{1 - \alpha_{+A}(\tau, T)} \cdot \frac{d}{dt} \alpha_{+A}(\tau, T), \qquad (4.2.2.3)b$$

$$\frac{d\xi_A}{dt} = \frac{1 - \xi_A}{1 - \alpha_{+A}(\tau, T)} \cdot \frac{d}{dt} \alpha_{+A}(\tau, T) . \qquad (4.2.2.3)c$$

Coefficient $1-\xi_A$ in equations (4.2.2.3))b and (4.2.2.3)c no longer indicates ξ_+ in process $M_+ \to A$, so that these two expressions will be eliminated since it is again not consistent with a coefficient factor that is proportional to the precursor phase.

Following the same manner as the above gives two remaining candidate algorithms for transition direction $M_{\perp} \rightarrow A$:

$$\frac{d\xi_{-}}{dt} = -\frac{\xi_{-}}{1 - \alpha_{-A}(\tau, T)} \cdot \frac{d}{dt} \alpha_{-A}(\tau, T) , \qquad (4.2.2.4)$$

$$\frac{d\xi_A}{dt} = \frac{\xi_-}{1 - \alpha_{-A}(\tau, T)} \cdot \frac{d}{dt} \alpha_{-A}(\tau, T) . \qquad (4.2.2.4)a$$

The elimination of the "b" and "c" governing equation possibilities for each single process indicates for each two process transition type: (TT1) to (TT4) in Ω_1 , there now remain four combination possibilities. For example, the combined $A \to M_+$, $A \to M_-$ process of transition type (TT2), might possibly be governed by either (4.2.2.1) or (4.2.2.1)a in conjunction with either (4.2.2.2) or (4.2.2.2)a. In addition there are still two possibilities for each detwinning transition in $\hat{\Omega}_2^+$ and $\hat{\Omega}_2^-$. Here it is interesting to note that the less complete model employed in the work by Pence *et al.* (1994) only allowed for transition

type (TT1) and (TT2) in the notation employed here. There, of the four combination possibilities for (TT2), the particular combination $\{(4.2.2.1), (4.2.2.2)\}$ was employed for $A \rightarrow M_+$, $A \rightarrow M_-$. Similarly, the particular combination $\{(4.2.2.3), (4.2.2.4)\}$ was employed for $M_+ \rightarrow A$, $M_- \rightarrow A$ (transition type (TT1)). We now inquire into the proper combination possibilities, and in this process arrive at those used in (Pence *et al.*, 1994) for (TT1) and (TT2).

4.3 Analysis on the Algorithm Associated with Transition Types

4.3.1 Unique Algorithm

Discussions in section 4.2.2 lead us to the observation that there remain four possible algorithms for each two process transition type in Ω_1 (TT1 to TT4) and two for each detwinning transition in $\hat{\Omega}_2^+$ and $\hat{\Omega}_2^-$. From many reasonable solicitudes, such as symmetry, basic assumptions on phase transformation, etc., most of them can be excluded as we are going to see next. Here we give two separate lines of argument. The first is based on symmetry and mathematical well-posedness. The second is based on an assumption regarding the transformation process.

The first argument begins with a symmetry consideration between M_{+} and M_{-} in the pair combination governing (TT1) and (TT2). This immediately reduces the pair combination in the following way:

(TT1):
$$\{(4.2.2.3), (4.2.2.4)\}$$
 or $\{(4.2.2.3)a, (4.2.2.4)a\}$.

(TT2):
$$\{(4.2.2.1), (4.2.2.2)\}$$
 or $\{(4.2.2.1)a, (4.2.2.2)a\}$.

The other two transition types (TT3) and (TT4) lose $M_{\downarrow}/M_{\downarrow}$ symmetry and so do not neces-

sarily allow for such reductions. Returning now to transition types (TT1) and (TT2), we note for (TT2) that the pair combination $\{(4.2.2.1)a, (4.2.2.2)a\}$ overdetermines ξ_A , and does not determine ξ_+ and ξ_- individually. Hence one may conclude that (TT2) is governed by the pair $\{(4.2.2.1), (4.2.2.2)\}$. For transition type (TT1), it can be shown that the pair $\{(4.2.2.3)a, (4.2.2.4)a\}$ admits an explicit solution for $\xi_-(t)$, $\xi_A(t)$, $\xi_+(t)$. This solution is found to have the property that ξ_- depends on the constitutive function $\alpha_{+A}(\tau, T)$ and ξ_+ depends on the constitutive function $\alpha_{-A}(\tau, T)$. This statement implies that the determination of ξ_- and ξ_+ depends on processes $M_+ \to A$ and $M_- \to A$ respectively, which does not seem reasonable, so that it is preferable to use $\{(4.2.2.3), (4.2.2.4)\}$.

Recall that the basic one variant phase transformation rule cited in the approach by Ivshin and Pence (1994 b) is that phase transformation proceeds at a pace that is proportional to the phase that is transforming and is independent of the phase that is experiencing a net increase. For (TT1) the A-phase is experiencing a net increase and so this gives an independent and purely physical argument against equations involving $\frac{d\xi_A}{dt}$ in (TT1). However this same assumption for (TT2) would argue against equations involving $\frac{d\xi_A}{dt}$ and $\frac{d\xi_A}{dt}$ in (TT2), which is in contradiction to the pair combination that we have obtained here. This provides a hint that the pair equation governing (TT2) may require some further modification, as we shall show in the next section.

For (TT3), the combined $M_+ \to A$ and $A \to M_-$ process, it can be argued that the possible algorithms associated with (4.2.2.2)a should be excluded since the phase fraction of austenite ξ_A should involve dependence on both of the phase fractions ξ_+ and ξ_- . On the other hand, the algorithm for process $M_+ \to A$ has been chosen as (4.2.2.3) in (TT1). Hence for the purpose of consistently using the same algorithm in all transition types, one must select $\{(4.2.2.3), (4.2.2.2)\}$. Transition type (TT4), the combined $M_- \to A$ and

 $A \rightarrow M_+$ process is similar to (TT3), The selected algorithm for (TT4) is {(4.2.2.1), (4.2.2.4)}.

Because there is no austenite in the detwinning processes (TT5) and (TT6) in $\hat{\Omega}_2^+$ and $\hat{\Omega}_2^-$ respectively, we do not need to contemplate those algorithms associated with the phase fraction of austenite. Thus, for the coherence considerations between the algorithms of $M_- \to A$ ($M_+ \to A$) and $M_- \to M_+$ ($M_+ \to M_-$), in the whole (τ , T)-plane, the algorithm selected for (TT5) is (4.2.2.4); the algorithm selected for (TT6) is (4.2.2.3).

4.3.2 Algorithm Consistency between One and Two Variant Problems

So far, we have selected equations for governing the transition types in the two-variant model. However, the extension of the algorithms from one-variant to two-variant models needs further investigations to ensure that the extended algorithms can describe both one-variant and two-variant situations for a self-accommondated process. To examine the consistency between one-variant and two-variant models, let us consider a loading path of increasing/decreasing temperature at zero-load in the two variant model, for conditions involving symmetric martensite variants. The corresponding transition types from section 3.1 are (TT1) and (TT2) for temperature increase and temperature decrease respectively. We begin with temperature decrease starting at $T > A_f$ so that the M_+/M_- symmetry in initial conditions keeps M_+/M_- symmetry for all time. In this case one should note that $\xi_M = \xi_+ + \xi_- = 2\xi_+ = 2\xi_-$. For this zero-load case of temperature decrease, algorithm $\{(4.2.2.1), (4.2.2.2)\}$ for transition type (TT2) can be rewritten in terms of ξ_M as

$$\frac{d\xi_M}{dt} = -\frac{2\xi_A}{\hat{\alpha}_{max}(T)} \cdot \frac{d}{dt} \hat{\alpha}_{max}(T) \text{ for } A \to M, \qquad (4.3.2.1)$$

if equation (4.2.1.5) for (TT2) is used. Similarly, for temperature increase, algorithm {(4.2.2.3), (4.2.2.4)} for transition type (TT1) can be rewritten as

$$\frac{d\xi_M}{dt} = -\frac{\xi_M}{1 - \hat{\alpha}_{min}(T(t))} \cdot \frac{d}{dt} \hat{\alpha}_{min}(T) \text{ for } M \to A, \qquad (4.3.2.2)$$

if equation (4.2.1.5) for (TT2) is used again.

Therefore, comparisons for $M \rightarrow A$ between the governing equation (4.1.1.2) of the one-variant and the governing equation (4.3.2.2) of the two-variant models show agreement. However comparisons for $A \rightarrow M$ between governing equation (4.1.1.1) of the onevariant and the governing equation (4.3.2.1) of the two-variant models show disagreement by a factor 2. This disagreement induces us to review the explanation of those constitutive functions at the beginning of section 4.2.2. It is noted that constitutive functions $\alpha_{A+}(\tau, T)$ and $\alpha_{A}(\tau, T)$ indicate state functions of austenite phase fractions narrating phase transformations from 100% austenite to each individual martensite variant respectively. Furthermore, when temperature decreases from a reference either above or below A_f at stressfree condition, the austenite phase is always evenly transformed into equal amounts of M_{\perp} and M_{+} martensite variants. However in section 4.2.2, this effect was not reflected in the set of (4.2.2.1) and (4.2.2.2). Therefore, to build this reasonable extrapolation into the extended governing algorithms of the two-variant model during the extension, the selected governing equations (4.2.2.1) and (4.2.2.2) for $A \rightarrow M_{+}$ and $A \rightarrow M_{-}$ should be modified by

$$\frac{d\xi_{+}}{dt} = -\frac{\xi_{A}}{2\alpha_{A+}(\tau, T)} \cdot \frac{d}{dt}\alpha_{A+}(\tau, T) \text{ for } A \to M_{+}, \tag{4.3.2.3}$$

$$\frac{d\xi_{-}}{dt} = -\frac{\xi_{A}}{2\alpha_{A-}(\tau, T)} \cdot \frac{d}{dt}\alpha_{A-}(\tau, T) \text{ for } A \to M_{-}, \qquad (4.3.2.4)$$

respectively.

The equations governing each transition type are summarized in TABLE 4. This algorithm, for the six transition types in either X-unfolding, pY-unfolding or Y-unfolding, ensures consistency within the two-variant model, and properly reduces to the one-variant model in the zero-load situation.

TABLE 4. Transition Types with Their Algorithm

AREAS	TRANSITION TYPE	ALGORITHM
	$(TT1) M_+ \to A, M \to A$	((4.2.2.3), (4.2.2.4))
Ω_1	$(TT2) \stackrel{?}{A} \rightarrow M_+, A \rightarrow M$	((4.3.2.3), (4.3.2.4))
	$(TT3) M_+ \to A, A \to M$	((4.2.2.3), (4.3.2.4))
	$(TT4) M_{-} \rightarrow A, A \rightarrow M_{+}$	((4.2.2.4), (4.3.2.3))
Ω_{2}^{+} or $\hat{\Omega}_{2}^{+}$	$(TT5) M_{-} \rightarrow M_{+}$	(4.2.2.4)
Ω_2^\cdot or $\hat{\Omega}_2^\cdot$	$(TT6) M_+ \to M$	(4.2.2.3)
BALANCE	$\xi_A(t) + \xi_+(t) + \xi(t) = 1 \ (1.2.0.1)$	

5 INTEGRABILITY AND PATH DEPENDENCE

The phase fraction evolution of the three species, which describes transformations between austenite and martensite or detwinning processes between the two martensite variants, is determined on the basis of the ordinary differential equations listed in the TABLE 4. The overall balance requires that the phase fractions satisfy relation (1.2.0.1). For this process, we assume that T(t) and $\tau(t)$ are given functions, ie., $(\tau(t), T(t))$ forms a state-path in which time t varies from a beginning time t_i to an arbitrary future time t so long as the transition type remains the same. General analytical solutions for the phase fractions can be given in terms of path integrals. These integrals along the state path may, or may not, be evaluatable in terms of the path endpoints. Equivalently, the algorithm within a transition type may, or may not, be path-independent. In this section we investigate the solution for each transition type as well as conditions which indicate path-independence within the transition type. Some of the precursor studies, which guide some aspects of this section's development, were suggested by Ivshin in unpublished work.

5.1 Integration of The Hysteresis Equations for The Phase Fractions

There are totally six transition types in the Y-unfolding: (TT1) to (TT4) which hold in Ω_1 , (TT5) which holds $\hat{\Omega}_2^+$ and (TT6) which holds in $\hat{\Omega}_2^-$. In the following we are going to present a solutions for the phase fraction evolution during a time interval $[t_i, t]$, in which

one of the six transition types occurs.

5.1.1 Integration of Transition Type (TT1)

If in a time interval $[t_i, t]$ transition type (TT1) $M_+ \to A, M_- \to A$ occurs, then the governing equations are (4.2.2.3), (4.2.2.4) and (1.2.0.1) (see TABLE 4). Through dropping dt in equations (4.2.2.3) and (4.2.2.4), and then integrating the two, we obtain

$$\xi_{+}(t) = E(t_{i}) \cdot (1 - \alpha_{+A}(\tau(t), T(t))), \qquad (5.1.1.1)$$

$$\xi_{-}(t) = D(t_i) \cdot (1 - \alpha_{-A}(\tau(t), T(t))), \qquad (5.1.1.2)$$

where, the coefficients are determined by

$$E(t_i) = \frac{\xi_+(t_i)}{1 - \alpha_{+A}(\tau(t_i), T(t_i))},$$
 (5.1.1.3)

$$D(t_i) = \frac{\xi_{-}(t_i)}{1 - \alpha_{A}(\tau(t_i), T(t_i))}.$$
 (5.1.1.4)

Hereupon, the corresponding austenite phase fraction is obtained from the balance equation (1.2.0.1).

$$\xi_{A}(t) = 1 - E(t_{i}) \cdot (1 - \alpha_{+A}(\tau(t), T(t))) - D(t_{i}) \cdot (1 - \alpha_{-A}(\tau(t), T(t))) . \tag{5.1.1.5}$$

For this situation, ξ_A , ξ_+ and ξ_- are all *path-independent* in the (τ, T) -plane. That is, beginning at known values $\xi_A(t_i)$, $\xi_+(t_i)$ and $\xi_-(t_i)$ at the initial time t_i , the values of $\xi_A(t)$, $\xi_+(t)$ and $\xi_-(t)$ at any future time t depend only upon the current values of the state

 $(\tau(t), T(t))$ and not upon the path connecting $(\tau(t_i), T(t_i))$ to $(\tau(t), T(t))$. Of course here it is required that the path only involves transition type (TT1) $M_+ \to A$, $M_- \to A$.

5.1.2 Integration of Transition Type (TT2)

For a time interval $[t_i, t]$ in which (TT2) $A o M_+$, $A o M_-$ occurs, the governing equations for this transition type are (4.2.2.1), (4.2.2.2) and (1.2.0.1). With a proper derivation on the three equations we arrive at

$$\xi_{\mathbf{A}}(t) = F(t_i) \cdot \sqrt{\alpha_{\mathbf{A}_{-}}(\tau(t), T(t)) \cdot \alpha_{\mathbf{A}_{+}}(\tau(t), T(t))}, \qquad (5.1.2.1)$$

where the coefficient $F(t_i)$ is given by

$$F(t_i) = \frac{\xi_A(t_i)}{\sqrt{\alpha_{A_i}(\tau(t_i), T(t_i)) \cdot \alpha_{A_i}(\tau(t_i), T(t_i))}}.$$
 (5.1.2.2)

Substituting (5.1.2.1) into (4.2.2.1) and (4.2.2.2) generates upon integration:

$$\xi_{+}(t) = \int_{t_{i}}^{t} \left(\frac{-F(t_{i})}{2} \cdot \sqrt{\frac{\alpha_{A-}(\tau(t), T(t))}{\alpha_{A+}(\tau(t), T(t))}} \cdot \frac{d}{dt} \alpha_{A+}(\tau(t), T(t)) \right) dt + \xi_{+}(t_{i}), \qquad (5.1.2.3)$$

$$\xi_{\cdot}(t) = \int_{t_i}^{t} \left(\frac{-F(t_i)}{2} \cdot \sqrt{\frac{\alpha_{A+}(\tau(t), T(t))}{\alpha_{A-}(\tau(t), T(t))}} \cdot \frac{d}{dt} \alpha_{A-}(\tau(t), T(t)) \right) dt + \xi_{\cdot}(t_i).$$
 (5.1.2.4)

Here the derivatives in the above integration are

$$\frac{d}{dt}\alpha_{A+}(\tau(t), T(t)) = \nabla \alpha_{A+}(\tau(t), T(t)) \cdot \frac{d}{dt}r(t), \qquad (5.1.2.5)$$

$$\frac{d}{dt}\alpha_{A}(\tau(t), T(t)) = \nabla \alpha_{A}(\tau(t), T(t)) \cdot \frac{d}{dt}r(t), \qquad (5.1.2.6)$$

where

$$\mathbf{r}(t) = \mathbf{\tau}(t)\hat{\mathbf{e}}_{\tau} + T(t)\hat{\mathbf{e}}_{T}, \qquad (5.1.2.7)$$

$$\nabla f(\tau, T) = \frac{\partial f}{\partial \tau} \hat{e}_{\tau} + \frac{\partial f}{\partial T} \hat{e}_{T}, \qquad (5.1.2.8)$$

 \hat{e}_{τ} and \hat{e}_{T} are unit vectors along τ and T axes.

Result (5.1.2.1) shows that ξ_A is path-independent, since it depends only upon the initial and the final values of temperature and stress. However expressions (5.1.2.3) and (5.1.2.4) indicate that phase fractions ξ_+ and ξ_- are, in general, path-dependent. This is because the two integrals cannot generally be evaluated in terms of their endpoints in (τ, T) -plane, unless special restrictions are put on the envelope functions.

To see this, assume that ξ_{+} and ξ_{-} are path-independent, then their expressions (5.1.2.3) and (5.1.2.4) have to satisfy Cauchy-Riemann condition (Apostol, 1962), which give

$$\nabla \alpha_{\mathbf{A}}(\tau, T) \cdot \overline{\nabla \alpha_{\mathbf{A}}(\tau, T)} = \nabla \alpha_{\mathbf{A}}(\tau, T) \cdot \overline{\nabla \alpha_{\mathbf{A}}(\tau, T)} = 0 \quad , \tag{5.1.2.9}$$

Here the operator with hyper bar is defined as

$$\overline{\nabla f(\tau, T)} = \frac{\partial f}{\partial T} \hat{\mathbf{e}}_{\tau} - \frac{\partial f}{\partial \tau} \hat{\mathbf{e}}_{T}. \tag{5.1.2.10}$$

The scalar form of equation (5.1.2.9) is

$$\frac{\partial}{\partial \tau} \alpha_{A-}(\tau, T) \cdot \frac{\partial}{\partial T} \alpha_{A+}(\tau, T) = \frac{\partial}{\partial T} \alpha_{A-}(\tau, T) \cdot \frac{\partial}{\partial \tau} \alpha_{A+}(\tau, T). \tag{5.1.2.11}$$

The path-independent condition (5.1.2.9) (or (5.1.2.11)) will be further discussed in section 5.1.6, where it is shown that this condition can not be satisfied.

5.1.3 Integration of Transition Type (TT3)

If transition type (TT3) $M_+ \to A$, $A \to M_-$ occurs in a time interval $[t_i, t]$, then, the governing equations are (4.2.2.3), (4.2.2.2) and (1.2.0.1). The solution of equation (4.2.2.3) again gives the result (5.1.1.1), so that ξ_+ is path-independent in (τ, T) -plane. With equations (4.2.2.3), (4.2.2.2) and result (5.1.1.1), one can obtain

$$\xi_{A}(t) = \sqrt{\alpha_{A}(\tau(t), T(t))} \cdot \int_{t_{i}}^{t} \frac{E(t_{i})}{\sqrt{\alpha_{A}(\tau(t), T(t))}} d\alpha_{+A}(\tau(t), T(t)) + \frac{\xi_{A}(t_{i})}{\sqrt{\alpha_{A}(\tau(t_{i}), T(t_{i}))}} \cdot \sqrt{\alpha_{A}(\tau(t), T(t))}$$
(5.1.3.1)

Plugging (5.1.1.1) and (5.1.3.1) into (1.2.0.1) then gives the phase fraction ξ .

In general, ξ_A and ξ_A are path-dependent in the (τ, T) -plane. We can find the condition for path-independence from the expression (5.1.3.1) by applying Cauchy-Riemann condition to it. This gives the condition

$$\nabla \alpha_{A}(\tau, T) \cdot \overline{\nabla \alpha_{+A}(\tau, T)} = \nabla \alpha_{+A}(\tau, T) \cdot \overline{\nabla \alpha_{A}(\tau, T)} = 0 , \qquad (5.1.3.2)$$

its scalar form is expressed as

$$\frac{\partial}{\partial \tau} \alpha_{A}(\tau, T) \cdot \frac{\partial}{\partial T} \alpha_{+A}(\tau, T) = \frac{\partial}{\partial T} \alpha_{A}(\tau, T) \cdot \frac{\partial}{\partial \sigma} \alpha_{+A}(\tau, T) . \qquad (5.1.3.3)$$

This condition, which is similar to (5.1.2.11), will also be discussed in section 5.1.6.

5.1.4 Integration of Transition Type (TT4)

Transition type (TT4) $M_- \to A$, $A \to M_+$ is similar to (TT3) under interchange of ξ_+ and ξ_- . The governing equations are (4.2.2.1), (4.2.2.4) and (1.2.0.1) for transition type (TT4). The solution of equation (4.2.2.4) again gives (5.1.1.2), which indicates that ξ_- is path-independent. The phase fraction of austenite can be found by solving equations (4.2.2.1) and (4.2.2.4) with the consideration of result (5.1.1.2), that is

$$\xi_{A}(t) = \sqrt{\alpha_{A+}(\tau(t), T(t))} \cdot \int_{t_{i}}^{t} \frac{D(t_{i})}{\sqrt{\alpha_{A+}(\tau(t), T(t))}} d\alpha_{-A}(\tau(t), T(t)) + \frac{\xi_{A}(t_{i})}{\sqrt{\alpha_{A+}(\tau(t_{i}), T(t_{i}))}} \cdot \sqrt{\alpha_{A+}(\tau(t), T(t))}$$
(5.1.4.1)

And by use of (1.2.0.1), (5.1.1.2) and (5.1.4.1), one then obtains ξ_+ .

The phase fractions of austenite and M_+ martensite are in general path-dependent in (τ, T) -plane in general. Applying Cauchy-Riemann condition to (5.1.4.1) gives the special path-independent condition of the two variables as

$$\nabla \alpha_{\mathbf{A}+}(\tau, T) \cdot \overline{\nabla \alpha_{-\mathbf{A}}(\tau, T)} = \nabla \alpha_{-\mathbf{A}}(\tau, T) \cdot \overline{\nabla \alpha_{\mathbf{A}+}(\tau, T)} = 0 \quad , \tag{5.1.4.2}$$

and its scalar form is

$$\frac{\partial}{\partial \sigma} \alpha_{A+}(T,\sigma) \cdot \frac{\partial}{\partial T} \alpha_{-A}(T,\sigma) = \frac{\partial}{\partial T} \alpha_{A+}(T,\sigma) \cdot \frac{\partial}{\partial \sigma} \alpha_{-A}(T,\sigma). \tag{5.1.4.3}$$

Again the above condition will also be further considered in section 5.1.6.

5.1.5 Integration for Detwinning Process

All the solutions and path-independent conditions obtained above are suited to the dual process region Ω_1 . In the detwinning zones $\hat{\Omega}_2^+$ and $\hat{\Omega}_2^-$, without any austenite, the only active transition types are (TT5) and (TT6) respectively. For transition type (TT5) $M_- \to M_+$, the governing equations are (4.2.2.4) and (1.2.0.1) with $\xi_A = 0$. Thus result (5.1.1.2) is the solution of ξ_- , which gives

$$\xi_{-}(t) = D(t_i) \cdot (1 - \alpha_{-A}(\tau(t), T(t))), \qquad (5.1.5.1)$$

$$\xi_{+}(t) = 1 - (D(t_i) \cdot (1 - \alpha_{-A}(\tau(t), T(t)))). \tag{5.1.5.2}$$

For transition type (TT6), the governing equations are (4.2.2.3) and (1.2.0.1) again with $\xi_A = 0$. The expression (5.1.1.1) gives the solution of ξ_+ as

$$\xi_{+}(t) = E(t_{i}) \cdot (1 - \alpha_{+A}(\tau(t), T(t))), \qquad (5.1.5.3)$$

$$\xi_{-}(t) = 1 - (E(t_i) \cdot (1 - \alpha_{+A}(\tau(t), T(t)))). \tag{5.1.5.4}$$

The phase fractions in both (TT5) and (TT6) are path-independent.

5.1.6 Path Independence of the depleted Species within a Transition Type

For transition types (TT1), (TT5) and (TT6), all of the phase fractions $\xi_{-}(t)$, $\xi_{A}(t)$ and $\xi_{+}(t)$ are path-independent in the sense that, once the initial conditions are specified, they depend on only the current values of (τ, T) . However for the remaining three transition types (TT2), (TT3) and (TT4), only one of the phase fractions has been shown to display such path-independence, namely: austenite phase fraction ξ_{A} in (TT2), positively oriented martensite phase fraction ξ_{+} in (TT3) and negatively oriented martensite phase fraction ξ_{-} in (TT4). These are precisely the phase species that are being absolutely depleted. For example, transition type (TT3) involves $M_{+} \rightarrow A$ and $A \rightarrow M_{-}$, thus the M_{+} species is being absolutely depleted, the M_{-} species is being absolutely augmented, and the A species is $in\ flux$ (whether it is depleted or augmented depends on which of the two transitions $M_{+} \rightarrow A$ and $A \rightarrow M_{-}$ is stronger). As regards transition type (TT1), here both M_{+} and M_{-} are being absolutely depleted, and, consistent with the above comments, the associated phase fractions are path independent. The path independence of ξ_{A} for transition type (TT1) can then be regarded as a consequence of the overall balance (1.2.0.1).

5.2 Path Dependence and Path Independence within a Transition Type

5.2.1 General Path-Independent Condition

So far we have arrived at three path-independent conditions (5.1.2.9), (5.1.3.2) and (5.1.4.2) in transition types (TT2), (TT3) and (TT4) respectively. However, in view of the fact that the envelope function dependency on (τ, T) is mediated by the β -function that describe the nuetrality curves (see (4.2.1.1) - (4.2.1.4)), condition (5.1.2.9) for (TT2) can

be rewritten as

$$\hat{\alpha}'_{max}(\beta^{+}) \cdot \hat{\alpha}'_{max}(\beta^{-}) \cdot (\beta^{+}_{T} \cdot \beta^{-}_{\tau} - \beta^{+}_{\tau} \cdot \beta^{-}_{T}) = 0, \qquad (5.2.1.1)$$

and (5.1.3.2) for (TT3) and (5.1.4.2) for (TT4) can be rewritten as

$$\hat{\alpha}'_{max}(\beta^{-}) \cdot \hat{\alpha}'_{min}(\beta^{+}) \cdot (\beta_{T}^{+} \cdot \beta_{\tau}^{-} - \beta_{\tau}^{+} \cdot \beta_{T}^{-}) = 0, \qquad (5.2.1.2)$$

$$\hat{\alpha}'_{max}(\beta^+) \cdot \hat{\alpha}'_{min}(\beta^-) \cdot (\beta_T^+ \cdot \beta_T^- - \beta_T^+ \cdot \beta_T^-) = 0, \qquad (5.2.1.3)$$

respectively.

Recall from Section 4.1.2 that $\hat{\alpha}'_{max}$ and $\hat{\alpha}'_{min}$ are equal to zero if (τ, T) are in the zones that are inactive for the process under consideration, that is the transitions either have not began or have gone to completion. Our interest is thus the case when neither $\hat{\alpha}'_{max}$ nor $\hat{\alpha}'_{min}$ vanishes. The three path-independent conditions then simplify to

$$\nabla \beta^{+}(\tau, T) \cdot \overline{\nabla \beta^{-}(\tau, T)} = 0. \qquad (5.2.1.4)$$

It will be shown in the next section that this condition can never be satisfied by the present β -functions.

5.2.2 Path-dependent Analysis for the case of $A_s > M_s$

In this section all discussion is confined to the pY-unfolding with identical moduli of austenite and martensite, and confined to a material with $M_s < A_s$. The other case $(M_s > A_s)$ is treated in the next section. Materials obeying $M_s < A_s$ involve a dead zone in the temperature driven (zero-load) transformation hysteresis. This gives certain simplifica-

tions. It is important to note that all the possibly path-dependent cases occur in certain parts of region Ω_1^+ , and that the associated special condition for path-independence is the requirement (5.2.1.4) on the nuetrality curves. As mentioned above, we are interested in the path-independent conditions in areas where the first derivatives of the two envelopes do not vanish. In transition type (TT2), the domain on which $\hat{\alpha}'_{max}$ is nonzero is

$$d_2 = \{(\tau, T) | M_f < \beta^{+}(\tau, T) < M_s, M_f < \beta^{-}(\tau, T) < M_s \}.$$

In domain d_2 (Figure 20) the path-independent condition of ξ_+ and ξ_- is given by (5.2.1.4). However, since $\beta_T^+ > 0$, $\beta_T^- > 0$, $\beta_\tau^- > 0$ and $\beta_\tau^+ < 0$, it follows that

$$\beta_T^+ \cdot \beta_\tau^- - \beta_\tau^+ \cdot \beta_T^- > 0, \qquad (5.2.2.1)$$

in d_2 . Hence transition type (TT2) in d_2 as determined by equations (4.3.2.3) and (4.3.2.4) generates path-dependent values for ξ_+ and ξ_-

Turning to transition types (TT3) and (TT4), the areas of nonzero $\hat{\alpha}'_{max}$ and $\hat{\alpha}'_{min}$ are given by

$$d_3 = \{(\tau, T) | M_f \leq \beta^{-}(\tau, T) \leq M_s, A_s \leq \beta^{+}(\tau, T) \leq A_f \},$$

$$d_4 = \{ (\tau, T) | M_f \le \beta^+(\tau, T) \le M_s, A_s \le \beta^-(\tau, T) \le A_f \},$$

respectively (Figure 20). For both of these two transition types, the path-independent condition (5.2.1.4), for ξ_A and ξ_- of (TT3) as well as for ξ_A and ξ_+ of (TT4), can never be satisfied in d_3 and d_4 severally because relation (5.2.2.1) is held again. Thus, for transition type (TT3) ξ_A and ξ_- are path-dependent in d_3 while for transition type (TT4) ξ_A and ξ_+ are path-dependent in d_4 .

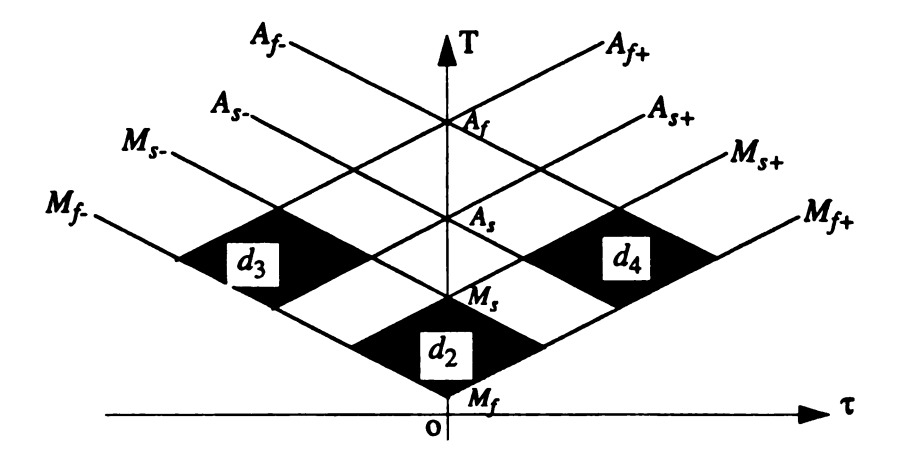


Figure 20. For the case $A_s > M_s$, three path-dependent zones d_2 , d_3 and d_4 are separated in Ω_1^+ . ξ_+ and ξ_- are path-dependent in d_2 if transition type (TT2) occurs (S-paths). ξ_A and ξ_- are path-dependent in d_3 if transition type (TT3) occurs (W-paths). ξ_A and ξ_+ are path-dependent in d_4 if transition type (TT4) occurs (E-paths).

Recall in Ω_1^+ that the determination of transition types correlates with state path directionality in a way that is geometrically associated with compass headings: N, E, S, W. Geometrically we have shown that: ξ_+ and ξ_- are path-dependent in d_2 for S-paths, ξ_A and ξ_- are path-dependent in d_3 for W-paths, ξ_A and ξ_+ are path-dependent in d_4 for E-paths. All the above conclusions can be viewed in TABLE 5.

TABLE 5. Path-dependent Category for $M_s < A_s$

PATH-DEPEDENT ZONES	PATH-DEPENDENT TRANSITION TYPES	PATH-DEPENDENT DIRECTIONS
d_2	(TT2)	S-paths
d_3	(TT3)	W-paths
<i>d</i> ₄	(TT4)	E-paths

5.2.3 Path-dependent Analysis for the case of $M_s > A_s$

The more complicated situation $M_s > A_s$ will be discussed in this section. Again, the pY-unfolding with identical shear moduli of austenite and martensite is considered here. The path-dependent condition is still (5.1.2.4) for transition types (TT2), (TT3) and (TT4), and the definitions for the three path-dependent zones remain unchanged as in the last section. The difference for the present circumstance is that the absence of a dead zone means that the three path-dependent zones d_2 , d_3 and d_4 overlap each other (Figure 21), which creates certain overlapping areas where either two or three transition types may simultaneously involve path-dependence.

For convenience, we define following six subdomains to further investigate the pathdependent condition,

$$a_2 = d_2 - d_3 - d_4$$
, $a_3 = d_3 - d_2 - d_4$, $a_4 = d_4 - d_2 - d_3$, $a_{23} = d_2 \cap d_3 - d_4$, $a_{24} = d_2 \cap d_4 - d_3$, $a_{234} = d_2 \cap d_3 \cap d_4$,

which are shown in Figure 21. With a similar discussion as that in section 5.2.2 the path-dependent zones, transition types and corresponding direction cones are listed in TABLE 6. Each transition type can only be triggered by the corresponding transition path, ie., (TT1) is ignited by N-paths and so on. It is observable from TABLE 6 and Figure 21 that in the relative stability zone for M_{-} , such as d_3 , the possibility for phase fraction ξ_{-} being path-dependent is larger than the others. A similar result can be observed for phase fraction ξ_{+} in d_4 .

TABLE 6. Path-dependent Category for $M_s > A_s$

PATH-DEPEDENT ZONES	PATH-DEPENDENT TRANSITION TYPES	PATH-DEPENDENT DIRECTIONS
a_2	(TT2)	S-paths
<i>a</i> ₃	(TT3)	W-paths
a ₄	(TT4)	E-paths
a ₂₃	(TT2), (TT3)	S-, W-paths
a ₂₄	(TT2), (TT4)	S-, E-paths
a ₂₃₄	(TT2), (TT3), (TT4)	S-, W-, E-paths

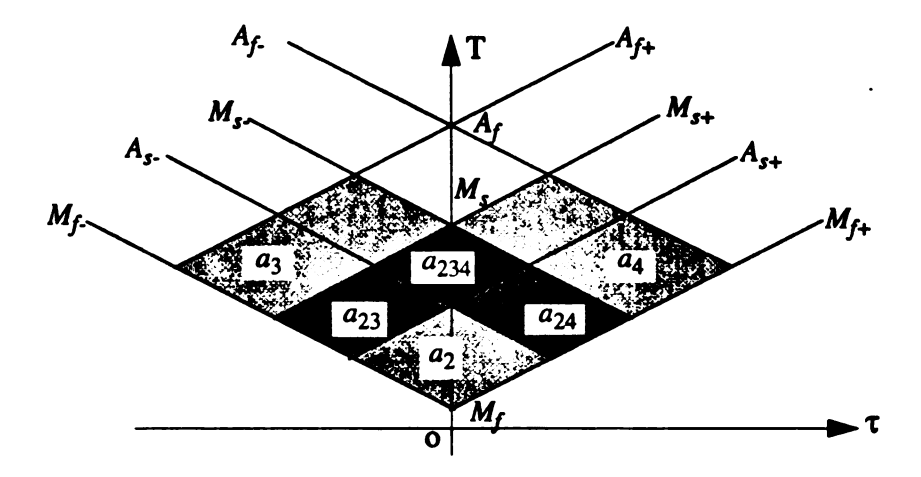


Figure 21. For the case $A_s < M_s$, six path-dependent zones a_2 , a_3 , a_4 , a_{23} , a_{24} and a_{234} are separated in Ω_1^+ . The situations occurring in a_2 , a_3 and a_4 are the same with those in d_2 , d_3 and d_4 of the case $A_s > M_s$ shown in Figure 20. In a_{23} , if transition type (TT2) is in process then the phase fractions ξ and ξ are path-dependent, while if (TT3) occurs then ξ_A and ξ are path-dependent. In a_{24} , the condition is similar to that in a_{23} under interchange of (TT3) and (TT4) as well as ξ and ξ . In a_{234} , ξ and ξ are path-dependent if (TT2) occurs, ξ_A and ξ are path-dependent if (TT3) occurs, and, ξ_A and ξ are path-dependent if (TT4) is in process.

5.3 Example

To illustrate this path dependence, consider a material with $M_s < A_s$ and contemplate three separate stable paths in d_2 , all of which involve only transition type (TT2) throughout. The three paths: l_1 , l_2 and l_3 are shown in Figure 22. They all start at point $(\tau, \sigma) = (0, M_s)$ with initial conditions $\{\xi_-, \xi_A, \xi_+\} = \{0, 1, 0\}$ and end at point $(\tau, \sigma) = (0, M_f)$. The three state paths are the forms of

$$l_1: \{(\tau, T) | \tau = 0\};$$

$$\begin{split} l_2 \colon \{ (\tau, T) | (T &= -\Omega k_1 \tau + M_s, M_s \geq T \geq \frac{M_s + M_f}{2}); \\ (T &= \Omega k_1 \tau + M_f, M_f \leq T \leq \frac{M_s + M_f}{2}) \}, \\ l_3 \colon \{ (\tau, T) | (T &= \Omega k_1 \tau + M_s, M_s \geq T \geq \frac{M_s + M_f}{2}); \\ (T &= -\Omega k_1 \tau + M_f, M_f \leq T \leq \frac{M_s + M_f}{2}) \}, \end{split}$$

respectively. Where, Ω is a real number which must be greater that 1 to stay in d_2 . It is desired to find the phase fractions $\{\xi_-, \xi_A, \xi_+\}$ at the end point $(0, M_f)$ on the three different paths.

The nuetrality functions that we use here are (2.3.2.3) and (2.3.2.4) for pY-unfolding with equality of the moduli of austenite and martensite, where $k_1 = \frac{\gamma^*}{\eta_A^o - \eta_M^o} = 0.1 \,\mathrm{m}^3$ °K/J (Ivshin and Pence, 1994 b). Thus, all the three paths are inside domain d_2 for any $\Omega > 1$ and the directions (derivative $\frac{dT}{d\tau}$) of all the points on the three paths are confined to the open cone zone S. The envelope functions used here are linear piecewise defined as the following:

$$\hat{\alpha}_{max}(\beta) = \begin{cases} 0, & \forall \quad \beta \leq M_f \\ \frac{\beta - M_f}{M_s - M_f}, & \forall \quad M_f \leq \beta \leq M_s \\ 1, & \forall \quad \beta \geq M_s \end{cases}$$
 (5.3.0.1)

$$\hat{\alpha}_{min}(\beta) = \begin{cases} 0, & \forall \quad \beta \leq A_s \\ \frac{\beta - A_s}{A_f - A_s}, & \forall \quad A_s \leq \beta \leq A_f \\ 1, & \forall \quad \beta \geq A_f \end{cases}$$
 (5.3.0.2)

Based on the definitions (4.2.1.1) to (4.2.1.4), the functions $\alpha_{A+}(\tau, T)$, $\alpha_{+A}(\tau, T)$, $\alpha_{A-}(\tau, T)$ and $\alpha_{A-}(\tau, T)$ can be found by substituting (2.3.2.3) and (2.3.2.4) into (5.3.0.1) and (5.3.0.2). It is then desired to determine phase fractions $\{\xi_-, \xi_A, \xi_+\}$ at the end point $(\tau, T) = (0, M_f)$ on the three paths, each as a function of Ω . A mathematical reduction leads to complicated integral expressions that can formally be integrated with the help of either handbooks or symbolic algebra. Numerically, these phase fractions for different values of Ω are found and given in TABLE 7. Since path l_2 and path l_3 are symmetric with respect to T-axis, so that the values of ξ_+ and ξ_- corresponding to path l_2 and path l_3 switch each other. These results also confirm that ξ_A is path-independent, ξ_+ and ξ_- are path-dependent in transition type (TT2).

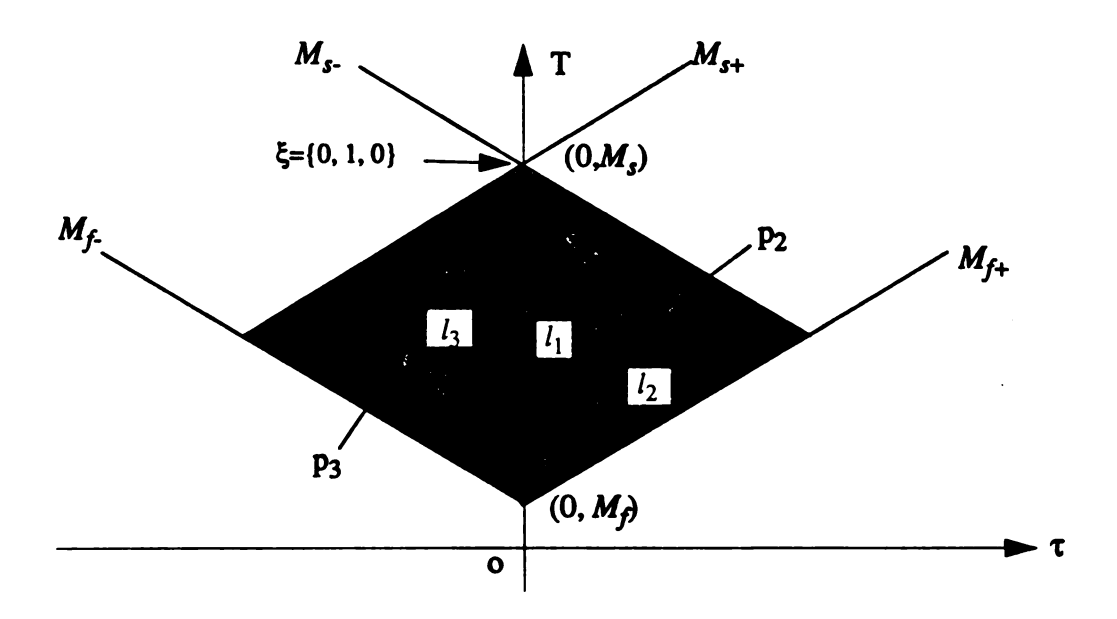


Figure 22. Three paths l_1 , l_2 and l_3 go from $(\tau, \sigma) = (0, M_s)$ to $(0, M_f)$ in the path-dependent zone of transition type (TT2) with initial condition $\{\xi_-, \xi_A, \xi_+\} = \{0, 1, 0\}$. Transition type (TT2) occurs on all three paths. Path l_2 consists of two straight segments which meet at point $p_2 = (\frac{1}{2\Omega k_1}(M_s - M_f), \frac{1}{2}(M_s + M_f))$. Path l_3 is similar. The phase fractions ξ_- and ξ_+ are path dependent while ξ_A is not. The values of the triple $\{\xi_-, \xi_A, \xi_+\}$ at the ends of the three paths are listed in TABLE 7.

TABLE 7. Phase Fractions at the End $(0, M_f)$ of the Three Paths: l_1, l_2, l_3

Ω	l_1	l_2	<i>l</i> ₃
1	{0.5, 0, 0.5}	{0, 0, 1}	{1, 0, 0}
1.01	{0.5, 0, 0.5}	{0.036752, 0, 0.963248}	{0.963248, 0, 0.036752}
1.1	{0.5, 0, 0.5}	{0.120019, 0, 0.879981}	{0.879981, 0, 0.120019}
1.5	{0.5, 0, 0.5}	{0.250921, 0, 0.749079}	{0.749079, 0, 0.250921}
2	{0.5, 0, 0.5}	{0.319921, 0, 0.68009}	{0.68009, 0, 0.319921}
5	{0.5, 0, 0.5}	{0.430292, 0, 0.569708}	{0.569708, 0, 0.430292}
20	{0.5, 0, 0.5}	{0.482665, 0, 0.517335}	{0.517335, 0, 0.482665}
100	{0.5, 0, 0.5}	{0.495634, 0, 0.503466}	{0.503466, 0, 0.495634}
1000	{0.5, 0, 0.5}	{0.499653, 0, 0.500347}	{0.500347, 0, 0.499653}
20000	{0.5, 0, 0.5}	{0.499983, 0, 0.500017}	{0.500017, 0, 0.499983}
8	{0.5, 0, 0.5}	{0.5, 0, 0.5}	{0.5, 0, 0.5}

5.4 Discussions on the Solutions

The phase fraction evolution for different transition types obtained in section 5.1 are suited to the X-unfolding, pY-unfolding and Y-unfolding. Because different nuetrality curves produce different responses to the envelope functions, the phase fraction evolution

in X, pY and Y-unfolding could be different corresponding to the same transition types and the same thermomechanical circumstances. Obviously, in Ω_1 both of the X- and pY-unfolding generate the same results for the phase fractions because the nuetrality curves for the two unfolding are identical in Ω_1 . However, for the Y-unfolding, since the detwinning flow and finish are independently specified, the description of phase transformations $A \leftrightarrow M_+$ in $\tau < 0$ and $A \leftrightarrow M_-$ in $\tau > 0$ are different from the description of the other two unfoldings. Predominantly, the Y-unfolding decreases stress ranges of existence of M_+ in $\tau < 0$ and of M_- in $\tau > 0$, which is caused by the smaller detwinning flow and finish stresses τ_s and τ_f found in the experimental literature compared to the "natural values" associated with the X- and pY-unfoldings.

All phase fraction solutions are determined in an infinitesimal time interval where only one of those transition types occurs. Chasing a given state path in (τ, T) -plane, phase fractions vary in one transition type for a segment on the path, and then may change to another transition types for the following segment on the path. All the three phase fractions $\{\xi_-, \xi_+, \xi_+\}$ are path-independent for transition type (TT1), (TT5) or (TT6), which means that they can be uniquely determined at a point in (τ, T) -plane provided initial conditions are given. In addition to this, ξ_A in (TT2), ξ_- in (TT3) and ξ_+ in (TT4), which represent consumed phases in each of the three transition types, are path-independent. On the other hand, phase fractions of transformed phases ξ_-/ξ_+ in (TT2), ξ_A/ξ_- in (TT3) and ξ_A/ξ_+ in (TT4) are path-dependent in the areas as shown in Figure 20 and Figure 21.

6 BEHAVIOR OF THE MODEL

After a careful discussion on the algorithms and associated studies, we now turn to view the macroscopic thermomechanical behavior of the two variant model by considering some numerical simulations. We emphasize that these simulations are only suited to a case of one dimensional behavior for a material containing only austenite and two martensite variants. This could include a compatible twin structure that is imagined as a symmetric lattice structure in which one lattice is sheared in one direction and the corresponding lattice is sheared in the opposite direction. Phase transformation occurs between austenite and martensite variants in Ω_1 , and detwinning occurs between the two symmetric martensite structures in $\hat{\Omega}_2^+$ and $\hat{\Omega}_2^-$.

6.1 Isothermal Behavior

In this section, we are going to confine all simulations for isothermal mechanical processes. This includes isothermal loading/unloading at high (above A_f) and low (below M_f) temperatures, in which pseudoelastic and shape memory behaviors will be generated. More than this, certain loading/unloading processes at some temperatures between A_f and M_f are also considered. Further, internal hysteresis loops will be conducted at the end of this section.

All the simulation parameters are taken from TABLE 2 of Section 2.5 except

 $\mu_A = 4.0 \times 10^4$ and $\mu_M = 2.5 \times 10^4$ MPa are going to be employed here. In particular, $M_s < A_s$ for this material. The phase diagram used here is Y-unfolding. The envelope functions are the piecewise forms of one argument as given in the following,

$$\alpha_{max}(\beta) = \begin{cases} 0 & \beta < M_f \\ \frac{1}{2} \left(1 - \cos \left(\frac{\beta - M_f}{M_s - M_f} \right) \pi \right) & M_f \le \beta \le M_s, \\ 1 & \beta > M_s \end{cases}$$
 (6.1.0.1)

$$\alpha_{min}(\beta) = \begin{cases} 0 & \beta < A_s \\ \frac{1}{2} \left(1 - \cos \left(\frac{\beta - A_s}{A_f - A_s} \right) \pi \right) & A_s \le \beta \le A_f \\ 1 & \beta > A_f \end{cases}$$
 (6.1.0.2)

6.1.1 Pseudoelastic Behavior

Pseudoelasticity occurs when loading in the high temperature austenite phase generates biased martensite, subsequent unloading causes complete reversion of the biased martensite to austenite provided $T > A_f$. This kind of behavior has been investigated in many works, such as by Fu, et al. (1993), Ivshin and Pence (1994 b), etc.. Here, as one of many basic features of the two variant model, pseudoelastic behaviors in both tension and compression at test temperature $T_t = 335$ °K are given in Figure 23. Three such behaviors at three different test temperature levels: $T_t = 315$ °K, $T_t = 325$ °K and $T_t = 335$ °K are presented (calculated by Mathematica) in Figure 24 for $\tau > 0$. In each complete hysteresis loop the lateral slopes are different because of the different moduli of austenite and martensite.

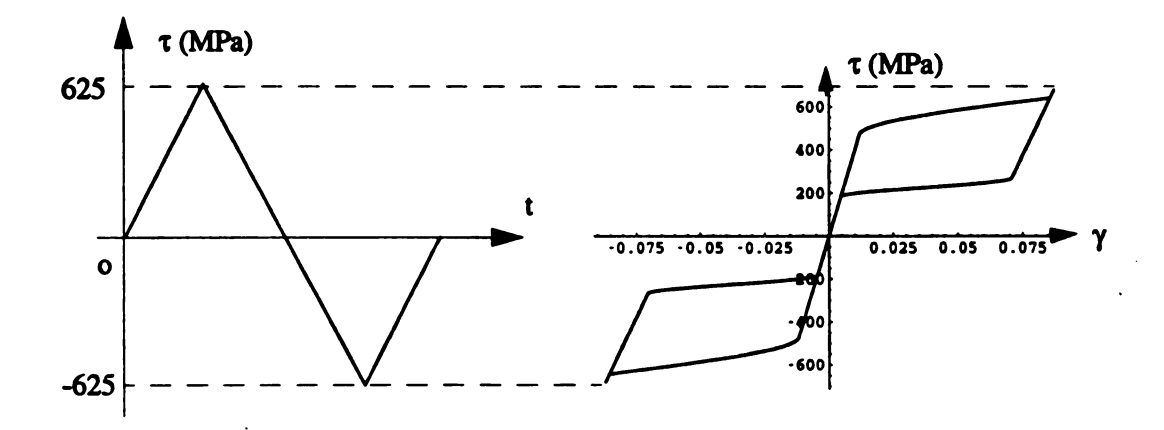


Figure 23. Pseudoelastic behaviors in both tension and compression conditions at test temperature $T_t = 335$. In $\tau > 0$, $A \leftrightarrow M_+$ processes are involved with the loading/unloading, while, in $\tau < 0$, $A \leftrightarrow M_-$ processes are involved with the opposite loading/unloading.

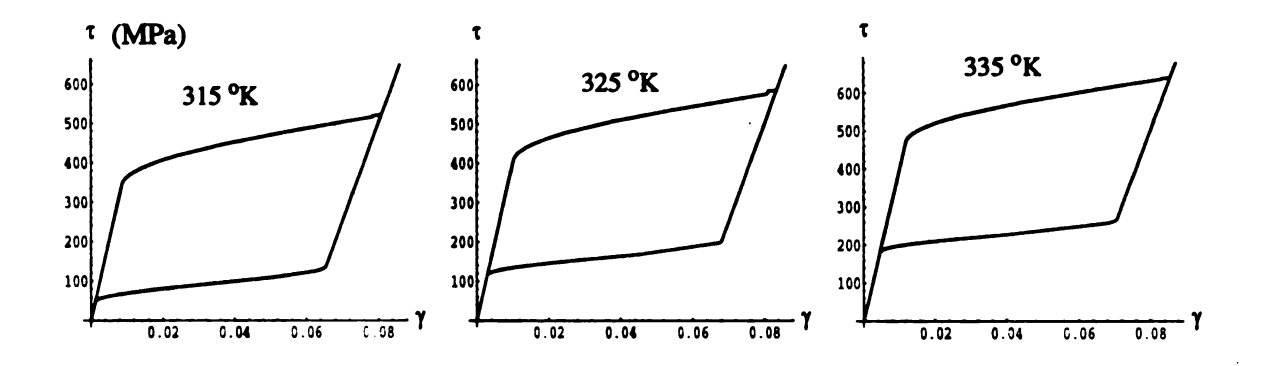


Figure 24. Pseudoelastic behaviors for $M_s < A_s$ at different temperature levels: $T_t = 315$, 325, 335 °K, all of which are greater than $A_f = 308$ °K.

Since $M_s < A_s$ for the material considered here there is *dead zone* between the flow stresses of $A \to M_+$ and $M_+ \to A$ (Figure 27). The *height* $\Delta \tau^T$ of the dead zone at test

temperature T_t is determined by the following formula,

$$\Delta \tau^{\mathrm{T}} = \frac{2(A_s - M_s)}{\sqrt{k_1 + 4k_2(T_t - M_s)} + \sqrt{k_1 + 4k_2(T_t - A_s)}}.$$
 (6.1.1.1)

Here (2.4.2.2) gives $k_1 = 0.144 \text{ m}^3 \text{ o}\text{K/J}$, $k_2 = 0.362 \times 10^{-4} \text{ m}^3 \text{ o}\text{K/(J MPa)}$ for this particular material. Since $k_2 > 0$, it follows that the height $\Delta \tau^T$ of the dead zone decreases with test temperature T_t increase and vice versa for $T_t > A_f$ (see Figure 24). The reason for this phenomena in the present model is that $\mu_A \neq \mu_M$ through parameter k_2 determined by equation (2.4.2.2). In the special case of equal shear moduli ($\mu_A = \mu_M$), one finds $k_2 = 0$, which indicates that $\Delta \tau^T = 2(A_s - M_s)/(2\sqrt{k_1})$.

Comparing with the other models, this one is similar to Falk's model (1980) but is much more general. In Falk's energy model, forward transformation $A \rightarrow M$ happens along the top dashed line when the applied load reaches the maximum of the left ascending branch (elastic loading of austenite) of the load-deformation diagram (Figure 25). The reverse transformation $M \rightarrow A$ occurs along the bottom dashed line when the unload reaches the minimum of the right ascending branch of the same diagram. Consequently, a pseudoelastic hysteresis loop is formed between the ascending branches and the two dashed lines, which indicates the energy dissipation during the process. The present model, which can cover all the above description if one treats the top and bottom dashed lines as the same as top and bottom bands, can generally describe the deformation related to both phase transformation and elasticity simultaneously. In addition, the height $\Delta \tau^{\rm T}$ decrease with temperature increase could reflect some experimental measurements such as those illustrated in the work by Funakubo (1987). This trend is also predicted by Landau-Devonshire's model (Muller and Xu, 1991), for which the load-deformation diagrams in

different temperatures are shown in Figure 26. However, in Muller and Xu's work (1991), an opposite phenomenon was observed experimentally, which shown the loop height slightly increases with the temperature increase. Therefore a corresponding model was suggested to describe this in their approach.

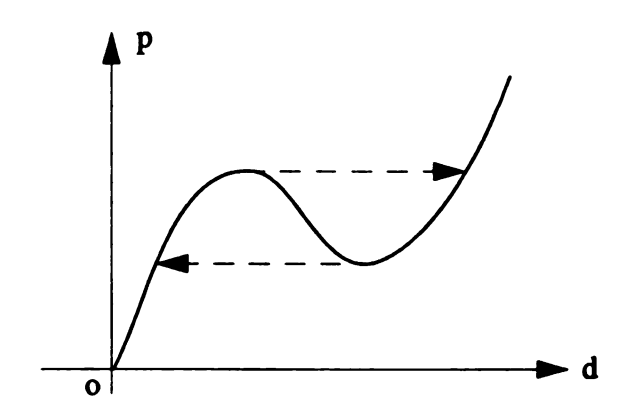


Figure 25. By Falk's model (1980), austenite transforming to martensite occurs at the highest point on the left ascending branch (top dashed line) upon loading. The reverse transformation, martensite to austenite occurs at the lowest point on the right ascending branch upon unloading.

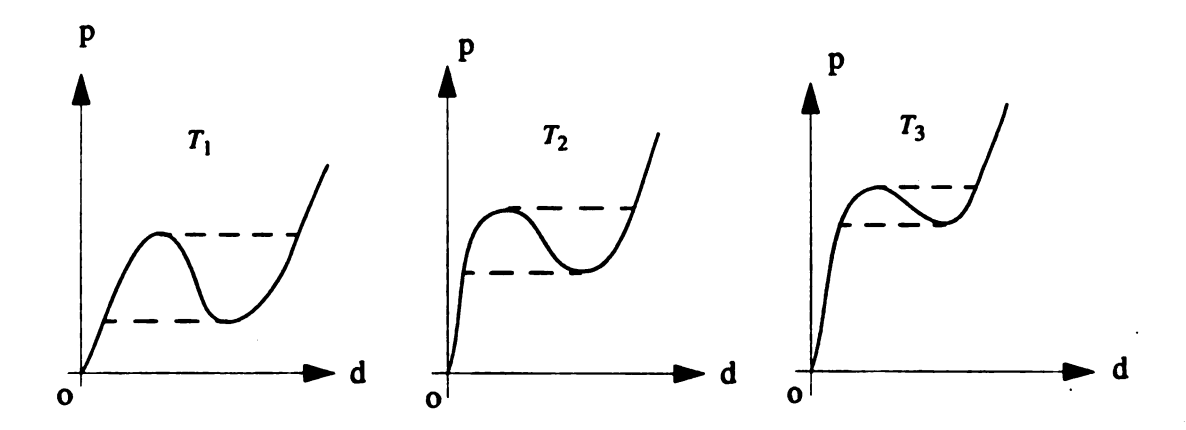


Figure 26. By Landau-Devonshire's model, load-deformation diagrams in three different temperatures ($T_1 < T_2 < T_3$) show that the heights of the hysteresis loops decrease with the temperature increase.

6.1.2 Internal Hysteresis Loops

Internal hysteresis loops are an important behavior. For the specified material with M_s $< A_s$, we will study how the internal hysteresis loop is conducted in the present model. In particular, we retrieve the results similar to those of the work by Ivshin and Pence (1994 b) from their one variant investigation and in so doing provide a mathematical treatment of an intensity filtering phenomenon.

For illustration we employ the pseudoelastic behavior at test temperature $T_t = 335$ °K $> A_f$ (Figure 27). The $A \rightarrow M_+$ and $M_+ \rightarrow A$ start stresses are denoted as $\tau^{AM}(T_t)$ and $\tau^{MA}(T_t)$ respectively, so that the *top band* and *bottom band* of the dead zone are defined by

$$\tau^{AM}(T_i) = \frac{-k_1 + \sqrt{k_1^2 - 4k_2(M_s - T_i)}}{2k_2}, \qquad (6.1.2.1)$$

$$\tau^{MA}(T_t) = \frac{-k_1 + \sqrt{k_1^2 - 4k_2(A_s - T_t)}}{2k_2},$$
(6.1.2.2)

respectively. With respect to Figure 27, loading from pure austenite to point a (above the stress $\tau = \tau^{AM}(T_t)$ but below the stress at which the $A \to M_+$ transformation is complete) gives a mixed state of A and M_+ . Then unloading remains elastic until point b on the bottom band. The slope value of this unloading portion from a to b is between that of elastic austenite (on the left side) and elastic martensite (on the right side) because the material state is a mixture of austenite and martensite (in general $\mu_A > \mu_M$). Further unloading from point b leads the curve to point b0, during which process $M_+ \to A$ 1 occurs. Point b1 coalesces with point b2 if the unloading is large enough to cause b3 to go to completion.

If reloading from point b, then the curve goes back elastically to point d on the same track as the unloading. This would be followed by $A \to M_+$ processes during loading to point e. Point e approaches point g if the loading causes $A \to M_+$ to go to completion. This is a behavior different from the plastic hardening in which reloading from point b will return elastically to point a.

On the other hand, if reloading from point c, then the behavior is elastic to point h with a mixture state of austenite and martensite inherited from point c. It then travels from h toward g monotonically during which $A \rightarrow M_+$ occurs.

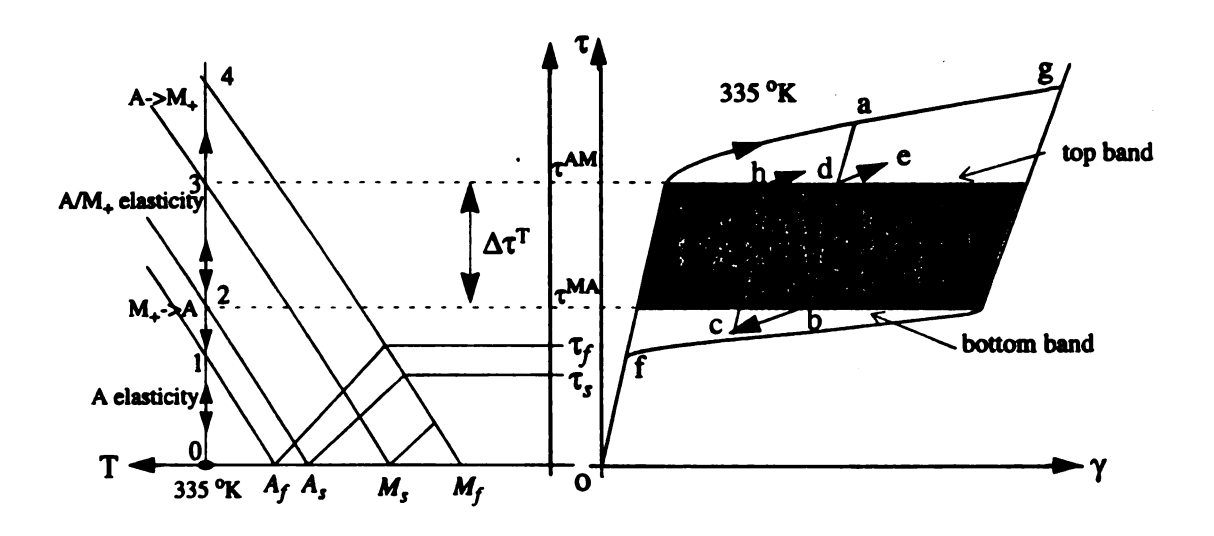


Figure 27. A dead zone between the top and bottom bands in the stress-strain diagram is illustrated. This dead zone corresponds to the portion between points 2 and 3 in the phase diagram. Points f and g correspond in stress-strain diagram to points 1 and 4 in the phase diagram. The internal loop formation condition is that unloading has to reach the bottom band and loading has to reach the top band shown as a-d-b-c-h path.

It is conspicuous from the above analysis for the material obeying $M_s < A_s$ that forward transformation $A \to M_+$ can only occur once the load reaches the top band $\tau =$

 $\tau^{AM}(T_t)$. The reverse transformation $M_{\perp} \to A$ can only occur once the unloading reaches the bottom band $\tau = \tau^{MA}(T_t)$. Any loading/unloading wholly between the two bands is conducted elastically at the modulus associated with the mixture. Consequently, a necessary condition for a an internal loop formation is that a cycling load has to have the maximum load larger than the top band and have the minimum load smaller than the bottom band. This is different with the model made by Muller and his colleagues (1991, 1993), in which the internal transformation is governed by a straight line connecting the martensite start stress and the austenite start stress in the stress-strain hysteresis loop. Another approach by Tanaka et al. (1994) involves internal transformation that is governed by two curved lines, one of which is connected with the martensite start stress and controls transformation $A \rightarrow M$ for loading internal paths. The other is connected with the austenite start stress and controls transformation $M \rightarrow A$ for unloading internal paths. The reason for the curved internal transformation lines is that they believe that the formation of the internal loops (subloops) depends upon the prior transformation through the dependence of internal transformation stresses on the transformation history. In the present model, the evolution of internal loops depends on the transformation history but the internal transformation stresses are taken as constants which implies that the phase diagram is fixed.

It can be also shown with the present model that, if loading from pure austenite state to a point above the top band, again say, point a, is followed by unloading to any point above point d, then oscillating the load in a small domain around the selected point will eventually eliminate all austenite phase and end up with pure M_+ phase. Similarly, an oscillation of loads in a small domain around a point on or below the bottom band will eliminate all the M_+ phase and end up with pure austenite phase A. This concludes that the top and bottom bands work, in a certain sense like, a phase filter to sift austenite A and M_+ variant

respectively when the specified oscillating load is applied away from the two bands. Finally oscillating around a point between the bands will give convergence to a mixture state that is independent of initial conditions. This phenomenon is connected with the infinitesimal loop behavior discussed in Ivshin and Pence (1994 a).

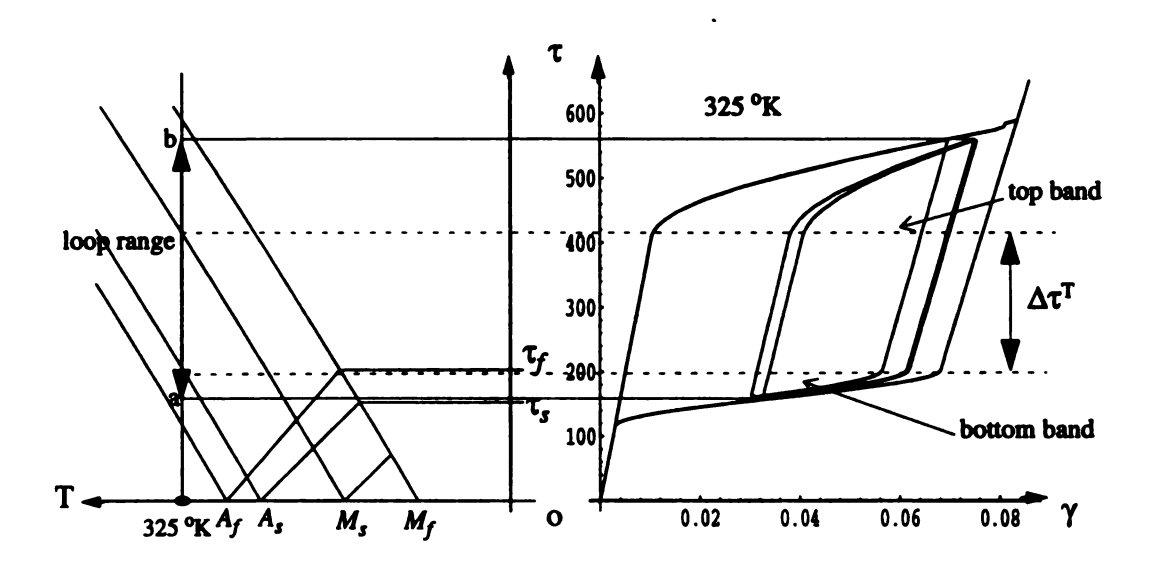


Figure 28. The stress-strain trajectory approaches a stable internal loop in the stress-strain diagram with oscillating scope of stress between points a and b (between τ^b and τ^t in stresses) in the phase diagram.

As a simulation result, an internal saturated hysteresis loop (Figure 28) is obtained at $T_t = 325$ °K under three cycles between $\tau^b = 160$ and $\tau^t = 560$ MPa in stress. It can be observed from Figure 28 that the internal loops drift to the right with respect to the original one, and quickly approach a firm position. This corresponds to a tendency that strains in a same stress level may initially vary with the cycle number, but then quickly settle to a stable internal loop after several cycles. We are going to prove this point in the following for a stress oscillation $\tau^b \le \tau \le \tau^t$ where $\tau^b < \tau^{MA}$ and $\tau^t > \tau^{AM}$ as shown in Figure 29.

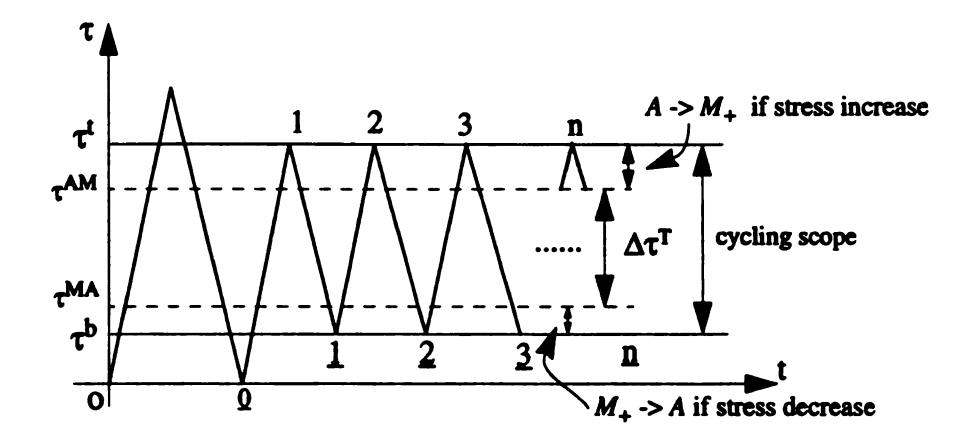


Figure 29. Cycling loads are applied between $\tau = \tau^b < \tau^{MA}$ and $\tau = \tau^t > \tau^{AM}$ at test temperature $T > A_f$ to form internal hysteresis loops. It can be seen that the top and bottom bands are covered inside the cycling range.

It should be noted that $T > A_f$ and $\tau > 0$ imply that $\xi_- = 0$ so that only transformations $A \leftrightarrow M_+$ are involved in the particular loading/unloading process. Based on equation (4.3.2.3) the right-shear martensite phase fraction is generated for $A \to M_+$ when the stress increases between $\tau = \tau^{AM}$ and $\tau = \tau^t$ MPa,

$$\xi_{+} = 1 - \frac{(\xi_{A})_{\mathbf{p}-\underline{1}}}{\sqrt{(\alpha_{A+})_{\mathbf{p}-1}}} \sqrt{\alpha_{A+}}.$$
 (6.1.2.3)

Here $(\xi_A)_{\bar{Q}} = 1$ and $\underline{n} (=1, 2, 3, ...)$ indicates the point numbers on the lower stress line at $\tau = \tau^b$ MPa. Since all the points \underline{n} -1 are on $\tau = \tau^b < \tau^{MA}$, it follows that all the values of $(\alpha_{A+})_{n-1} = 1$. Based on equation (4.2.2.3) the austenite phase fraction is found as the following for $M_+ \to A$ when the stress decreases between $\tau = \tau^{MA}$ and $\tau = \tau^b$,

$$\xi_A = 1 - \frac{(\xi_+)_n}{1 - (\alpha_{+A})_n} (1 - \alpha_{+A}),$$
 (6.1.2.4)

here n (=1, 2, 3, ...) indicates the point numbers on the upper stress line at $\tau = 426.6$ MPa. Since all the point n are on $\tau = 426.6$ MPa > τ^{AM} , it follows that all of the values of $(\alpha_{+A})_n = 0$. Thus the values of ξ_+ at each top peak for $\tau = \tau^t$ are $(\xi_+)_n = 1 - (\xi_A)_{n-1} \sqrt{(\alpha_{A+})_n}$ while the values of ξ_A at each bottom peak on $\tau = \tau^b$ are $(\xi_A)_n = 1 - (\xi_+)_n (1 - (\alpha_{+A})_n)$. Since α_{A+} is simply a function of τ and T, all the $(\alpha_{A+})_n$ are equal, as are all $(\alpha_{+A})_n$. For convenience, let $(\alpha_{A+})_n = u$ and $(\alpha_{+A})_n = v$ (n =1, 2, 3, ... and n =1, 2, 3, ...). Therefore, the M_+ phase fraction at point n on $\tau = \tau^t$ can be written as

$$(\xi_{+})_{n} = \left(\sum_{i=1}^{n} (uv)^{i-1}\right) (\xi_{+})_{1}. \tag{6.1.2.5}$$

Since the cycling load/unload conducts an incomplete transformation for both forward and reverse transitions $A \leftrightarrow M_+$, we have 0 < u, v < 1. Thus (6.1.2.5) converges to a limit

$$(\xi_{+})_{\infty} = \frac{(\xi_{+})_{1}}{1 - uv} = \frac{1 - \sqrt{u}}{1 - uv},$$
 (6.1.2.6)

which is larger than $(\xi_+)_1$. By (6.1.2.4) and (6.1.2.6) the austenite phase fraction on $\tau = \tau^b$ converges to a limit

$$(\xi_A)_{\underline{\infty}} = 1 - \frac{1 - \sqrt{u}}{1 - uv} (1 - v).$$
 (6.1.2.7)

The overall strain expression based on (2.1.0.2) can be rewritten,

$$\gamma = \frac{\tau}{\mu_A} + \left(\frac{\tau}{\mu_M} - \frac{\tau}{\mu_A} + \gamma^*\right) \xi_+, \qquad (6.1.2.8)$$

for this particular loading/unloading condition. Thus the strain converges to fixed values on both top and bottom peaks of the cycling which means that the internal loops in this example move to the right and approach a saturated position. The "right move" tendency corresponds to a situation for phase transformations that more martensite (or twins) is (are) generated during the cyclic load before the saturation is reached. This is similar to the softening feature of materials under high temperature creep.

6.1.3 Shape Memory Effect and Isothermal Behavior below A_f

Shape memory effects occur when the alloy is deformed into a biassed martensite phase and does not revert to a self-accommodated morphology upon unloading. Its initial shape is recovered when heated into the stable austenite regime, and then cooled back to the original temperature.

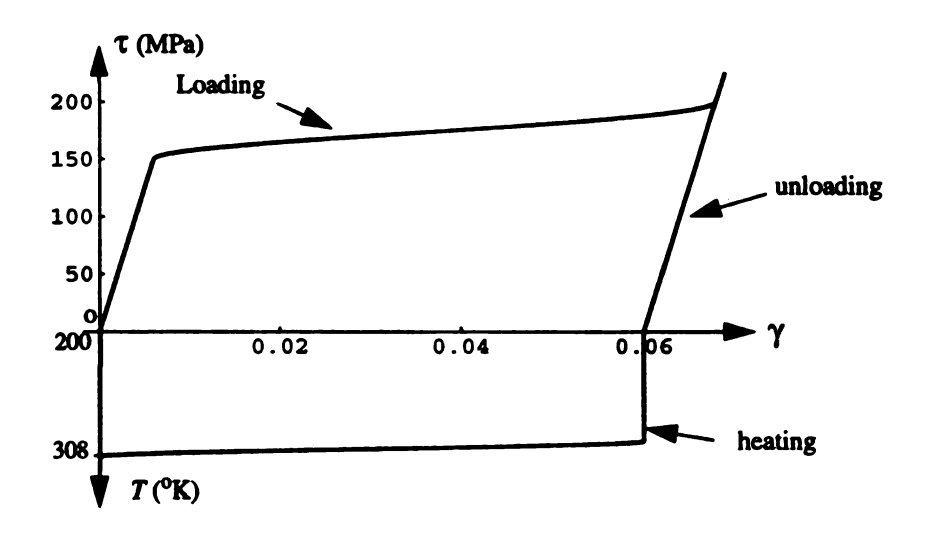


Figure 30. Shape memory effects occur during loading-unloading-heating-cooling processes.

Here the test temperature of loading/unloading $T_t = 200$ °K which is below $M_f (= 235$ o K). After unloading the temperature is then increased to A_{f} . The initial phase fraction condition used in the present case is obtained by decreasing the temperature from above A_f to the test temperature under a free-stress situation (CFAF), thus it is random martensite ξ = {0.5, 0, 0.5}. Upon loading (Figure 30) equal elastic deformation occurs in the two martensite variants for stress below the detwinning flow τ_s =150 MPa. This is followed by a detwinning process $M_{-} \rightarrow M_{+}$ which involves the migration of twinning interfaces within the two martensite variant mixture. This kind of motion of twinning interfaces needs gradual increases of external driving forces to overcome the interface resistance to motion. This process is complete at $\tau = \tau_f$ Further loading then involves pure elastic behavior of the fully detwinned martensite (M_{+}) (the tail part on Figure 30). Unloading from the maximum stress point to a stress free condition makes the stress/strain relation track on a linear path with the martensite modulus as the slope. This gives a residual strain equal to the phase transformation strain upon unloading to zero stress. Heating the specimen to the temperature A_f transforms $M_+ \to A$ and so eliminates all the residual strain. Cooling again gives random martensite and so leaves the strain unchanged.

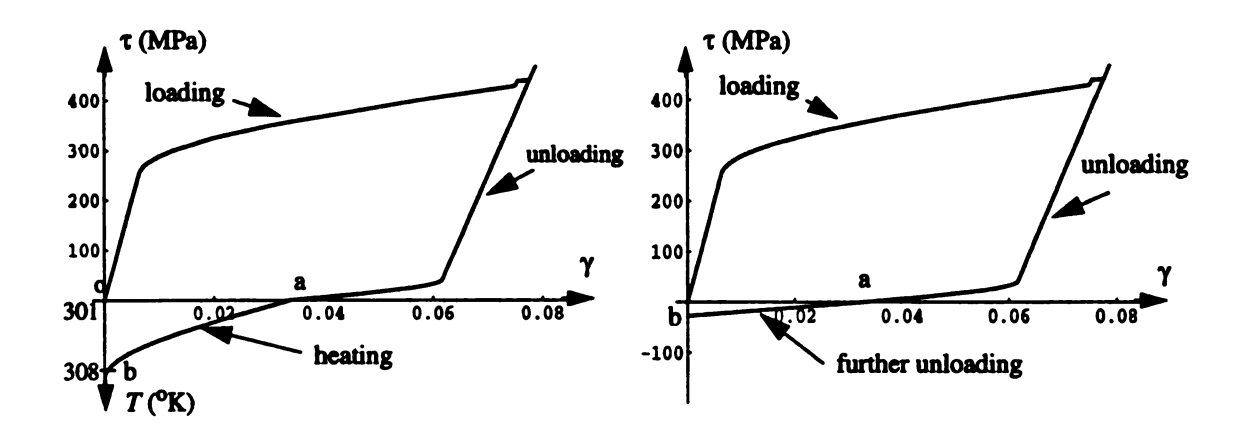


Figure 31. Two different procedures recover the residual strain. (a) shows the residual strain recovered upon heating, (b) shows that the residual strain can be recovered by further unloading. Here the test temperature is 301 $^{\rm o}$ K during the loading/unloading process and the original phase fraction is $\xi = \{0, 1, 0\}$.

In general, the residual strain associated with unloading is caused by certain special martensite variants remaining, and it can be recovered upon heating to above A_f . Discussions related with this issue have been conducted by either experimental measurements and theoretical approaches (Funakubo, 1987). In addition, the present model not only gives strain annihilation by heating/cooling (as just shown) but also illustrates that the residual strain can be recovered by "further unloading". Here the unloading is always with respect to loading, for example, at certain temperature levels, increasing the stress causes $A \rightarrow M_+$ to become active, which is the loading process. In the opposite, decreasing the stress causes $A \rightarrow M_+$ to become active, which is the unloading process. When the stress returns to zero, process $M_+ \rightarrow A$ may or may not be complete. The complete case comports to pseudoelasticity while the incomplete case remains at residual strain. Based on the

present model, any such remaining strain can be recovered by heating and cooling (a to b in Figure 31. (a)). Conversely, further unloading, which means continuous decrease of the stress to negative values, is an alternative way to either complete or partially complete the process $M_+ \to A$ (a to b in Figure 31. (b)). Actually, this further unloading is an opposite loading with respect to the loading of increase stress, which is favored for the growth of martensite variant M_- . Thermodynamically, this corresponds to a situation for which the energy barrier for phase transformation $M_+ \to A$ is smaller than that of detwinning $M_+ \to M_-$ in the temperature range between A_f and T_{fs} (see section 2.6). A similar condition is held for $M_- \to A$ when stress increases to a positive value smaller than τ_f .

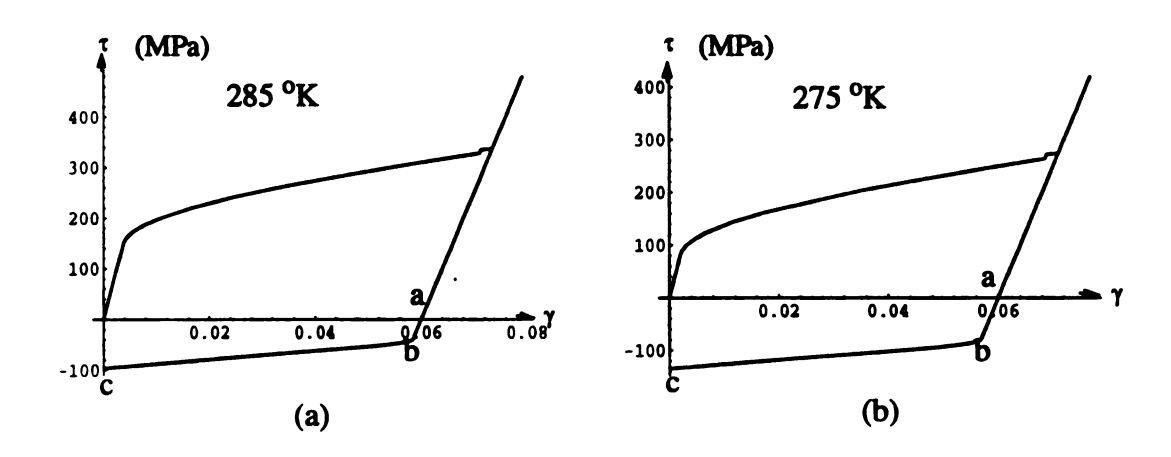


Figure 32. The residual strains are recovered by further unloading $(a \to b \to c)$. The plateau of the transformation $A \to M_+$ decreases with the test temperature decrease. In the opposite, the yielding plateau of the reverse transformation $M_+ \to A$ increases in the negative direction of the τ -axis as the test temperature decreases.

To demonstrate this phenomenon, consider an example with a initial condition $\{\xi_-, \xi_A, \xi_+\}=\{0, 1, 0\}$ at test temperature $T_t=301$ °K below A_f (=308 °K). Two stress/strain behav-

iors are obtained for the residual strain recovery by either heating or by further unloading (Figure 31). If the test temperature is now decreased then the stress/strain profiles move down along τ -axis (Figure 32). This *Bauschinger effect* type of phenomenon can be observed in a certain test temperature range (Figure 32 (a)), which is a concept from classical plastic theory to reflect an experimental observation that, after a certain amount of forward plastic deformation in tension or compression, the material yields at a lower stress when the direction of loading is reversed than for continued forward deformation.

Ferroelastic behaviors (Bondaryev and Wayman, 1988) are simulated at test temperature $T_t = 200$ °K with initial condition $\xi = \{0.5, 0, 0.5\}$ (Figure 33).

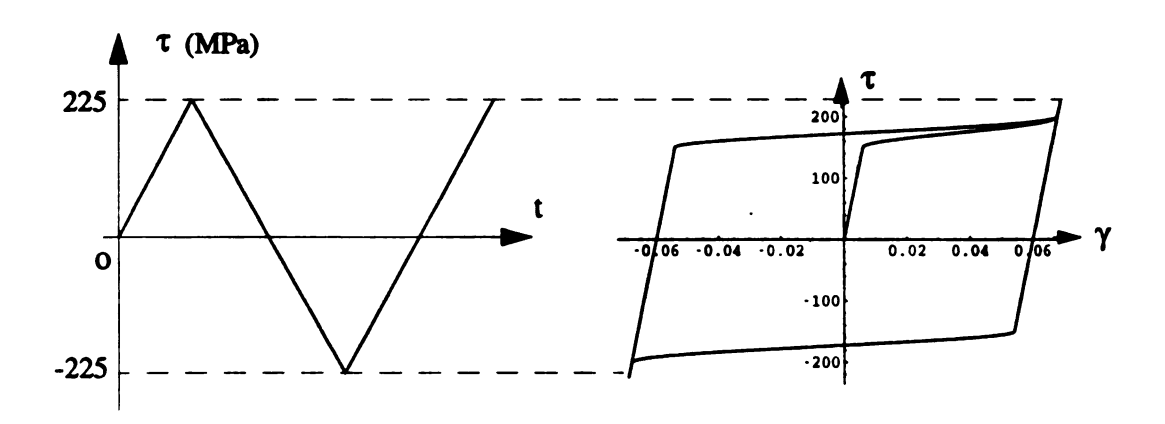


Figure 33. Ferroelastic behaviors in both tension and compression conditions at test temperature $T_t = 200$. In $\tau > 0$, $M_- \rightarrow M_+$ process is involved with the transformation, while, in $\tau < 0$, $M_+ \rightarrow M_-$ process is involved with the transformation.

In addition to pseudoelasticity and shape memory, there are other isothermal behaviors between A_f and M_f of interest. Since the initial conditions have a large effect on the ensuing stress/strain relation associated with loading and unloading, in the following we will show two groups of graphics regarding the two kinds of initial conditions CFAF and

HFMF introduced in Section 2.5. Recall that CFAF is obtained by cooling the temperature from above A_f to the test temperature, which corresponds to an initial condition of maximum austenite (Figure 34). The other (HFMF) is obtained by heating the temperature from below M_f to the test temperature, which corresponds to an initial condition of maximum equal amount martensite (Figure 35). It is noted that the model allows for transformations $M_- \to A$ to occur in $\tau > 0$, and also allows for transformation $M_+ \to A$ to occur in $\tau < 0$. Increasing the stress to cause $M_- \to A$ in $\tau > 0$ could be regarded as further unloading with respect to decreasing the stress (loading) to cause $A \to M_-$ in $\tau < 0$ at the same temperature level. A similar discussion for $M_+ \to A$ to occur corresponding to decrease the stress in $\tau < 0$ can be arrived too.

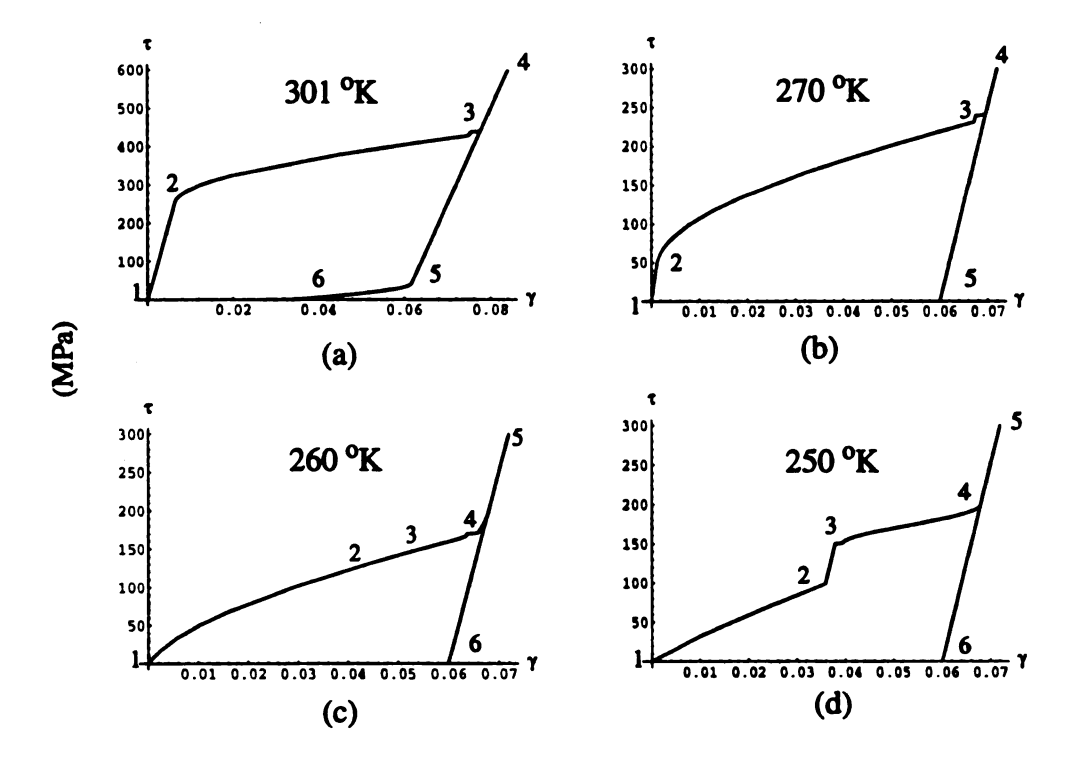


Figure 34. Initial conditions are obtained by cooling the temperature from above A_f to the test temperature in a stress free circumstance (CFAF). General features of the transformation process for loading/unloading were described in Figure 14. In (a) the initial condition is $\{0, 1, 0\}$. $1 \rightarrow 2$: austenite elastic deformation; $2 \rightarrow 3$: phase transformation $A \rightarrow M_{+}$; $3 \rightarrow 4$: M_{+} elastic deformation; $4 \rightarrow 5$: M_{+} elastic unloading; $5 \rightarrow 6$: partial reverse transformation $M_+ \to A$ which gives a certain amount of residual strain left at the end of the unloading. In (b) the initial condition is still $\{0, 1, 0\}$ because $270^{\circ} \text{K} > M_s$ (=263 ^oK). $1 \rightarrow 2 \rightarrow 3 \rightarrow 4$: conduct the same deformation mechanism as those segments in (a) correspondingly; $4 \rightarrow 5$: M_{+} elastic unloading. In (c) the initial condition is {0.0135, 0.973, 0.0135}. $1 \rightarrow 2$: phase transformation $A \rightarrow M_+$; $2 \rightarrow 3$: combined transformations $A \rightarrow M_{+}$ and $M_{-} \rightarrow A$; $3 \rightarrow 4$: detwinning $M_{-} \rightarrow M_{+}$; $4 \rightarrow 5$: M_{+} elastic deformation; $5 \rightarrow 6$: M_{+} elastic unloading. Since the phase fraction of M_{-} is small, there is no significant change in segments $1 \rightarrow 2$, $2 \rightarrow 3$ and $3 \rightarrow 4$. In (d) the initial condition is $\{0.222, 0.556,$ 0.222). $1 \rightarrow 2$: phase transformation $A \rightarrow M_+$; $2 \rightarrow 3$: elastic twinned martensite; $3 \rightarrow 4$: detwinning $M_{-} \rightarrow M_{+}$; $4 \rightarrow 5$: M_{+} elastic deformation; $5 \rightarrow 6$: M_{+} elastic unloading. In (b), (c) and (d) the residual strains are the phase transformation strain γ .

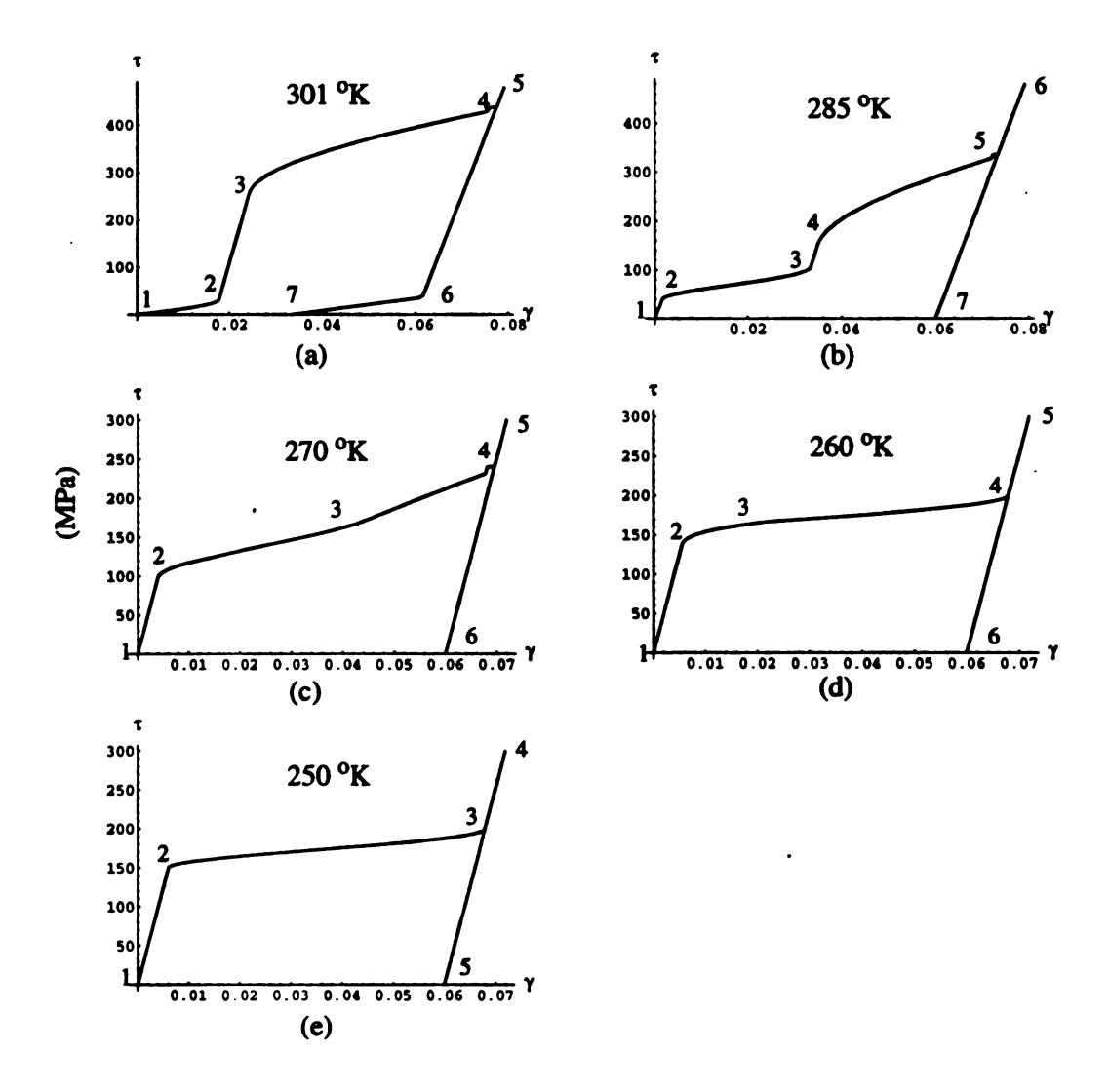


Figure 35. Initial conditions are obtained by heating the temperature from below M_f to the test temperature in a zero-stress condition (HFMF). General features of the transformation process for loading/unloading were described in Figure 15. In (a) the initial condition is $\{0.2801, 0.4397, 0.2801\}$. $1 \rightarrow 2$: phase transformation $M \rightarrow A$; $2 \rightarrow 3$: elasticity of combined austenite and right-shear martensite; $3 \rightarrow 4$: phase transformation $A \rightarrow M_+$; $4 \rightarrow 5$: M_+ elasticity; $5 \rightarrow 6$: elastic M_+ unloading; $6 \rightarrow 7$: partial reverse transformation $M_+ \rightarrow A$ upon continuous unloading which gives a certain amount of residual strain left at the end of the unloading. In (b) the initial condition is $\{0.5, 0, 0.5\}$ which is also the initial conditions for (c), (d) and (e). $1 \rightarrow 2$: fully twinned martensite elasticity; $2 \rightarrow 3$: phase transformation $M \rightarrow A$; $3 \rightarrow 4$: elasticity of combined austenite and right-shear martensite; $4 \rightarrow 5$: phase transformation $A \rightarrow M_+$; $5 \rightarrow 6$: M_+ elasticity; $6 \rightarrow 7$: elastic M_+ elastic unloading. In (c) $1 \rightarrow 2$: elasticity of twinned martensite; $2 \rightarrow 3$: combined

phase transformation $M_- \to A$ and $A \to M_+$; $3 \to 4$: phase transformation $A \to M_+$; $4 \to 5$ and $6 \to 7$ are similar to $5 \to 6$ and $6 \to 7$ in (b) respectively. In (d) $1 \to 2$: elasticity of twinned martensite; $2 \to 3$: combined phase transformation $M_- \to A$ and $A \to M_+$; $3 \to 4$: detwinning $M_- \to M_+$; $4 \to 5$ and $5 \to 6$ are similar to the corresponding sections in (c). The only difference of (e) with (d) is that there is only one section to conduct detwinning $M_- \to M_+$, which is $2 \to 3$. In (b), (c), (d) and (e) the residual strains left are phase transformation strain γ^* .

6.1.4 Load Cycling and Saturation

Based on the present model, saturated hysteresis loops usually occur in dual direction transformations where two or more phases compensate each other and eventually reach a balanced state of associated phases for the oscillating load process. This behavior, for example, was observed in the process $A \leftrightarrow M_{\perp}$ at high temperature oscillating of loads in Section 6.1.2. A oscillated stress-strain behavior with $0 \le \tau \le 150$ (MPa) is simulated at T = 270 °K < A_s (Figure 36). In this process with HFMF initial condition ($\xi = \{0.5, 0, 0.5\}$), all the three phases M_{-} , A and M_{+} are involved in different periods. Since the oscillated load is operated in $\tau > 0$, $M_{\perp} \to A$ and $A \to M_{\perp}$ occur during loading while only elastic relaxation takes place in the mixture state during unloading. M. phase is roughly devoured out after the fourth cycle, while A phase remains until the tongue-shape response reaches the far right lateral straight line (Figure 36 (b)). There is no stable saturated loop because there is no phase compensation in the unloading process. The yielding point on the outside profile (the same with Figure 35 (c)) is higher than the internal yielding points. This is because there is no austenite involved with the transformation at the very first loading so that the yielding does not occur until the path hits the nuetrality curve A_{s} . This triggers $M_{\perp} \to A$ which then supplies austenite for the immediate $A \to M_{\perp}$ process. Since austenite has been generated during the first cycle, the yielding occurs at lower stress in the following cycles as shown in Figure 36. The phase fraction distributions at the beginning of each cycle are listed in TABLE 8. The austenite reaches its maximum value right after the first cycle.

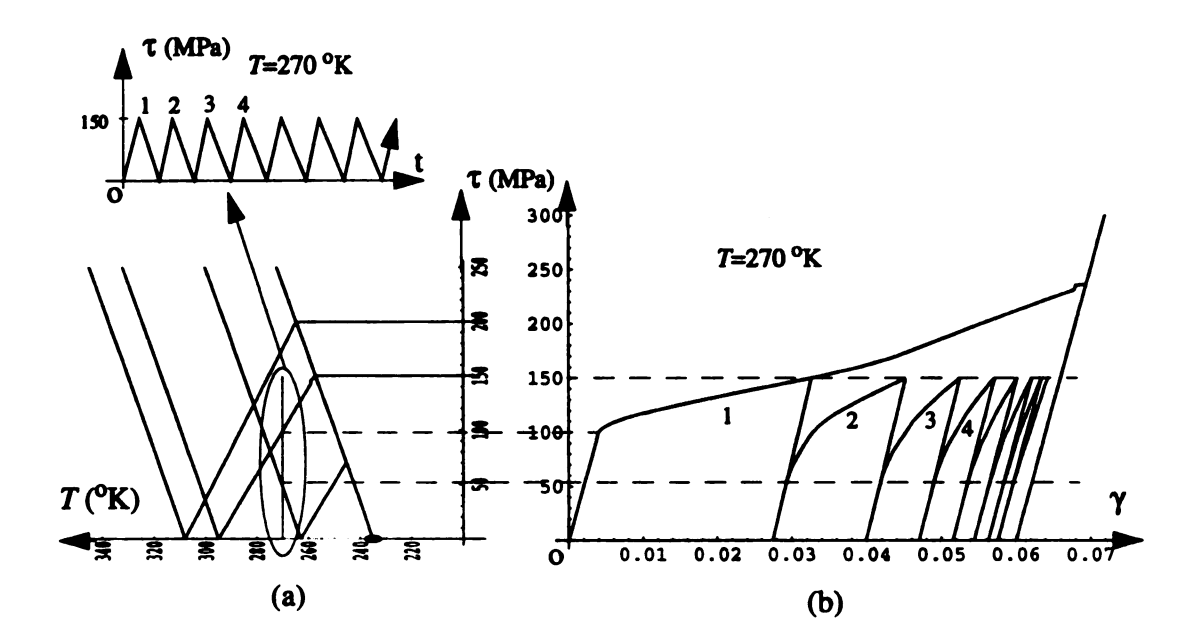


Figure 36. Isothermal response (b) under cyclic loads (a) at test temperature T = 270 °K (M_s < 270 °K < A_s). The initial condition is from HFMF with $\xi = \{0.5, 0, 0.5\}$. The outside profile is the same with Figure 35 (c). $M_- \rightarrow A$ and $A \rightarrow M_+$ occur upon loading while elastic relaxations in mixture phase states occur upon unloading. M_- phase is roughly consumed out after the fourth cycle. Austenite remains until the tongue-shape stress-strain response reaches the far right lateral straight line of the outside profile.

TABLE 8. Phase Fraction Distributions

cycle	phase fractions	
1	{0.5000, 0.0000, 0.5000}	
2	{0.1012, 0.3403, 0.5585}	
3	{0.0205, 0.2940, 0.6855}	
4	{0.0042, 0.2084, 0.7874}	
5	{0.0000, 0.1414, 0.8586}	
6	{0.0000, 0.0935, 0.9065}	
7	{0.0000, 0.0617, 0.9383}	
8	{0.0000, 0.0407, 0.9593}	
:	:	
∞	{0.0000, 0.0000, 1.0000}	

6.2 Differences between Loading-Cooling and Cooling-Loading Paths

According to Duerig, et al., 1988, "For reasons which are not entirely clear, plastic deformation will occur below the martensitic yield strength in many materials if one applies the load while cooling through M_s " (pp. 183-184). We now show that behavior of this type arises naturally in the present model. The essential feature of this argument were presented in the approach by Wu, Pence and Grummon (1996). In particular we consider two routes for obtaining oriented martensite (M_{\perp}) at a low temperature and high stress beginning from stress-free austenite at high temperature. Here the high temperature is taken to be T = 325 °K (> A_f) and the low temperature is taken as T = 225 °K (< M_f). Various final values of stress τ_i will be considered. For each such stress value, one of the two routes involves loading at T = 325 °K from $\tau = 0$ to τ_i , followed by cooling at $\tau = \tau_i$ from T= 325 °K to T = 225 °K. The other route involves cooling at τ = 0 from T = 325 °K to T = 225 °K, followed by loading at T = 225 °K from $\tau = 0$ to τ_i . We refer to these two routes as loading-cooling and as cooling-loading paths respectively (Figure 37). In all cases the final phase fraction state is martensitic: $\{\xi_-, \xi_A, \xi_+\} = \{\xi_-, 0, \xi_+\}$. However for a certain range of τ , namely $\tau < \tau_f$, one obtains that the value of ξ_+ generated by the loading-cooling path is greater than that generated by the cooling-loading path.

The envelope functions to be used in the following are of the forms (6.1.0.1) and (6.1.0.2). All the material properties are given by TABLE 2 of section 2.5.

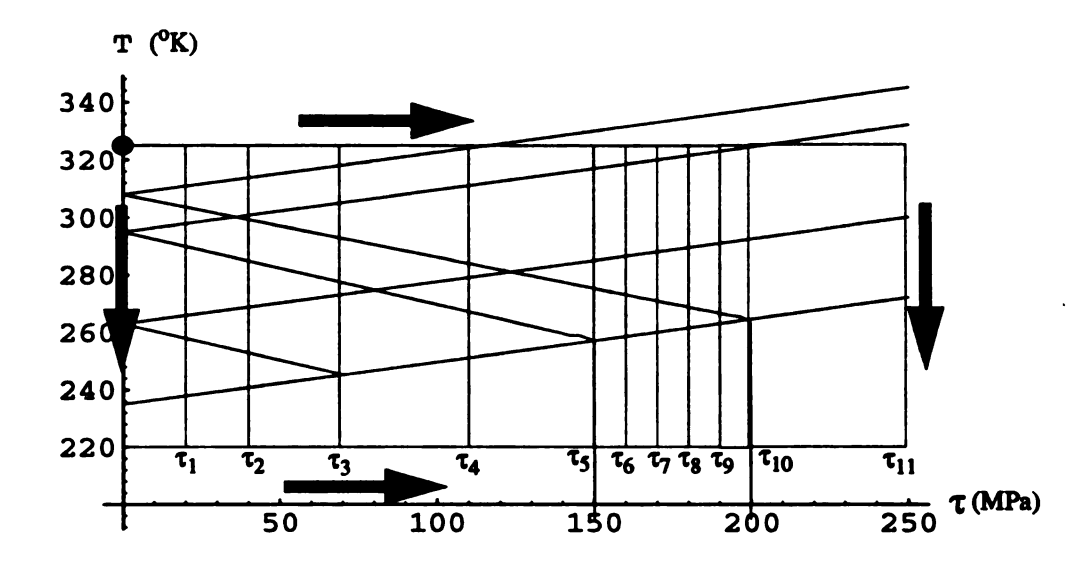


Figure 37. Two groups of driving paths starting at point (0, 325) on *T*-axis with initial condition {0, 1, 0} go to point (20, 220), (40, 220), (68.9, 220), (110, 220), (150, 220), (160, 220), (170, 220), (180, 220), (190, 220) respectively.

Following the above two kinds of driving paths the model predicts a natural path-dependent phenomenon of shape memory materials. In the loading-cooling paths, the loading portion triggers trivial (TT4), so as to only conduct austenite elastic deformations, and the cooling portion triggers (TT2). Since $\tau > 0$ transformation $A \to M_+$ occurs earlier than $A \to M_-$ upon cooling, therefore, at the end of the driving path the phase fraction ξ_+ is larger than phase fraction ξ_- (and $\xi_A = 0$). There is a critical stress τ^* (= τ_3) that is the intersection stress between nuetrality curves M_{f+} and M_{s-} :

$$\tau^* = \frac{-(k_1 - k_s) + \sqrt{(k_1 - k_s)^2 + 4k_2(M_s - M_f)}}{2k_2}.$$
 (6.2.0.1)

For the present parameters used here (TABLE 2 of Section 2.5), this critical stress τ^* =

68.9 MPa. If $\tau_i < \tau^*$, then further cooling to temperature 220 °K will generate both of the martensite variants. If the stress surpasses τ^* during loading, then further cooling to temperature 220 °K will generate 100% M_+ martensite ({0, 0, 1}) because transformation $A \to M_-$ upon cooling can only be conducted in a stress domain [0, τ^*) in $\tau > 0$.

In the cooling-loading driving paths, (TT2) is triggered by the cooling portion and (TT5) is triggered the loading portion. Cooling from temperature 325 °K to 220 °K along T-axis is a self-accommondated process, so as to produce an equal amount of the two variants of martensite. Then loading at temperature 220 °K will only cause elastic deformations of this equal self-accommodated martensite until the detwinning flow stress τ_s . Increasing the stress beyond τ_s then induces the detwinning process $M_- \to M_+$.

The unequal final amounts of the phase fractions of the martensite variants produced by the two different kinds of the driving paths are illustrated in Figure 38. On the other hand, since the loading-cooling paths generate more M_+ if $\tau < \tau_f$ they give a larger deformation than the cooling-loading paths. In other words, the first process of loading-cooling only generates an elastic deformation in the austenite. The following process (cooling) generates a deformation associated with phase transformation $A \to M_+$ which is larger than the elastic deformation. However, following the cooling-loading driving paths, there is no deformation in the self-accommondated cooling process. The loading portion then will only generate an elastic deformation of martensite before the stress reaches the detwinning stress τ_s .

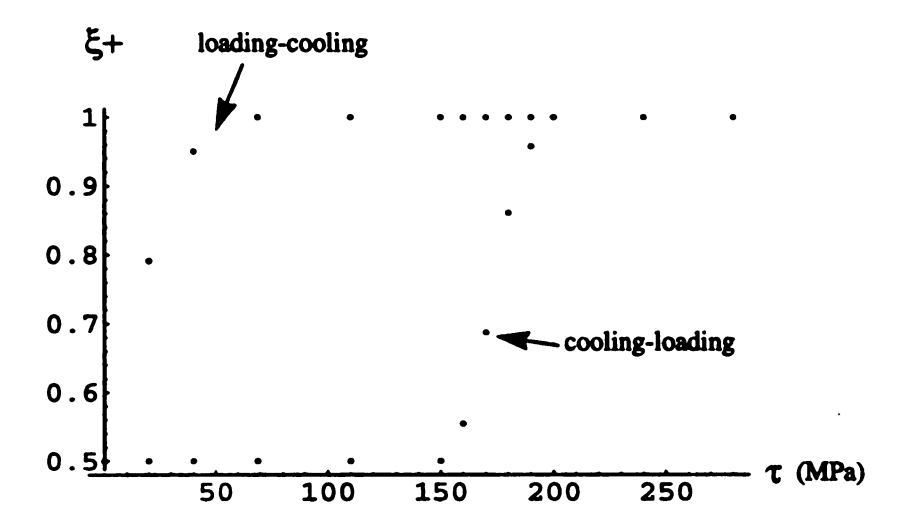


Figure 38. Phase fractions of the martensite variant M_+ upon driving paths of loading-cooling (upper point plot) and cooling-loading (lower point plot). Here $\tau^{\bullet} = 68.9$, $\tau_{s} = 150$ and $\tau_{f} = 200$ MPa.

6.3 Comparison with Other Models

In Brinson's approach (1993) martensite phase fractions are distinguished as stress-induced martensite M^d (favored at a specified stress) and thermo-induced martensite M^t , the latter of which is regarded as self-accommondated. This contrasts to the model under consideration here in which the martensite phase fractions are distinguished in terms of variant structures. Note, however, that a connection between these two viewpoints is established by grouping our minority variant with an equal amount of the majority variant to obtain a self-accommondated martensite structure that can be identified with Bekker and Brinson's thermo-induced martensite. Then the excess majority variant is identified as purely stress induced martensite. That is, one takes

$$\xi_t = 2min(\xi_+, \xi_-), \xi_d = \xi_+ + \xi_- - \xi_t.$$
 (6.3.0.1)

To illustrate this transformation, we define two sets of portions of all state paths. The first one P_+ is a set of all portions of the state paths along which the relation $\xi_+ > \xi_-$ is held. The other one P_- is a set of all portions of the state paths along which the relation $\xi_+ < \xi_-$ is held. If a state path or part of the state path belongs to P_+ , following it M_+ is the majority variant, so that

$$\xi_1 = 2\xi_2, \quad \xi_2 = \xi_2 - \xi_2,$$
 (6.3.0.2)

or in the reverse forms

$$\xi = \xi/2, \quad \xi_{+} = \xi_{d} + \xi/2.$$
 (6.3.0.3)

The governing equations corresponding the above situation for all the six transition types, in terms of ξ_l and ξ_d are:

(TT1):

$$\frac{d\xi_t}{dt} = -\left(\frac{\xi_t}{1-\alpha_{-A}}\right)\frac{d\alpha_{-A}}{dt}, \frac{d\xi_d}{dt} = \frac{1}{2}\left(\frac{\xi_t}{1-\alpha_{-A}}\right)\frac{d\alpha_{-A}}{dt} - \frac{1}{2}\left(\frac{2\xi_d + \xi_t}{1-\alpha_{+A}}\right)\frac{d\alpha_{+A}}{dt}.$$
 (6.3.0.4)

(TT2):

$$\frac{d\xi_t}{dt} = -\left(\frac{1-\xi_d-\xi_t}{\alpha_{A^-}}\right)\frac{d\alpha_{A^-}}{dt}, \frac{d\xi_d}{dt} = \left(\frac{1-\xi_d-\xi_t}{2\alpha_{A^-}}\right)\frac{d\alpha_{A^-}}{dt} - \left(\frac{1-\xi_d-\xi_t}{2\alpha_{A^+}}\right)\frac{d\alpha_{A^+}}{dt}. \quad (6.3.0.5)$$

(TT3):

$$\frac{d\xi_t}{dt} = -\left(\frac{1 - \xi_d - \xi_t}{\alpha_{A^-}}\right)\frac{d\alpha_{A^-}}{dt}, \frac{d\xi_d}{dt} = \left(\frac{1 - \xi_d - \xi_t}{2\alpha_{A^-}}\right)\frac{d\alpha_{A^-}}{dt} - \frac{1}{2}\left(\frac{2\xi_d + \xi_t}{1 - \alpha_{+A}}\right)\frac{d\alpha_{+A}}{dt}. \quad (6.3.0.6)$$

(TT4):

$$\frac{d\xi_t}{dt} = -\left(\frac{\xi_t}{1-\alpha_{-A}}\right)\frac{d\alpha_{-A}}{dt}, \frac{d\xi_d}{dt} = \frac{1}{2}\left(\frac{\xi_t}{1-\alpha_{-A}}\right)\frac{d\alpha_{-A}}{dt} - \left(\frac{1-\xi_d-\xi_t}{2\alpha_{A+}}\right)\frac{d\alpha_{-A}}{dt}.$$
 (6.3.0.7)

(TT5):

$$\frac{d\xi_t}{dt} = -\left(\frac{\xi_t}{1 - \alpha_{-A}}\right)\frac{d\alpha_{-A}}{dt}, \, \xi_d = 1 - \xi_t. \tag{6.3.0.8}$$

(TT6):

$$\frac{d\xi_t}{dt} = \left(\frac{2 - \xi_t}{1 - \alpha_{+A}}\right) \frac{d\alpha_{+A}}{dt}, \, \xi_d = 1 - \xi_t. \tag{6.3.0.9}$$

The path-independent issue about the above symbolic description can be obtained by expression (6.3.0.2) and the previous achievement in Section 5.1. Thus ξ_A , ξ_d and ξ_t are path independent for transition type (TT1), (TT5) and (TT6), whereas only ξ_A is path independent for (TT2). Note now, however, for (TT3), where only ξ_+ is path independent, that this is insufficient to give path independence for either ξ_A , ξ_d or ξ_t . A similar lack of any path independent component ξ_A , ξ_d and ξ_t occurs for (TT4).

It should be noted that the above equations or their solutions corresponds to a situation that ξ_+ is rich. Following a continuous state path in the (σ, T) -plane, the sovereign phase between ξ_+ and ξ_- may exchange each other. If in some portions that ξ_- is rich, one should use another group of governing equations for the six transition types, which are modified by the following relation based on the rule (6.3.0.1).

$$\xi_{1} = 2\xi_{+}, \quad \xi_{2} = \xi_{1} - \xi_{+}, \quad (6.3.0.10)$$

7 APPLICATION OF THE MODEL TO AN ACTUATOR DESIGN

As illustrated in the previous chapters, shape memory alloys conduct many interesting and useful behaviors under thermomechanical loads. One of these, shape memory, is primarily responsible for many smart device designs. Actually, the shape memory effect is an ability of a material to recover a significant inelastic deformation upon heating (Figure 30). This significant inelastic deformation is caused by either phase transformations between austenite and martensite or martensite variant reorientations. Based on this kind of deformation mechanism, functional thermomechanical devices are designed for various purposes in different aspects. In the following we are going to model the behavior of a potential reciprocal device, Two-Stroke Thermal Engine (TSTE), with the present two variant model. This contraption is designed to carry out a reciprocal movement upon thermal heating/cooling pulses controlled for example by an electrical signal. These trigger austenite martensite transformations and martensite variant reorientations in the device.

7.1 Analysis on Basic Structure of TSTE

The TSTE is made of two identical SMA elements which are confined between fixed frame constraints so that the overall length is constant. We use (I) and (II) to indicate the left and right elements respectively (Figure 39). Normalize the two lengths of the two ele-

ments by characteristic lengths which are taken to be the length of the element in a state of stress-free austenite, say, l_1 for the element (I) and l_2 for the element (II). Thermal expansion effects are neglected. At any point in the operation, the strain in each element is assumed to be uniform, and is due both to elastic stress and to transformation strains associated with the phase variant state of the element, $\xi^{I} = \{\xi^{I}_{-}, \xi^{I}_{A}, \xi^{I}_{+}\}$ and $\xi^{II} = \{\xi^{II}_{-}, \xi^{II}_{A}, \xi^{II}_{+}\}$. The phase fractions in each element obey the phase balance condition (1.2.0.1).

The reference configuration is obtained by the following three steps: (1) cooling both elements to a temperature T_o below M_f so as to transfer all austenite phase to random martensite phase, (2) stretching element (I) to a fully detwinned martensite phase (positively oriented) and then releasing the force, (3) connecting the two elements by a thickless rigid thermal isolation to form a interface between the two elements. This generates a stressfree reference configuration with element (I) positively oriented and element (II) fully twinned. The initial phase fractions corresponding to the reference state are $\xi^{I} = \{0, 0, 1\}$ and $\xi^{II} = \{0.5, 0, 0.5\}$.

The stress here is therefore regarded as a normal stress that is associated with normal strain caused by the interface movement due to the thermal heating/cooling pulses. To emphasize this feature we replace $\{\tau, \gamma, \mu\}$ by $\{\sigma, \epsilon, E\}$. Therefore, we use σ_I and σ_{II} (instead of τ_{sub}) to indicate the normal stresses in elements (I) and (II) respectively, and ϵ^* (instead of γ^*) to indicate the corresponding transformation strain. Since there is as yet no external load to be carried, the stresses equilibrate: $\sigma_I = \sigma_{II} = \sigma$.

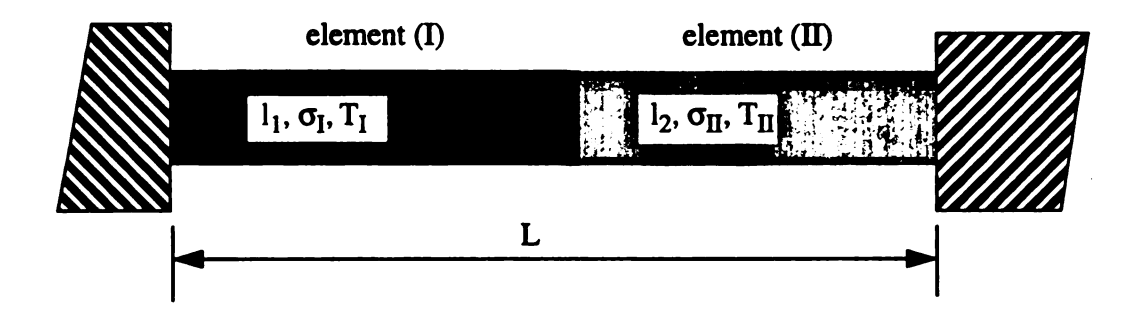


Figure 39. Structure of the TSTE confined in a fixed frame.

We will always operate the detwinned element (operating element) by applying a heating/cooling pulse while the other random twin element (response element) is passively driven due to the perfect interface bounding. Heating causes the oriented martensite to transform to austenite so as to annihilates the detwinning strain, which then pulls on the other element causing it to now detwin. Cooling the transformed austenite converts it to random martensite while the other element, now detwinned, undergoes elastic relaxation. Therefore, after a heating/cooling operation on one element, the states of the two elements should exchange with each other. An ideal operation involves a perfect switch between the two elements at the end of each operation. As we will see below, elastic deformation causes a departure from the ideal behavior. The switching of the state of the two elements supplies an initial condition for the following heating/cooling pulse on the other element. Repeatedly inputting a temperature pulse to the current detwinned side will generate some kind of cyclic response. In this study we want to characterize the limiting cyclic output. A similar study has been conducted by Ivshin and Pence (1992), in which a limit cyclic response of two-way shape memory effect was simulated when a laminated sample with residual stresses was considered. That study, however, only involved a one variant martensite model, and also did not involve alternating reciprocal action.

7.2 Deformation Consistency

The temperatures T_I and T_{II} in the two elements are regarded as explicit input variables, while stress σ , along with phase fractions ξ^I and ξ^{II} , are treated as output variables. Note since $\xi = \{\xi_-, \xi_A, \xi_+\}$ that there are totally seven output variables. The phase fraction balance gives two equations: $\xi^I_- + \xi^I_A + \xi^I_+ = 1$, $\xi^{II}_- + \xi^{II}_A + \xi^{II}_+ = 1$. There are two evolution equations governing the phase fractions ξ^I for the element (I), and two governing ξ^{II} for the element (II). The particular evolution equations to be used for each element will depend upon the transition type in action. So far there are six equations and seven unknowns, which is not a well posed problem. The final equation comes from the constraint condition for the movement of the perfectly bonded interface which involves all the input and output variables. This equation can be expressed as the following by setting the overall displacement away from stress-free austenite equal to the original displacement due to stress-free transformation strain in element (I),

$$l_{1}\{\xi_{-}^{I},\xi_{A}^{I},\xi_{+}^{I}\}\cdot\{\varepsilon_{-},\varepsilon_{A},\varepsilon_{+}\}+l_{2}\{\xi_{-}^{II},\xi_{A}^{II},\xi_{+}^{II}\}\cdot\{\varepsilon_{-},\varepsilon_{A},\varepsilon_{+}\}=l_{1}\varepsilon^{*},$$
 (7.2.0.1)

where

$$\{\varepsilon_{\cdot}, \varepsilon_{A}, \varepsilon_{+}\} = \left\{\frac{\sigma}{E_{M}} - \varepsilon^{*}, \frac{\sigma}{E_{A}}, \frac{\sigma}{E_{M}} + \varepsilon^{*}\right\}. \tag{7.2.0.2}$$

The interface displacement from its original location is determined by

$$\delta = l_1(\varepsilon^* - \{\xi_{-}^I, \xi_{A}^I, \xi_{+}^I\} \cdot \{\varepsilon_{-}, \varepsilon_{A}, \varepsilon_{+}\}), \qquad (7.2.0.3)$$

in terms of element (I), or

$$\delta = l_2\{\xi_-^{\mathrm{II}}, \xi_A^{\mathrm{II}}, \xi_+^{\mathrm{II}}\} \cdot \{\varepsilon_-, \varepsilon_A, \varepsilon_+\}, \qquad (7.2.0.4)$$

in terms of element (II).

Determinations of $\xi^{I} = \{\xi_{-}^{I}, \xi_{A}^{I}, \xi_{+}^{I}\}$ and $\xi^{II} = \{\xi_{-}^{II}, \xi_{A}^{II}, \xi_{+}^{II}\}$ depend upon the state path (σ, T) through transition type criteria and the evolution equations, where the temperature T as an input is given, and the stress σ needs to obey equation (7.2.0.1). Therefore, the imposed procedure is fully coupled. To solve this problem an initial judgement based upon the input information has to be made for choosing the transition type or the particular evolution equation for those phase fractions. This process will be seen in the following section.

Here, we only consider two elements with equal lengths in the stress-free austenite state, ie., $l_1 = l_2 = l$. Thus, equation (7.2.0.1) along with equation (7.2.0.2) becomes

$$\left(\frac{\sigma}{E_{M}} - \epsilon^{*}\right)(\xi_{-}^{I} + \xi_{-}^{II}) + \frac{\sigma}{E_{A}}(\xi_{A}^{I} + \xi_{A}^{II}) + \left(\frac{\sigma}{E_{M}} + \epsilon^{*}\right)(\xi_{+}^{I} + \xi_{+}^{II}) = \epsilon^{*}.$$
 (7.2.0.5)

The linear piecewise envelope functions as shown in equations (5.3.0.1) and (5.3.0.2), and the Y-unfolding derived in section 2.4.2 are going to be employed in the forthcoming analysis.

7.3 Heat-Cool Element(I): The First Stroke

In this section we will discuss the stress-temperature relation during the first heating/cooling (the first stroke) on the element (I) with a the special initial condition $\xi^{I} = \{0, 0, 1\}$ and $\xi^{II} = \{0.5, 0, 0.5\}$. The specialty of this initial condition is that, the operating element which is under heating/cooling is fully detwinned, and the response element which is in a constant temperature is in an even random martensite state. It will be seen that the initial condition for the following stroke will be $\xi^{II} = \{\Delta, 0, 1-\Delta\}$ and $\xi^{I} = \{0.5-\Delta, 0, 0.5+\Delta\}$ with $\Delta > 0$. There are three processes in the heating and three in the cooling, which are distinguished by either different transformation type or the absence of a phase transformation. Actually, the major displacement of the interface between the two elements is caused in the heating portion. However, a small displacement recovery takes place in the cooling portion.

7.3.1 Heating Process

We are now going to determine state paths $(\sigma, T_{\rm I})$ and $(\sigma, T_{\rm II})$ on the phase diagram. The initial conditions of $\xi^{\rm I} = \{0, 0, 1\}$ and $\xi^{\rm II} = \{0.5, 0, 0.5\}$ give that initially $\Delta = 0$. Heating element (I) causes the state path $(\sigma, T_{\rm I})$ for element (I) to increase up the T-axis from the initial point $(\sigma, T_{\rm I}) = (0, T_o = M_f)$ to the point $(0, A_s)$ while the state path $(\sigma, T_{\rm II})$ for element (II) stays at the initial point $(\sigma, T_{\rm II}) = (0, T_o = M_f)$. In this process for $T_{\rm I} < A_s$ there is no movement of the interface between the two elements because of the absence of phase transformations and the neglect of thermal expansion effects.

Heating $T_I > A_s$ in an infinitesimal temperature range $[A_s, T_I^i]$ (the corresponding stress range is $[0, \sigma^i]$) initiates (TT1) in element (I), which increases the stress σ in the two

elements since the active $M_+ \to A$ makes element (I) shorter so as to drag the interface toward the left $(M_- \to A)$ is inactive since $\xi_-^I = 0$). An analytical solution for T_I and σ can be found for this process segment based on the length constraint (7.2.0.5) and the phase evolution equations ((4.2.2.3), (4.2.2.4)) of (TT1) for the phase fraction ξ_-^I (note the element (II) is in elastic with a constant temperature T_o so that $\xi_-^{II} = \{0.5, 0, 0.5\}$):

$$T_{\rm I} = A_s + k_1 \sigma + k_2 \sigma^2 + \frac{2E_A (A_f - A_s) \sigma}{E_A E_M \varepsilon^* + (E_A - E_M) \sigma}.$$
 (7.3.1.1)

Since the first derivative of (7.3.1.1) with respect to stress σ

$$\frac{dT_{\rm I}}{d\sigma} = k_1 + 2k_2\sigma + \frac{2E_A^2 E_M \varepsilon^* (A_f - A_s)}{\left[E_A E_M \varepsilon^* + (E_A - E_M)\sigma\right]^2}$$
(7.3.1.2)

satisfies the (TT1) criteria (3.2.1.5) for $d\sigma > 0$ in the whole domain $[0, \sigma^i]$, further heating T_I beyond this infinitesimal temperature range $[A_s, T_I^i]$ continues to trigger (TT1) in element (I), so that expression (7.3.1.1) tracks the response σ until either the process goes to completion or the stress σ reaches the detwinning flow σ_s .

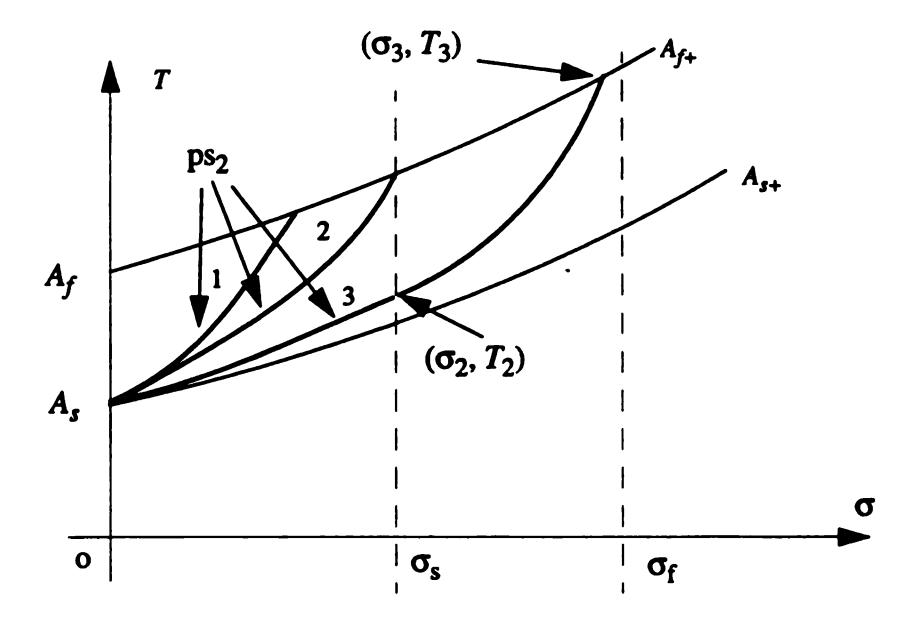


Figure 40. The path segment ps₂ has three possibilities: 1, 2, 3, as shown in the above. Path 3 is the desired situation and approachable for many shape memory alloys, which will be discussed in the following.

The stress σ inside the two elements increases, and may or may not reach the detwinning flow stress σ_s before the completion of $M_+ \to A$ in element (I). This implies that continued $T_{\rm I}$ increase will cause the state path $(\sigma, T_{\rm I})$ to follow a path of the form of either path 1, 2 or 3 as shown in Figure 40. Simultaneously, the state path $(\sigma, T_{\rm II})$ is horizontal in the (σ, T) -plane since the temperature $T_{\rm II}$ is held fixed in element (II). Useful device response requires a situation where the $M_+ \to A$ process in element (I) is sufficient to cause detwinning in element (II). This will happen if the elastic strains are insufficient to relieve the original transformation strain, that is if the following requirement is satisfied

$$\varepsilon^* > \varepsilon_A^s + \varepsilon_M^s, \tag{7.3.1.3}$$

where,

$$\varepsilon_A^s = \frac{\sigma_s}{E_A}, \, \varepsilon_M^s = \frac{\sigma_s}{E_M}.$$
 (7.3.1.4)

The physical interpretation of expressions (7.3.1.3) and (7.3.1.4) can be viewed in Figure 41. Generally, the TiNi alloy gives $\varepsilon^* * \varepsilon_A^s + \varepsilon_M^s$ (Hou and Grummon, 1995), so that continuous heating to trigger process $M_+ \to A$ will cause the stress σ to surpass σ_s so as to initiate detwinning in element (II).

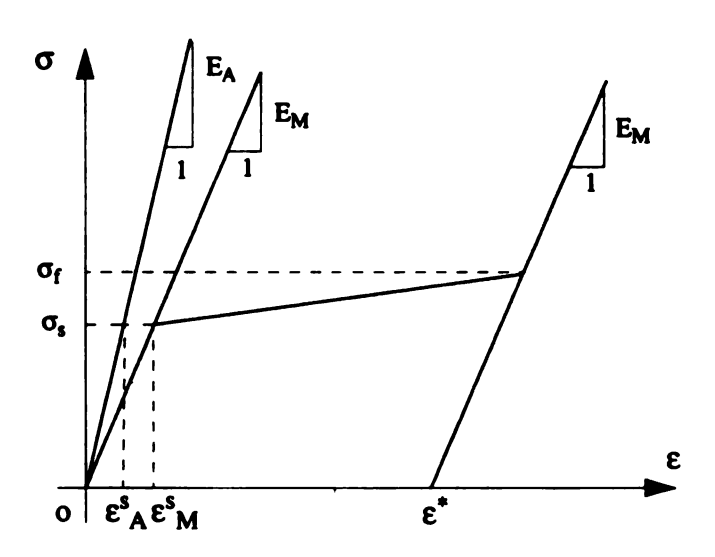


Figure 41. A physical interpretation for the condition that ensures that detwinning occurs during heating in a stroke.

Condition (7.3.1.3) indicates that the state path (σ , $T_{\rm I}$) follows a path of the form of path 3. Continued heating with $T_{\rm I} > T_2$ now triggers detwinning in element (II). Since the

detwinning provides a softening process, the motion of the interface between the two elements will dramatically increase with this $T_1 > T_2$ increase, which in turn, causes the state path (σ, T_1) to veer away from the nuetrality curve A_{s+} towards the nuetrality curve A_{f+} which it encounters at point (σ_3, T_3) . This process will be derived in the following discussion.

The phase evolution equations ((4.2.2.3), (4.2.2.4)) for the phase fraction ξ^{I} under (TT2), the phase evolution equation (4.2.2.4) for the phase fraction ξ^{II} under (TT5), along with the length constraint (7.2.0.5) gives the following state path of σ and T_{I} for $\sigma_{s} < \sigma < \sigma_{f}$:

$$T_{\rm I} = A_s f(\sigma, T_{\rm II}) + k_1 \sigma + k_2 \sigma^2 + \frac{2E_A (A_f - A_s) \sigma}{E_A E_M \varepsilon^* + (E_A - E_M) \sigma},$$
 (7.3.1.5)

where,

$$f(\sigma, T_{II}) = \frac{E_A E_M \varepsilon^* \frac{\beta^* (\sigma, T_{II})}{A_s} + (E_A - E_M) \sigma}{E_A E_M \varepsilon^* + (E_A - E_M) \sigma}, \qquad (7.3.1.6)$$

and

$$\beta'(\sigma, T_{II}) = \frac{(A_f - A_s)(M_f + k_1 \sigma + k_2 \sigma^2) + (A_s k_f - A_f k_s)\sigma}{A_f - A_s + (k_f - k_s)\sigma}.$$
 (7.3.1.7)

The parameters k_f and k_s in the above equation are determined by (2.4.2.1) and (2.4.2.3) respectively in section 2.4.2.

This description holds until its intersection (σ_3 , T_3) with the nuetrality curve A_{f+} . Solv-

ing $T_1 = A_f + k_1 \sigma + k_2 \sigma^2$ and (7.3.1.5) coincidentally gives

$$E_A E_M \varepsilon^* (A_f - \beta^* (\sigma, T_{II})) = (A_f - A_s)(E_A + E_M) \sigma$$
 (7.3.1.8)

for the intersection point. This implies that β (σ, T_{II}) can reach A_f only if $\sigma \to 0$, which does not occur in the present situation. Since β (σ, T_{II}) is the nuetrality curve to describe the detwinning process, element (II) does not fully detwin, ie. $\sigma_3 < \sigma_f$ (Figure 40). In addition, the phase fractions of the two elements at point (σ_3, T_3) are $\xi^I = \{0, 1, 0\}$ and $\xi^{II} = \{\Delta_a, 0, 1 - \Delta_a\}$. Continued heating with $T_I > T_3$ results in the path (σ, T_I) becoming vertical due to stress that is maintained at σ_3 and the element (II) state path (σ, T_{II}) would remain stalled at its endpoint (σ_3, T_o) . Hence any heating beyond T_3 does not contribute any additional device actuation. It is also important to note that Δ_a is unchanged during the subsequent cooling process of the element (I).

7.3.2 Cooling Process

When cooling $T_{\rm I}$ from T_3 the state path $(\sigma, T_{\rm I})$ starts as a vertical line involving $\sigma = \sigma_3$ since initially there are no transformations to relieve the stress. This persists until the vertical element (I) stroke path encounters the nuetrality curve M_{s+} at point (σ_4, T_4) where $\sigma_4 = \sigma_3$. Now further cooling will trigger $A \to M_+$ in element (I). This also gives elastic relaxation in element (II) in a infinitesimal temperature range $[T_4, T_1^{\rm I}]$ (the corresponding stress range: $[\sigma_4, \sigma^{\rm I}]$). The relation between $T_{\rm I}$ and σ can be found by use of the constraint equation (7.2.0.5) and phase evolution equation (4.3.2.3) for $\xi^{\rm I}$ (note that phase fraction $\xi^{\rm II}$ is unchanged in the form of $\xi^{\rm II} = \{\Delta_a, 0, 1-\Delta_a\}$ in this infinitesimal range),

$$T_{\rm I} = M_f + k_1 \sigma + k_2 \sigma^2 + (M_s - M_f) \left[\frac{2E_A \sigma + E_A E_M \varepsilon^* (1 - 2\Delta_a)}{E_A E_M \varepsilon^* + (E_A - E_M) \sigma} \right]^2.$$
 (7.3.2.1)

Since the first derivative of expression (7.3.2.1) with respect to σ

$$\frac{dT_{I}}{d\sigma} = k_{1} + 2k_{2}\sigma +$$

$$2(M_{s} - M_{f}) \frac{2E_{A}\sigma + E_{A}E_{M}\epsilon^{*}(1 - 2\Delta_{a})}{[E_{A}E_{M}\epsilon^{*} + (E_{A} - E_{M})\sigma]} E_{A}E_{M}\epsilon^{*}[E_{A} + E_{M} + 2(E_{A} - E_{M})\Delta_{a}]$$
(7.3.2.2)

satisfies the (TT2) criteria (3.2.1.6) for $d\sigma < 0$ in the whole domain $[0, \sigma^j]$, further cooling T_I beyond this infinitesimal temperature range $[T_4, T_I^j]$ continues to trigger (TT2) $(A \to M_+)$ in element (I). This indicates that the expression (7.3.2.1) applies to the cooling procedure until the state path (σ, T_I) reaches the nuetrality curve M_{s-} at the point (σ_5, T_5) .

Further cooling of temperature $T_{\rm I}$ below $T_{\rm 5}$ triggers (TT2) in element (I) involving both $A \to M_+$ and $A \to M_-$ processes. Substituting phase fraction expressions (5.1.2.3) and (5.1.2.4) for (TT2) into (7.2.0.5) gives

$$\int_{\sigma_{s}}^{\sigma} \left[\sqrt{\frac{\alpha_{A-}^{I}}{\alpha_{A+}^{I}}} \left(\frac{\partial \alpha_{A+}^{I}}{\partial \sigma} + \frac{\partial \alpha_{A+}^{I}}{\partial T_{I}} \frac{dT_{I}}{d\sigma} \right) - \sqrt{\frac{\alpha_{A+}^{I}}{\alpha_{A-}^{I}}} \left(\frac{\partial \alpha_{A-}^{I}}{\partial \sigma} + \frac{\partial \alpha_{A-}^{I}}{\partial T_{I}} \frac{dT_{I}}{d\sigma} \right) \right] d\sigma =$$

$$-\frac{2}{F_{s}} \left[1 - \Delta \xi_{5}^{I} - \Delta \xi_{5}^{II} - \frac{(E_{A} + E_{M})\sigma}{E_{A}E_{M}} \frac{(E_{A} - E_{M})\sigma}{E_{A}E_{M}} (1 - F_{5} \sqrt{\alpha_{A+}^{I}} \frac{\alpha_{A-}^{I}}{\alpha_{A-}^{I}}) \right]$$
(7.3.2.3)

where,

$$\Delta \xi_{5}^{I} = (\xi_{+}^{I})_{5} - (\xi_{-}^{I})_{5},$$

$$\Delta \xi_{5}^{II} = (\xi_{+}^{II})_{5} - (\xi_{-}^{II})_{5} = (\xi_{+}^{II})_{4} - (\xi_{-}^{II})_{4} = 1 - 2\Delta_{a},$$

$$\alpha_{A+}^{I} = \alpha_{A+}(\sigma, T_{I}) = (\beta^{+}(\sigma, T_{I}) - M_{f}) / (M_{s} - M_{f}),$$

$$\alpha_{A-}^{I} = \alpha_{A-}(\sigma, T_{I}) = (\beta^{-}(\sigma, T_{I}) - M_{f}) / (M_{s} - M_{f}),$$

$$F_{5} = \sqrt{\alpha_{A+}(\sigma_{5}, T_{5})} / \sqrt{\alpha_{A+}(\sigma_{5}, T_{5})\alpha_{A-}(\sigma_{5}, T_{5})} = 1 (\alpha_{A-}(\sigma_{5}, T_{5}) = 1).$$

Taking the first derivative to (7.3.2.3) with respect to stress σ generates

$$P(\sigma, T_{\rm I}) \frac{dT_{\rm I}}{d\sigma} = Q(\sigma, T_{\rm I}) + C_1 - 2C_2 \sqrt{\alpha_{\rm A+}^{\rm I} \alpha_{\rm A-}^{\rm I}},$$
 (7.3.2.4)

where

$$\begin{split} C_1 &= \frac{4}{F_5 E_M \varepsilon}, \ C_2 = \frac{E_A - E_M}{E_A E_M \varepsilon}, \\ P(\sigma, T_1) &= \sqrt{\frac{\alpha_{A^-}^I}{\alpha_{A^+}^I} \frac{\partial \alpha_{A^+}^I}{\partial T_1}} - \sqrt{\frac{\alpha_{A^+}^I}{\alpha_{A^-}^I} \frac{\partial \alpha_{A^-}^I}{\partial T_1}} + C_2 \sigma \left(\sqrt{\frac{\alpha_{A^-}^I}{\alpha_{A^+}^I} \frac{\partial \alpha_{A^+}^I}{\partial T_1}} + \sqrt{\frac{\alpha_{A^+}^I}{\alpha_{A^-}^I} \frac{\partial \alpha_{A^-}^I}{\partial T_1}} \right), \\ Q(\sigma, T_1) &= \sqrt{\frac{\alpha_{A^+}^I}{\alpha_{A^-}^I} \frac{\partial \alpha_{A^-}^I}{\partial \sigma}} - \sqrt{\frac{\alpha_{A^-}^I}{\alpha_{A^+}^I} \frac{\partial \alpha_{A^+}^I}{\partial \sigma}} - C_2 \sigma \left(\sqrt{\frac{\alpha_{A^-}^I}{\alpha_{A^+}^I} \frac{\partial \alpha_{A^+}^I}{\partial \sigma}} + \sqrt{\frac{\alpha_{A^+}^I}{\alpha_{A^-}^I} \frac{\partial \alpha_{A^-}^I}{\partial \sigma}} \right). \end{split}$$

The state path (σ, T_I) in this portion is governed by the ODE (7.3.2.4) and the corresponding initial condition: $T_I|_{\sigma = \sigma_5} = T_5$. The path segment starts at $(\sigma, T) = (\sigma_5, T_5)$. An important issue is the stress associated with cool-down to $T_I = M_f$. In the next section it is shown that $\sigma = 0$ at $T_I = M_f$ so that this segment ps₆ has the form shown in Figure 42.

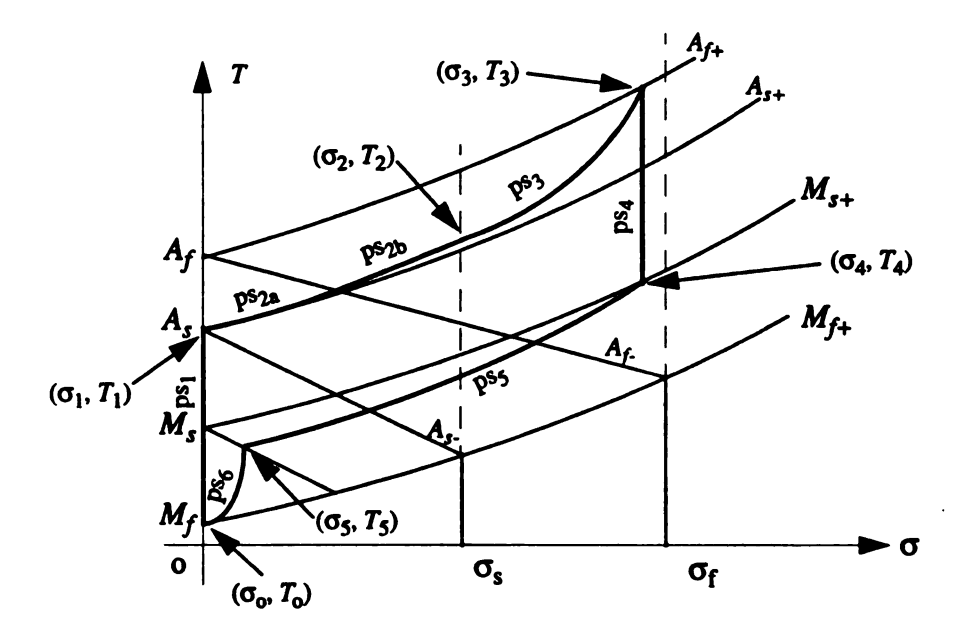


Figure 42. Six (σ, T_I) -path segments and their connecting points related with the first stroke (heating/cooling element (I)) are schematically presented in the phase diagram for $\sigma > 0$.

7.3.3 An Uniqueness Point for the Solution of the Equation (7.3.2.4)

In this section we will focus on the state path ps₆ as governed by equation (7.3.2.4). It is shown that this path concludes at the point $(0, M_f)$ with σ decreasing monotonically from the initial value $\sigma = \sigma_5$. The demonstration holds for the linear envelope functions (5.3.0.1) and (5.3.0.2) and the constitutive functions (4.2.1.1) to (4.2.1.4), and the Y-unfolding derived in section 2.4.2. To show that the solution is monotone, (7.3.2.4) is reformed as

$$\frac{dT_{\rm I}}{d\sigma} = \frac{Q(\sigma, T_{\rm I}) + C_1 - 2C_2 \sqrt{\alpha_{\rm A+}^{\rm I} \alpha_{\rm A-}^{\rm I}}}{P(\sigma, T_{\rm I})},$$
(7.3.3.1)

the above P and Q functions are

$$P(\sigma, T_{\rm I}) = \frac{1 + C_2 \sigma}{M_s - M_f} \sqrt{\frac{\beta^{-}(\sigma, T_{\rm I}) - M_f}{\beta^{+}(\sigma, T_{\rm I}) - M_f}} + \frac{C_2 \sigma - 1}{M_s - M_f} \sqrt{\frac{\beta^{+}(\sigma, T_{\rm I}) - M_f}{\beta^{-}(\sigma, T_{\rm I}) - M_f}},$$

$$Q(\sigma, T_{\rm I}) = \frac{(1 + C_2 \sigma)(k_1 + 2k_2 \sigma)}{M_s - M_f} \sqrt{\frac{\beta^{\dagger}(\sigma, T_{\rm I}) - M_f}{\beta^{\dagger}(\sigma, T_{\rm I}) - M_f}} + \frac{k_s^{\dagger}(C_2 \sigma - 1)}{M_s - M_f} \sqrt{\frac{\beta^{\dagger}(\sigma, T_{\rm I}) - M_f}{\beta^{\dagger}(\sigma, T_{\rm I}) - M_f}}.$$

Since it is always true that $\beta^-(\sigma, T_1) > \beta^+(\sigma, T_1)$ in the triangle zone enclosed by the T-axis, M_{f+} and M_{s-} , one has $P(\sigma, T_1) > 0$ for all $\sigma > 0$. On the other hand, in this triangle zone it is also true that $\sigma < 1/C_2 = (E_A E_M \epsilon^+)/(E_A - E_M)$ which implies $C_2 \sigma - 1 < 0$. Note that $k_s^- < 0$, $k_1 > 0$ and $k_2 > 0$. Therefore, one has $Q(\sigma, T_1) > 0$ for all $\sigma > 0$. Finally, since $0 \le \sqrt{\alpha_{A+}^1 \alpha_{A-}^1} \le 1$, one has $C_1 - 2C_2 \sqrt{\alpha_{A+}^1 \alpha_{A-}^1} > 0$ ($F_5 = 1$). Taken together, it is concluded that the solution of equation (7.3.2.4) (or (7.3.3.1)) is monotone.

The solution curve can not penetrate the terminal nuetrality curve M_{f+} . To verify this, assume that the solution curve $T_{I}(\sigma)$ goes toward M_{f+} . It is seen that there is a singularity for the solution of (7.3.2.4) on the terminal nuetrality curve M_{f+} since $\alpha_{A+}^{I}|_{M_{f+}} = 0$. The limit of $\frac{dT_{I}}{d\sigma}$ is

$$\lim_{\beta^{+}(\sigma, T_{1}) \to M} \left(\frac{dT_{1}}{d\sigma} \right) = k_{1} + 2k_{2}\sigma, \qquad (7.3.3.2)$$

which is equal to the slope of the terminal nuetrality curve M_{f+} . This indicates that the path ps₆ can never penetrate M_{f+} .

Finally, the path ps₆ $T_I(\sigma)$ definitely goes through the point $(0, M_f)$. To prove this, assume that there is a limit of the solution $T_I(\sigma)$:

$$\lim_{\sigma \to 0+} T_{\rm I}(\sigma) = L. \tag{7.3.3.3}$$

This limit exists because $T_{\rm I}(\sigma)$ is monotone. If $L > M_f$ then the limit of the right hand side of (7.3.2.4) is

$$\lim_{\sigma \to 0+} P(\sigma, T_{\rm I}) \frac{dT_{\rm I}}{d\sigma} = 0, \qquad (7.3.3.4)$$

which is not equal to the limit of the left hand side of (7.3.2.4):

$$\lim_{\sigma \to 0+} [Q(\sigma, T_{\rm I}) + C_1 - 2C_2 \sqrt{\alpha_{\rm A+}^{\rm I} \alpha_{\rm A-}^{\rm I}}] = \frac{1 - k_s^2}{M_s - M_f} + C_1 \neq 0.$$
 (7.3.3.5)

Thus, it must be $L = M_f$ which implies that the solution $T_I(\sigma)$ definitely goes through the point $(0, M_f)$. The proof is thus complete.

The above proven conclusion illustrates that the stress between the two elements is erased at the end of the cooling (or when $T_{\rm I}$ reaches the temperature M_f). This shows that the elastic deformation of the element (II) of a martensite state upon heating the element (I) can be recovered by subsequently cooling the element (I) to the temperature M_f . Since during the whole cooling process the phase fraction of the element (II) remains constant: $\xi^{\rm II} = \{\Delta_a, 0, 1-\Delta_a\}$, the phase fraction of the element (I) could be determined as $\xi^{\rm I} = \{0.5-\Delta_a, 0, 0.5+\Delta_a\}$ by means of the consistency requirement (7.2.0.5).

7.4 Later Heat-Cool Strokes

The first stroke, as discussed above, is special, since it is the only stroke starting from a fully detwinned state of the element (I) and random martensite state of element (II): ξ^{I} =

 $\{0,0,1\}$ and $\xi^{II}=\{0.5,0,0.5\}$. All other strokes involving heating/cooling of the element (I) will start from $\xi^{I}=\{\Delta,0,1-\Delta\}$ amd $\xi^{II}=\{0.5-\Delta,0,0.5+\Delta\}$ for some positive Δ . Similarly, all strokes involving heating/cooling of element (II) will start from $\xi^{I}=\{0.5-\Delta,0,0.5+\Delta\}$ and $\xi^{II}=\{\Delta,0,1-\Delta\}$ for some positive Δ . Let the corresponding sequence in Δ so generated be: Δ_{1} , Δ_{2} , Δ_{3} , Δ_{4} ,... where $\Delta_{1}=\Delta_{a}$ and odd subscripts correspond to end-of-stroke states after heating/cooling of element (I) and even subscripts correspond to end-of-stroke states after heating/cooling of element (II).

The analysis of any one of those strokes, taking Δ_i to Δ_{i+1} can be treated in a similar fashion to the initial stroke involving the six path segments: ps_1 , ps_2 , ps_3 , ps_4 , ps_5 , ps_6 , in the particular element that undergoes heating/cooling. Each such segment will involve different phase fraction values that lead off each of the segments. Otherwise, the only major qualitative difference involves the analysis of the segment ps_2 (ps_1 is trivial transformation during heating process so that it is a vertical line along T-axis from $(0, T_0 = M_f)$ to $(0, A_s)$). On segment ps_2 , the initial value $\xi = \Delta_i$ in the active element now causes a $M_- \to A$ transformation in addition to the $M_+ \to A$ transformation; this alters the previous description of the ps_2 segment given in (7.3.1.1). In particular, this path segment is no longer straight even if the elastic moduli of austenite and martensite are equal. This dual transformation in the heated element continues until the path encounters the terminal nuetrality curve A_f . Certain phase diagrams might allow detwinning in the response element before completion of $M_- \to A$ in the active element. This corresponds to materials that have the following relation between material parameters

$$A_f + k_f \sigma_s > A_s + k_1 \sigma_s + k_2 \sigma_s^2,$$
 (7.4.0.1)

ie., the temperature on nuetrality curve A_{f} is larger than that on nuetrality curve A_{s+} at the

same stress level $\sigma = \sigma_s$ for $\sigma > 0$. With the material parameters used here, an opposite condition of (7.4.0.1) is found, so that $M_- \to A$ completes in the active element before detwinning occurs in the response element. Thus, in the simulation results presented below, we find that $M_- \to A$ occurs on the segment ps₂, which is consequently split into two subpaths ps_{2a} and ps_{2b}. The latter path ps_{2b} involves only $M_+ \to A$ transformation in the heated element, and so is described by the same equations that were used for the treatment of the primary ps₂ path for the active element (see equation (7.3.1.1)). All subsequent details are qualitatively the same. Especially, full austentization of the heated element occurs before full detwinning of the constant temperature element, thus giving $\Delta_{i+1} > 0$.

7.5 Limit Analysis on Thermal Cycles

A simulation involving concrete parameters will be conducted in this section. The complication of starting states with nonzero Δ_i and different moduli of austenite and martensite prompt us to consider a fully numerical treatment. The convergence of Δ after several thermal strokes applied on the two elements is reached for different values of the austenite and martensite moduli. This in turn generates a stable path-loop in the (τ, T) -plane and the (δ, T) -plane, where δ , the displacement, is given by either (7.2.0.3) or (7.2.0.4).

7.5.1 Numerical Convergence on Residual Phase Fraction

Linear envelope functions: (5.3.0.1) and (5.3.0.2), and the Y-unfolding are taking into

account for the present simulation. The parameters employed here are from the TABLE 2 except for the moduli. The temperature pulse, as an input applied on the two elements, is illustrated in Figure 43 where $T_o = M_f$. The ultimate temperature must be sufficient to fully austenitize the operating element under the constraint stresses generated by the process. These ultimate temperatures are different in each stroke but tend to an asymptote. The values of Δ corresponding to end-of-stroke states for different combination selections of the austenite and martensite moduli are given in TABLE 9 to TABLE 12. These Δ values can be obtained without considering the state path of full cycles or full strokes. They are determined by the constraint equation (7.2.0.5) and the fact that the phase fraction of the response element remains unchanged during cooling processes. This is completed by a sample Mathematica program. By doing this, first, general heating state paths are updated by the value of Δ corresponding to the previous stroke. Second, the intersection point between the updated heating state path and nuetrality curve A_{f+} is found to determine the phase fractions at this point. Finally, by use of the constraint condition (7.2.0.5) to conclude the Δ at the end of the current stroke. It is seen in all cases that the values of Δ rapidly converge to a stable value Δ_{∞} .

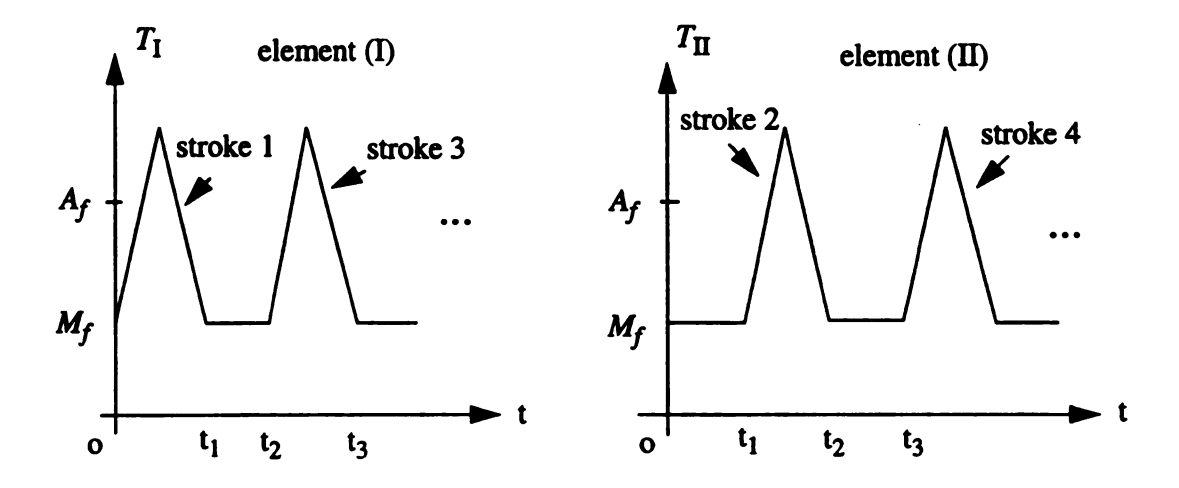


Figure 43. Temperature pulses applied on the two elements. The maximum temperature in heating must be sufficient to fully austenitize the operating element.

The following TABLEs show that the limit values Δ_{∞} tend to decrease with an increase of the moduli. This corresponds to a condition that the response element experiences greater detwinning because an increased stiffness gives a relatively small elastic deformation so that more of the deformation is related with the phase transformations. Based on the conditions of TABLE 9 and TABLE 12 both of which have the same sum of the moduli of austenite and martensite, it is also observed that the equal moduli situation gives more detwinning for the response element than the uneven moduli situation.

Since Δ is nonzero, the device as described here has not recovered the prevailing state at the very beginning of the operation: $\xi^{\rm I} = \{0, 0, 1\}$, $\xi^{\rm II} = \{0.5, 0, 0.5\}$. Hence the response is not a true "cycle" in the first couple strokes. Continued operation will always involve end-of-stroke states involving some Δ remnant that is not fully detwinned on the nominally oriented element. Repeatable or true cyclic behavior only occurs if the same Δ

remnant occurs at the end of each two-stroke cycle. In fact, for symmetric device described here $(l_1 = l_2 = l)$, the same Δ remnant must occur at the end of every stroke, albeit interchanged between the two elements. The question thus arises as to whether or not there is such a stable cycle, ie. an Δ , which gives cyclic behavior. Here smallness of Δ is a measure of the closeness to ideal behavior in terms of stroke distance. That is $\Delta_{\infty} = 0$ gives ideal behavior (maximum stroke), while, at the other extreme $\Delta_{\infty} = 1/4$ gives $\xi^{I} = \xi^{II} = \{0.25, 0, 0.75\}$ at the end of each stroke, corresponding to zero interface movement. This point can be viewed in the following discussion.

To clearly see the problem, we consider the displacement at the end of each stroke. With (7.2.0.3) and (7.2.0.4) employed here, the displacements at the end of each stroke with respect to the reference position are found as the following,

$$\delta_0 = 0;$$

$$\delta_1 = l(1-2\Delta_1)\epsilon^*;$$

$$\delta_2 = 2l\Delta_2\epsilon^*;$$

$$\vdots$$

$$\delta_i = \begin{cases} l(1-2\Delta_i)\epsilon^* & \text{if } i \text{ is odd} \\ 2l\Delta_i\epsilon^* & \text{if } i \text{ is even} \end{cases}$$

Then the effective stroke distances between two connected strokes are

$$sd_{1} = |\delta_{1} - \delta_{0}| = l(1 - 2\Delta_{1})\epsilon^{*};$$

$$sd_{2} = |\delta_{2} - \delta_{1}| = l\epsilon^{*}(1 - 2\Delta_{2} - 2\Delta_{1});$$

$$\vdots$$

$$sd_{i} = |\delta_{i} - \delta_{i-1}| = l\epsilon^{*}(1 - 2\Delta_{i} - 2\Delta_{i-1});$$

$$\vdots$$

When enough temperature pulses are operated on the two elements $(i \to \infty)$, our numerical results show that $\lim_{i \to \infty} \Delta_i = \lim_{i \to \infty} \Delta_{i-1} = \Delta_{\infty}$. Therefore, the limiting effective stroke distance is obtained as

$$\mathrm{sd}_{\infty} = l \varepsilon^{\bullet} (1 - 4 \Delta_{\infty}). \tag{7.5.1.1}$$

Thus, $\Delta_{\infty}=0$ represents a maximum stroke situation that the prevailing state: $\xi^{\rm I}=\{0,0,1\}$ and $\xi^{\rm II}=\{0.5,0,0.5\}$ can be recovered at the end of each stroke, while $\Delta_{\infty}=1/4$ indicates a useless situation. A measure of the ultimate stroke quality is thus $Q=1-4\Delta_{\infty}$. Note that $Q=0.5398,\ 0.6206,\ 0.6574,\ 0.5865$ for the cases given in TABLE 9 to TABLE 12 respectively.

TABLE 9. $\mu_A = 4.0*10^4$; $\mu_M = 2.0*10^4$ MPa

operating elements	strokes	Δ of response elements at end-of-stroke	ultimate temperatures (°K)
(I)	1	0.1171521977252063	335.123647800
(II)	2	0.1150009266592965	334.622190725
(I)	3	0.1150510309196698	334.633789633
(II)	4	0.1150498696891485	334.633520813
(I)	5	0.1150498966052308	334.633527044
(II)	6	0.1150498959813465	334.633526900
(I)	7	0.1150498959958073	334.633526900
(II)	8	0.1150498959954724	334.633526900
(I)	9	0.1150498959954803	334.633526900
(II)	10	0.1150498959954798	334.633526900
(I)	11	0.1150498959954798	334.633526900
limit	œ	Δ _∞ ≈ 0.1150499	334.633526900

TABLE 10. $\mu_A = 4.0*10^4$; $\mu_M = 2.8*10^4$ MPa

operating elements	strokes	Δ of response elements at end-of-stroke	ultimate temperatures (°K)
(I)	1	0.095965644548003	335.433784391
(II)	2	0.094826994366186	335.117197237
(I)	3	0.094843410530481	335.121891685
(II)	4	0.094843174457726	335.121824177
(I)	. 5	0.094843177852696	335.121825147
(II)	6	0.094843177803873	335.121825133
(I)	7	0.094843177804575	335.121825134
(II)	8	0.094843177804565	335.121825134
(I)	9	0.094843177804565	335.121825134
limit	6 0	Δ _∞ ≈ 0.09484318	335.121825134

TABLE 11. μ_A = 4.0*10^4; μ_M = 3.4*10^4 MPa

operating elements	strokes	Δ of response elements at end-of-stroke	ultimate temperatures (°K)
(I)	1	0.086460055018001	335.588237493
(II)	2	0.085641127661279	335.327082388
(I)	3	0.085650372005167	335.330032150
(II)	4	0.085650267840977	335.329998912
(I)	5	0.085650269014702	335.329999287
(II)	6	0.085650269001486	335.329999283
(I)	. 7	0.085650269001635	335.329999283
(II)	8	0.085650269001633	335.329999283
(I)	9	0.085650269001633	335.329999283
limit	80	Δ _∞ ≈ 0.08565027	335.329999283

TABLE 12. μ_A = 3.0*10^4; μ_M = 3.0*10^4 MPa

operating elements	strokes	∆ of response elements at end-of-stroke	ultimate temperatures (°K)
(I)	1	0.104853194379462	335.307846732
(II)	2	0.103344420472474	334.914231932
(I)	3	0.103371280735037	334.921227214
(II)	4	0.1033.70804176779	334.921103103
(I)	5	0.103370812632450	334.921105305
(II)	6	0.103370812482419	334.921105266
(I)	7	0.103370812485081	334.921105266
(II)	8	0.103370812485033	334.921105266
(I)	9	0.103370812485035	334.921105266
(II)	10	0.103370812485035	334.921105266
limit	∞	Δ _∞ ≈ 0.10337081	334.921105266

7.5.2 Stable Response Loops

We now consider more detailed numerical simulations of (σ, T) -paths for a particular case involving equal moduli. The parameters to be used in the following simulation are all listed in TABLE 2. Following the previous analysis of Sections 7.3 and 7.4, the (σ, T) -curves corresponding to the first stroke, are presented (by lighter dots) for both the elements in Figure 44. The (σ, T) -curves for the consequent stroke are given (by darker dots) in Figure 45. Note that the (σ, T_1) -curves for the response element is always a straight back and forth horizontal line. The difference between the first and the second strokes is that both $M_- \to A$ and $M_+ \to A$ are involved in the ps₂ process of the second stroke, while only $M_+ \to A$ is involved in the ps₂ process of the first stroke (refer to Figure 42), since the initial condition of the first stroke involved $\xi_- = 0$ in the operating element.

A combined view of $(\sigma, T_{\rm I})$ -and $(\sigma, T_{\rm II})$ -curves (the lighter dot is the $(\sigma, T_{\rm I})$ -curve for the first stroke) corresponding to the operating elements under ten cycles are shown in Figure 46. The moduli here are: $\mu_A = 3.0 \times 10^4$, $\mu_M = 3.0 \times 10^4$ MPa, so that the simulation is that associated with TABLE 12. It is to be noted that, after the first stroke, the various curves are indistinguishable (the darker dot curves), which indicates that the limit cycle corresponding to Δ_{∞} has been reached. These state paths are generated based on the analysis in sections 7.3 and 7.4. The intercomparable (δ, T) - and (δ, σ) -curves are illustrated in Figure 47 (a) and (b), which are obtained by use of equations (7.2.0.3) and (7.2.0.4), as well as the derived (σ, T) state paths. The lighter dot curves are again the displacement against temperature and stress, corresponding to the first stroke, while the darker dot curves correspond to the remaining nine strokes. The effective stroke distances can be found from expression (7.5.1.1) and Δ_{∞} listed in the above TABLEs. For example,

the effective stroke distance $sd_{\infty} = 0.5865l\epsilon$ for this particular case.

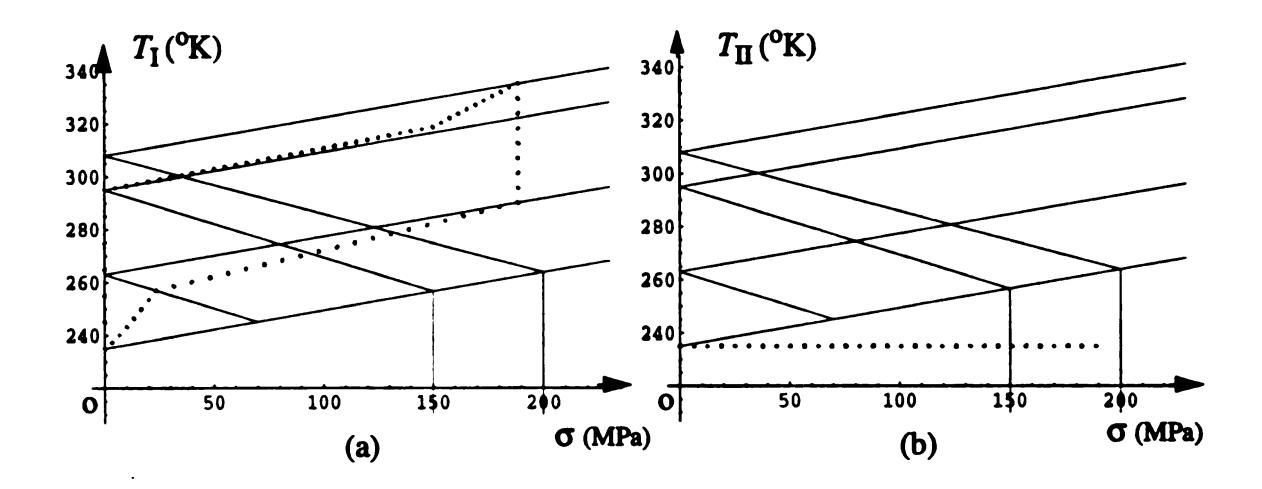


Figure 44. (σ , T)-paths for the first stroke for element (I) (a) and for element (II) (b). The operating element here is element (I) with initial temperature $T_0 = M_f$, which is equal to the constant temperature of the response element (II) during this process. Here the material properties come from TABLE 2. In particular the moduli are $\mu_A = \mu_M = 3.0 \times 10^4$ MPa. The value of Δ at the beginning is $\Delta = 0$, and at the end is $\Delta = 0.104853194379462$.

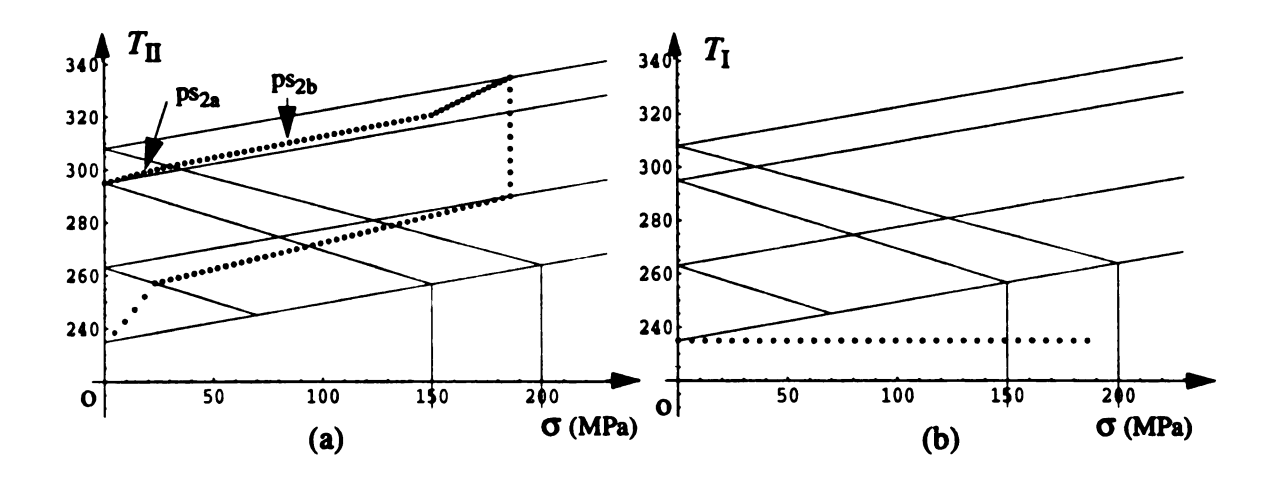


Figure 45. (σ , T)-curves in the second stroke are presented in (a) for the element (II) and in (b) for the element (I). The operating element is element (II) with initial temperature $T_0 = M_f$, which is equal to the constant temperature of element (I) during this process. In the first part of ps₂ both $M_- \to A$ and $M_+ \to A$ are involved in the phase transformation (refer to Figure 42). The value of Δ at the beginning is $\Delta = 0.104853194379462$, and at the end is $\Delta = 0.103344420472474$.

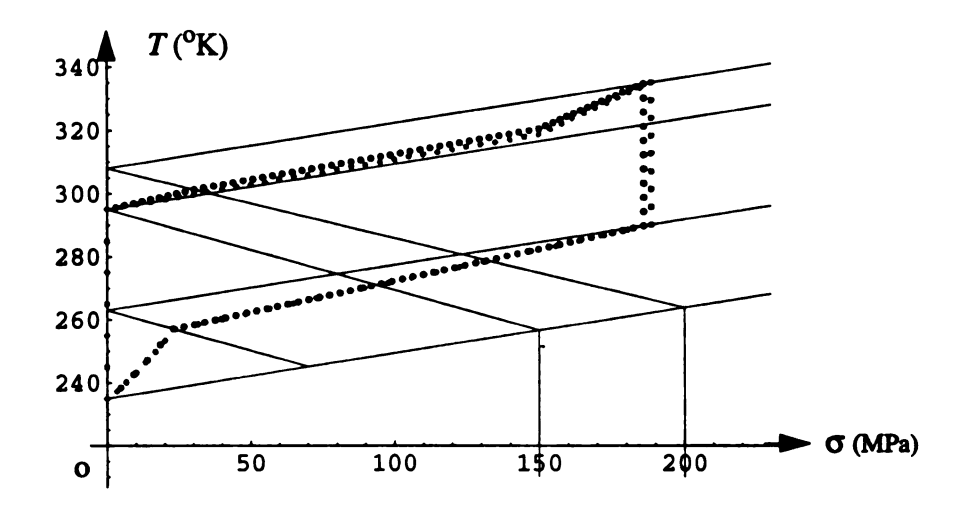


Figure 46. This graph shows (σ, T) -curves of the operating elements in ten strokes. A stable (σ, T) -loop (the darker one) is reached after the first cycle (the lighter one).

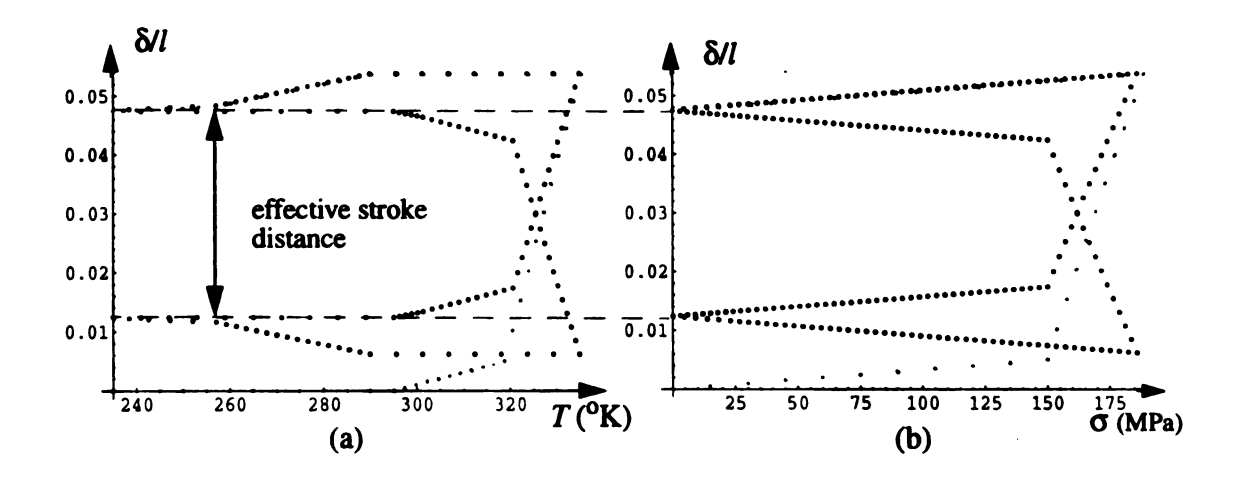


Figure 47. The corresponding displacement against stress (a) and temperature (b) after ten strokes. The lighter dots correspond to the first stroke. The darker dots correspond to the following nine strokes, which are indistinguishable at this scale. The head down loops correspond to operating element (II) while the head up loops correspond to operating element (II) in both (a) and (b).

7.6 Discussion

In principle, the deformation caused by thermal expansion is against that caused by phase transformation. The thermal expansion coefficients of austenite and martensite can be taken as $\alpha_A = 11 \times 10^{-6}$ 1/°K and $\alpha_M = 6.6 \times 10^{-6}$ 1/°K respectively. To gauge its effect, we choose the bigger one $\alpha = 11 \times 10^{-6}$ 1/K° a for both austenite and martensite. The temperature change to actuate a stroke is likely to be on the order of 100 °K based on the above simulation. Then the thermal expansion strain is about 0.0011 « $\epsilon^* = 0.06$. Thus, we conclude that a reasonable approximation allows the thermal expansion effect to be neglected.

Based on the previous achievement, the final cyclic behavior corresponds to a repeatable limit cycle. Such limit cycles arise naturally in earlier models of SMA behavior given by Ivshin and Pence (1992). Here a limit cycle means that cyclic input, such as repeated alternating temperature pulse excursions $T_{\rm I}(t)$ and $T_{\rm II}(t)$, generates cyclic output response, here $\xi^{\rm I}(t)$ and stroke δ . For a given cyclic input, the associated limit cycle or cycles (if any exist) may be sought in two general ways. The first involves starting from some initial condition of the output response, here $\xi^{\rm I}(0)$ and $\xi^{\rm II}(0)$, followed by performing a large number of input cycles. Limit cycles then arise as the possible large time convergence of the functions $\xi^{\rm I}(t)$ and $\xi^{\rm II}(t)$ to a repeatable cycle with the same cyclic frequency. Here initial conditions of the output response that happen to be on a limit cycle will generate output response that stays on the cycle, and, ideally, those initial conditions not on a limit cycle will give output response that drifts towards a nearby limit cycle. This was the method pursued above, where the limit cycle was essentially attained on the second stroke (Figure 44 to Figure 47). The other general method for determining limit cycles

involves setting up a mapping between output response variables sampled at the cyclic frequency and seeking fixed points of the mapping. Such fixed points give initial conditions that are on a limit cycle. Although Ivshin and Pence were able to pursue such a direct fixed point treatment in some of their previous studies (Ivshin and Pence, 1992), the more complicated nature of the problem under study here (involving more than one martensitic variant, and more than one shape memory element) points to the usefulness of obtaining these limit cycles by numerical simulation procedures.

8 CONCLUSION AND PROPOSED FUTURE WORK

The approach is to augment conventional continuum mechanical descriptions with internal variables that track fractional portioning of the material between austenite and the various martensite variants. A three-species model involving austenite and two complementary martensite variants provides sufficient generality to capture the martensite variant distributions that underlie shape memory, and the strain-accommodation associated with pseudoelasticity. Transformations between all of these species can be tracked on the basis of triggering algorithms that reflect both transformation hysteresis and the variations of phase fractions of triggering both stress and temperature.

Three phase diagrams are presented based on thermodynamic considerations and experimental measurements. The X-unfolding, as a prototype, is first derived from allowing phase transformation nuetrality curves to enter non-austenite areas to describe the detwinning processes. The detwinning in this unfolding strongly depends upon both stress and temperature. Further modification on the X-unfolding, about the entropy of austenite replaced by that of martensite in the non-austenite areas, provides the pY-unfolding. An interesting aspect of this phase diagram is that stresses associated with detwinning start and finish are determined in terms of the other material parameters. Basically, this pY-unfolding requires only the following experimentally determined parameters: the four phase transformation temperatures, the transformation strain, the Young's moduli of austenite and martensite, and the transformation latent heat. The more sophisticated phase dia-

gram, Y-unfolding, is generated by specifying the detwinning start and finish stresses independently based on experimental observations. The corresponding nuetrality curves of phase transformations are consequently modified following this change. The comparison of isothermal behaviors, between the theoretical prediction with the Y-unfolding and the experimental measurements on thin films by Hou and Grummon, shows that the model can well reflect the practical situation in some degrees (Grummon and Pence, 1996).

Discussions of the path-independent conditions in Chapter 5 reveal some fundamental features of the two variant algorithms of the model. These features are responsible for the hysteresis characteristics of shape memory alloys. The special behavior, discussed in Chapter 6, according to loading/cooling and cooling/loading state paths shows potential for the model to direct designing smart sensors. Pseudoelasticity, shape memory effects and many isothermal behaviors are predicted in Chapter 6.

The application of the model in Chapter 7 shows two aspects. One is that the model possesses both theoretical completeness in certain levels and potentiality to guide sample engineering designs. The other is the potential engineering application of the two element device (TSTE). A stable cyclic behavior is reached by performing the cyclic temperature pulse on the device. Further investigation associated with carrying external loads can follow up based on the present approach.

The interesting inverse problem investigated in the Appendix reflects another view on the model itself. Relations between stress, strain, temperature and entropy for each species are backed out of a three species phase diagram as given by experiment. We believe that there are still certain amounts of work to be done on the thermodynamic issue related with the choice of the particular entropy form of each individual phase. An example shows that there is a consistency between the approach in Chapter 2 and the inverse issue in the

Appendix under the same phase diagram.

So far in this study, we only focus on 1-D isothermal descriptions and some sample behaviors associated with both stress and temperature changes, in which stress and temperature are treated as an explicit input. More complicated situations, such as convective and adiabatic processes, can be extended from the present approach by adding certain thermodynamic considerations (Ivshin and Pence, 1994 b). In general, for the convective and adiabatic condition, often the case is that only either stress or temperature, but not both, are given as input and their relation is decided by extra thermodynamic equations (e.g. joule heating, convection, physical constraint).

For more general modeling work, TiNi alloys considered usually have either 24 habit plane martensite variants plus austenite, or 12 coherent martensite variants plus austenite. which are distributed in 3-D scopes. Fellows as Patoor et al (1994), Son and Hwang (1993), Boyd and Lagoudas (1994, 1996) contributed certain amount of work on the 3-D modeling work in different aspects. For instance, Patoor et al have developed a constitutive model to describe the transformation among all 24 martensite variants and austenite phase based on free energy issue. The model was set up first for the single crystal and then extended to the description of polycrystalline transformation by considering the self-consistent micromechanics method. Son and Hwang have acquired a thermodynamic model for both pseudoelasticity and shape memory effects. The transformation criteria of the model is similar to plastic yielding's in plasticity theories. Later, Boyd and Lagoudas have also developed a microscope constitutive model to phenomenologically narrate the behavior of pseudoelasticity and shape memory effects for polycrystalline shape memory alloys. The model using a free energy function and a dissipation potential contains three descriptions based on the combination number of internal state variables.

Another challenge future work conjunct with the present study is how to extend the present model to the more general case with multiple martensite variants and austenite in 3-D. This extension will include modifying the overall entropy and strain expressions (2.1.0.1) and (2.1.0.2) respectively based on the compatibility theory (Bhattacharya and Kohn, 1996). The corresponding 3-D criteria for phase transformations and reorientations is another open question. The potential way to solve the problem is based on the relation between 3-D stress distributions and orientations of various lattice structures of austenite and martensite variants.

9 REFERENCE

- 1 Apostol, T., Calculus, Blaisdell Mathematics Series. New York, London. First Edition 1962.
- 2 Achenbach, M. and I. Muller, Simulations of Material Behavior of Alloys with Shape Memory, Arch. Mech. 37(6), pp. 573-585(1985).
- 3 Achenbach, M., T. Atanackovic and I. Muller, A Model for Memory Alloys in Plane Strain, Int. J. Solids Structures Vol. 22, No. 2, pp. 171-193(1986).
- 4 Achenbach, M., A Model for an Alloy with Shape Memory, *Int. J. Plast.* 5, pp. 371-395(1989).
- 5 Banks, R. and O. Weres. 1976. In Shape Memory Effects in Alloys. J. Perkins. ed.. NY: Plenum Press.
- 6 Barrett, D. and B. Sullivan, A Three-Dimensional Phase Transformation Model for Shape Memory Alloys, *Journal of Intelligent Material Systems and Structures*, Vol. 6, pp. 831-839, Nov. 1995.
- 7 Bekker, A. and L. Brinson. A Macromodel of Thermo-Induced Martensite Transformation in a 1-D SMA Polycrystalline Body, AMD-Vol.189/PVP-Vol.292, *Mechanics of Phase Transformations and Shape Memory Alloys*, 45-58, ASME 1994.
- 8 Bhattacharya, K and R. Kohn, Symmetry, Texture and The Recoverable Strain of Shape-Memory Polycrystals, *Acta Mater.*, Vol. 44, No. 2, pp. 529-542, 1996.
- 9 Boyd, J. G. and D. C. Lagoudas, Thermomechanical Response of Shape Memory Composites, *Journal of Intelligent Material Systems and Structures*, Vol. 5, pp. 831-839, May, 1994.
- 10 Boyd, J. G. and D. C. Lagoudas, A Thermodynamical Constitutive Model for Shape Memory Materials. Part I. The Monolithic Shape Memory Alloy, *International Journal of Plasticity*, Vol. 12, No. 6. pp. 805-842, 1996.
- 11 Brinson, L. C., One-Dimensional Constitutive Behavior of Shape Memory Alloys: Thermomechanical Derivation with Non-Constant Material Functions and Redefined Martensite Internal Variable, J. of Intell. Mater. Syst. and Struct. Vol. 4-April, pp. 229-

- 242(1993).
- 12 Brinson, L. C. and M. S. Huang, Simplifications and Comparisons of Shape Memory Alloy Constitutive Models, J. of Intell. Mater. Syst. and Struct., 7, 1996, pp. 108-114.
- 13 Bondaryev, E. and C. Wayman, Some Stress-Strain-Temperature Relationships for Shape Memory Alloys, *Meta. Trans.* A, Vol. 19A, pp. 24072413, Oct. 1988.
- 14 Budiansky, B. and L. Truskinovsky, On the Mechanics of Stress-Induced Phase Transformation in Zirconia, J. Mech. Phys. Solids, Vol. 41, No. 9, pp. 1445-1459, 1993.
- 15 Coleman, B. D. and M. Gurtin, Thermodynamics with Internal State Variables, J. Chem. Phys., Vol. 47, No. 2, pp. 597613, July 15, 1967.
- 16 Coleman, B. D. and M. L. Hodgdon, A Constitutive Relation for Rate-independent Hysteresis in Ferromagnetically soft materials, *Int. J. Engng. Sci.* 24, pp. 897-919 (1986).
- 17 Coleman, B. D. and M. L. Hodgdon, On A Class of Constitutive Relations for ferromagnetic hysteresis, *Arch. Rational Mech. Anal.* 99, pp. 375-396 (1987).
- 18 Delaey, L., R. V. Krishnan, H. Tas and H. Warlimont, Thermoplasticity, Pseudoelasticity and the Memory Effects Associated with Martensitic Transformations---Part 1, J. Mater. Sci. 9, pp.1521-1543(1974)
- 19 Dye, T., 1990. An Experimental Investigation of the Behavior of "Nitinol", MS thesis, Virginia Tech.
- 20 Duerig, T, D. Stockel and A. Keeley, Actuator and Work Production Devices, *Engineering Aspects of Shape Memory Alloys*, Butterworth-Heinemann Ltd. 1990, pp. 181-194.
- 21 Falk, F., Model Free Energy, Mechanics, and Thermodynamics of Shape Memory Alloys, *Acta metall.* 28, pp. 1773-1780 (1980).
- 22 Falk, F., 1989. Pseudoelastic Stress-Strain Curves of Polycrystalline Shape Memory Alloys Calculated from Single Crystal Data, *Int. J. Engng Sci.*, 27: 227-284.
- 23 Fedelich, B., G. Zanzotto, One-dimensional Quasistatic Nonisothermal Evolution of Shape-memory Material inside The Hysteresis Loop, *Cont. Mech. Thermodyn.* 3, pp. 251-276(1991).
- 24 Fu, S., Y. Huo, and I. Muller, Thermodynamics of Pseudoelasticity---an Analytical Approach, *Acta Mechanica*, 99, pp. 1-19 (1993).
- 25 Funakubo, I., Shape Memory Alloys, 1987.

- 26 Graesser, E. and F. Cozzarelli, Shape Memory Alloys as New materials for Asiesmic Isolation, *Journal of Engineering Mechanics*, ASCE, 117(11), pp. 2590-2608 (1991).
- 27 Graesser, E. and F. Cozzarelli, A Proposed Three-dimensional Constitutive Model for Memory Alloys, J. of Intell. Mater. Syst. and Struct. Vol. 5-Jan. pp. 78-89(1994).
- 28 Grummon, D. S. and T. J. Pence, Thermotractive Titanium-Nickel Thin Films for Microelectromechanical Systems and Active Composites, to appear in *Symposium of Adv. in Mats for Smart System*, Dec. 1996 (Boston)
- 29 Huo, Y. and I. Muller, Nonequilibrium Thermodynamics of Pseudoelasticity, *Cont. Mech. Thermodyn.* 5, pp. 163-204 (1993).
- 30 Hou, L. and D. Grummon, Transformational Superelasticity in Sputtered Titanium-Nickel Thin Films, *Scripta Metallurgica et Materialia*, Vol. 33, No. 6, pp. 989-995, 1995.
- 31 Ivshin, Y. and T. Pence, A Constitutive Model for Hysteretic Phase Transition Behavior, *Int. J. Enging. Sci.*, Vol. 32, No. 4, pp. 681-704 (1994).
- 32 Ivshin, Y. and T. Pence, A Thermomechanical Model for a One Variant Shape Memory Material, J. of Intell. Mater. Syst. and Struct., Vol. 5, pp. 455-473 (1994).
- 33 Ivshin, Y. and T. Pence, A Simple Mathematical Model of Two-Way Memory Effect, 1992, Proceedings of the ICOMAT.
- 34 Krishnan, R., L. Delaey, H. Tas and H. Warlimont, Thermoplasticity, Pseudoelasticity and the Memory Effects Associated with Martensitic Transformations---Part 2, J. Mater. Sci. 9, pp. 1536-1544(1974).
- 35 Leo, P. H., T. W. Shield and O. P. Bruno, Transient Heat Transfer Effects on The Pseudoelastic Behavior of Shape-Memory Wires, *Acta metall. mater.* Vol. 41, No. 8, pp. 2477-2485 (1993).
- 36 Liang, C., 1990. "The Constitutive Modeling of Shape Memory Alloys", Ph.D. thesis. Virginia Tech.
- 37 Liang, C. and C. A. Rogers, One-Dimensional Thermomechanical Constitutive relations for Shape Memory Materials, *J. of Intell. Mater. Syst. and Struct.* 1(2), pp. 207-234(1990).
- 38 Likhachev, A. and Y. Koval, On The Differential Equation Describing The Hysteretic Behavior of Shape-memory Alloys, *Scripta Metallurgica*, Vol. 27, pp. 223-227 (1992).
- 39 Lim, T. J. and D. L. McDowell, Degradation of An Ni-Ti Alloy during Cyclic Loading, North American Conference on Smart Structures and Materials, SPIE, Orlando, FL, Feb. 1994.

- 40 Miyazaki, S., Y. Kohiyama and K. Otsuka, Plastic Deformation of Ti-Ni Alloys, *Proceedings of International Symposium on Intermetallic Compounds*, Japanese Institute of Metals International Symposium. 6th, 1991, Sendai, Japan.
- 41 Miyazaki, S. and K. Otsuka, Mechanical Behaviour Associated with the Premartensitic Rhombohedral-Phase Transition in a Ti₅₀Ni₄₇Fe₃ Alloy, *Philosophical Magazine A*, 1984, Vol. 50, No. 3, 393-408.
- 42 Miyazaki, S. and K. Otsuka, Deformation and Transition Behavior Associated with the R-Phase in Ti-Ni Alloys, *Metallurgical Transactions A*, Vol. 17A, Jan. 1986, 53-63.
- 43 Muller, I. 1979. A Model for a Body with Shape Memory, Arch. Rational Mechanics Anal., 70:61-67.
- 44 Muller, I. and H. Xu, On the Pseudo-elastic Hysteresis, *Acta Metall. Mater.* Vol. 39, No. 3, pp. 263-271(1991).
- 45 Patoor, E., A. Eberhardt and M. Berveiller, Micromechanical Modeling of the Shape Memory Behavior, AMD-Vol. 189/PVP-Vol. 292, *Mechanics of Phase Transformations and Shape Memory Alloys*, pp. 23-37, ASME 1994.
- 46 Pence, T., D. Grummon and Y. Ivshin, A Macroscopic Model for Thermoelastic Hysteresis in Shape-Memory Materials, AMD-Vol.189/PVP-Vol.292, *Mechanics of Phase Transformations and Shape Memory Alloys*, 45-58, ASME 1994.
- 47 Rogers, C. A., C. Liang and J. Jia. 1989. Behavior of Shape Memory Alloy Reinforced Composite Plates-Parts I and II. *Proceedings of the 30th Structures. Structural Dynamics and Materials Conference. Mobile, AL. April* 3-5, pp. 2011-2017.
- 48 Sun, Q. P. and Hwang, K. C., 1993, Micromechanics Modeling for the Constitutive Behavior of Polycrystalline Shape Memory Alloys I. Derivation of General Relations, J. Mech. Phys. Solids, Vol. 41, pp. 1-17; -II. Study of the Individual Phenomena, J. Mech. Phys. Solids, Vol. 41, pp. 19-33.
- 49 Takeda, M., M. Hashimoto and K. Sato, 1986. A New Displacement Sensor Using Pseudoelastic Titanium-Nickel Alloys, *Journal of Robotic Systems*, 3(4): 441-450.
- 50 Tanaka, K. and R. Iwasaki, A Phenomenological Theory of Transformation Superplasticity, *Eng. Fract. Mech.* 21(4), pp. 709-720(1985).
- 51 Tanaka, K.. A Phenomenological Sketch of Shape Memory Effect: One Dimensional Tensile Behavior, *Res. Mech.* 18, pp. 251-261(1986).
- 52 Tanaka, K., F. Nishimura and H. Tobushi, Phenomenological Analysis on Subloops in Shape Memory Alloys Due to Incomplete Transformations, *Journal of Intelligent Material Systems and Structures*, Vol. 5-July 1994.

- 53 Warlimont, H., L. Delaey, R. V. Krishnan and H. Tas, J. Mater. Sci. 9, pp. 1545-1555(1974).
- 54 Wasilewski, R., Stress-Assisted Martensite Formation in TiNi, Scripta Metallurgica, Vol. 5, pp. 127-130, 1971.
- 55 Wasilewski, R., The "Yield" Behavior of Stoichiometric TiNi across the Martensitic Transformation Range, *Scripta Metallurgica*, Vol. 5, pp. 131-135, 1971.
- 56 Wasilewski, R., Martensitic Transformation and Fatigue Strength in TiNi, Scripta Metallurgica, Vol. 5, pp. 207-212, 1971.
- 57 Wasilewski, R., The Effects of Applied Stress on the Martensitic Transformation in TiNi, *Met. Trans.* 2 (1971) 2973-2981.
- 58 Wen, Y., Method for Random Vibration of Hysteretic Systems, J. Engrg. Mech. Div., ASCE, 102(2), pp. 249-263.
- 59 Wayman, C. M., Some Applications of Shape-Memory Alloys, *Journal of Metals*, 32(16): 129-137, 1980.
- 60 Wu, X., T. Pence and D. Grummon, Model Tracking of Stress and Temperature-Induced Martensitic Transformations for Assessing Superelastic and Shape Memory Actuation, to appear in Symposium of Adv. in Mats for Smart System, Dec. 1996 (Boston).

10 APPENDIX

REFINEMENT OF THE TWO VARIANT PHASE DIAGRAM

As discussed in the chapter 2, under certain assumptions of entropy and strain of the pure phase species, phase diagrams have been obtained based on thermodynamic considerations. The Gibbs free energy is treated as though a state function of temperature and stress in either an individual phase or a mixture phase, by which Clausius-Clapeyron relations are generated to describe transformations between any two species and further to form phase diagrams. The phase diagram gained by this procedure is usually not exactly the same with experimental observations, specifically, in a detwinning process. Thus, the difference between theoretical derivations and experimental measurements supplies a motivation to consider a reverse problem. That is, if a phase diagram is given, it is very interesting to find the distribution forms of strain and entropy of the pure phases that provide the same thermodynamic consistency requirement. This problem is considered here.

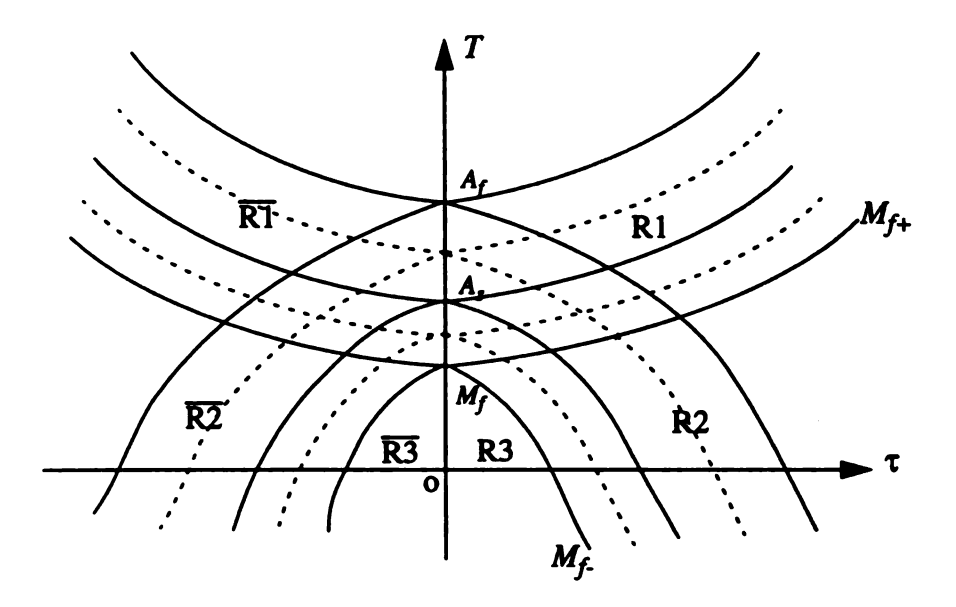


Figure 48. A given phase diagram as might be determined by experimental measurements. R1 is the region above nuetrality curve M_{f+} for $\tau \ge 0$; R2 is the region between M_{f+} and M_{f-} for $\tau \ge 0$; R3 is the region between M_{f-} and T-axis for $\tau \ge 0$. $\overline{R1}$, $\overline{R2}$ and $\overline{R3}$ are corresponding mirror images of R1, R2 and R3 about T-axis for $\tau < 0$.

10.1 Clausius-Clapeyron Relations

If a phase diagram is given, shown as Figure 48, the slopes of each neutrality curves are determined for the processes of martensitic transformations and martensite variant reorientations. For convenience, three regions, R1, R2 and R3, are defined in the half-plane $\tau \ge 0$, in which $A \leftrightarrow M_+$ and $A \leftrightarrow M_-$ occur in R1 and $M_- \to M_+$ occurs in R2 and R3. The mirror images of R1, R2 and R3 about $\tau = 0$ axis are $\overline{R1}$, $\overline{R2}$ and $\overline{R3}$. It is supposed that the Gibbs free energy is a state function of temperature and stress in both the individual phases and in any mixture state. Thus, the following Clausius-Clapeyron relations have to be satisfied in the half-plane $\tau \ge 0$ if one notes (2.1.0.7), (2.1.0.8) and

(2.3.1.1),

$$\eta_A - \eta_+ = -(\gamma_A - \gamma_+) / f_1(\tau) \text{ for } A \leftrightarrow M_+ \text{ in R1}, \qquad (10.1.0.1)$$

$$\eta_A - \eta_{-} = -(\gamma_A - \gamma_{-})/f_2(\tau, T) \text{ for } A \leftrightarrow M_{-} \text{ in R1}, \qquad (10.1.0.2)$$

$$\eta_+ - \eta_- = -(\gamma_+ - \gamma_-)/f_3(\tau, T) \text{ for } M_- \to M_+ \text{ in R2 and R3.}$$
 (10.1.0.3)

Here, $f_1(\tau)$, $f_2(\tau, T)$ and $f_3(\tau, T)$ are the slopes of each neutrality curve for $A \leftrightarrow M_+$, $A \leftrightarrow M_-$ and $M_- \to M_+$ respectively, which are regarded as experimentally supplied. Similarly, in the corresponding mirror image regions in the half-plane $\tau < 0$, R1, R2 and R3, following Clausius-Clapeyron relations have to be obeyed,

$$\eta_A - \eta_A = -(\gamma_A - \gamma_A)/\overline{f}_1(\tau) \text{ for } A \leftrightarrow M_A \text{ in } \overline{R1},$$
 (10.1.0.4)

$$\eta_A - \eta_+ = -(\gamma_A - \gamma_+) / \overline{f}_2(\tau, T) \text{ for } A \leftrightarrow M_+ \text{ in } \overline{R1}, \qquad (10.1.0.5)$$

$$\eta_+ - \eta_- = -(\gamma_+ - \gamma_-)/\overline{f}_3(\tau, T)$$
 for $M_+ \to M_-$ in $\overline{R2}$ and $\overline{R3}$. (10.1.0.6)

Here, $\overline{f}_1(\tau)$, $\overline{f}_2(\tau, T)$ and $\overline{f}_3(\tau, T)$ are the slopes of each neutrality curve for $A \leftrightarrow M_{\perp}$, $A \leftrightarrow M_{+}$ and $M_{+} \to M_{\perp}$ respectively for $\tau < 0$. The mirror image status of $\overline{R1}$, $\overline{R2}$ and $\overline{R3}$ that will hold in the event of symmetry requires the following relations, which are henceforth assumed:

$$f_1(\tau) = -\bar{f}_1(-\tau), \qquad (10.1.0.7)$$

$$f_2(\tau, T) = -\bar{f}_2(-\tau, T),$$
 (10.1.0.8)

$$f_3(\tau, T) = -\bar{f}_3(-\tau, T),$$
 (10.1.0.9)

In this more general phase diagram, the entropy and strain may each depend on both temperature and stress. The entropies are written as the following in the present study (Ivshin and Pence, 1994 b; Bekker and Brinson, 1994),

$$\eta_A(\tau, T) = C \ln \left(\frac{T}{T_o}\right) + \eta_A^o(\tau, T) ,$$
 (10.1.0.10)

$$\eta_{+}(\tau, T) = C \ln \left(\frac{T}{T_o}\right) + \eta_{+}^{o}(\tau, T),$$
(10.1.0.11)

$$\eta_{\cdot}(\tau, T) = C \ln \left(\frac{T}{T_o}\right) + \eta_{\cdot}^o(\tau, T)$$
(10.1.0.12)

Here, the stress is appended in the reference terms of entropy expressions. Since the heat capacity is defined as $T\frac{d\eta}{dT}$, it follows that the heat capacities in the three phases are given by $C + T\frac{d\eta_i^o}{dT}$, so that if η_i^o is independent of temperature then C is interpreted as actual heat capacity.

The mathematical Maxwell relations of Gibbs free energy being a state function in each pure phase gives the following

$$\frac{\partial \eta_A}{\partial \tau} = \frac{\partial \gamma_A}{\partial T}, \quad \frac{\partial \eta_+}{\partial \tau} = \frac{\partial \gamma_+}{\partial T}, \quad \frac{\partial \eta_-}{\partial \tau} = \frac{\partial \gamma_-}{\partial T}, \quad (10.1.0.13)$$

Assume that the stress-strain relation for austenite satisfies Hooke's law in all the cases, ie.,

$$\gamma_A = \frac{\tau}{\mu_A},\tag{10.1.0.14}$$

which implies that η_A^o depends upon only temperature based on the Maxwell relation (10.1.0.13). We presume that η_A^o is constant for the rest of this Appendix.

10.2 Determination of Strain in $A \leftrightarrow M_+$ Process

In R1, equations (10.1.0.1) and (10.1.0.13) give

$$\frac{\partial}{\partial T}(\gamma_A - \gamma_+) + \frac{1}{f_1(\tau)} \frac{\partial}{\partial \tau}(\gamma_A - \gamma_+) - \frac{\frac{d}{d\tau} f_1(\tau)}{f_1^2(\tau)}(\gamma_A - \gamma_+) = 0, \qquad (10.2.0.1)$$

for $A \leftrightarrow M_+$ process. The characteristic equation of (10.2.0.1) is

$$\frac{dT}{d\tau} = f_1(\tau). \tag{10.2.0.2}$$

Assume that (10.2.0.2) is integrable and its integration form is

$$\Pi_1(\tau, T) = \zeta, \qquad (10.2.0.3)$$

with property $\Pi_1(0, \zeta) = \zeta$, $M_f \le \zeta \le A_f$. To solve equation (10.2.0.1) the following boundary condition on $\tau = 0$ has to be posed for γ_A and γ_+ ,

$$\gamma_A \Big|_{\tau = 0} = \gamma_A^o(\zeta) \text{ and } \gamma_+ \Big|_{\tau = 0} = \gamma_+^o(\zeta),$$
 (10.2.0.4)

for $M_f \le \zeta \le A_f$. Expression (10.1.0.14) implies that $\gamma_A^o(\zeta) = 0$. Therefore, the solution of (10.2.0.1) with boundary condition (10.2.0.4) is found as

$$\gamma_{+}^{R1}(\tau, T) = \frac{\tau}{\mu_{A}} + \frac{f_{1}(\tau)}{f_{1}(0)} \gamma_{+}^{o}(\Pi_{1}(\tau, T)), \qquad (10.2.0.5)$$

the superscript RI on the right head of γ_+ indicates the solution in region R1.

From (10.1.0.1), (10.1.0.10), (10.2.0.5) and (10.1.0.11), the following relation about the entropies is derived,

$$\eta_{+}^{o}(\tau, T) = \eta_{A}^{o} - \frac{\gamma_{+}^{o}(\Pi_{1}(\tau, T))}{f_{1}(0)}.$$
 (10.2.0.6)

For $A \leftrightarrow M$ process in $\overline{R1}$, combining (10.1.0.4) and (10.1.0.13) follows

$$\frac{\partial}{\partial T}(\gamma_A - \gamma_{-}) + \frac{1}{\bar{f}_1(\tau)} \frac{\partial}{\partial \tau}(\gamma_A - \gamma_{-}) - \frac{\frac{d}{d\tau} \bar{f}_1(\tau)}{\bar{f}_1^2(\tau)}(\gamma_A - \gamma_{-}) = 0 , \qquad (10.2.0.7)$$

with its characteristic equation

$$\frac{dT}{d\tau} = \bar{f}_1(\tau). \tag{10.2.0.8}$$

Then, the following results are determined in a similar fashion (10.2.0.5) and (10.2.0.6),

$$\gamma_{-}^{\overline{R1}}(\tau,T) = \frac{\tau}{\mu_{A}} + \frac{\overline{f}_{1}(\tau)}{\overline{f}_{1}(0)} \gamma_{-}^{o}(\overline{\Pi}_{1}(\tau,T)), \qquad (10.2.0.9)$$

$$\eta_{-}^{o}(\tau, T) = \eta_{A}^{o} - \frac{\gamma_{-}^{o}(\overline{\Pi}_{1}(\tau, T))}{\overline{f}_{1}(0)},$$
(10.2.0.10)

if the boundary condition on $\tau = 0$ is given by

$$\gamma_{-|_{\tau=0}} = \gamma_{-}^{o}(\zeta)$$
. (10.2.0.11)

Here, $\overline{\Pi}_1(\tau, T) = \zeta$ for $M_f \le \zeta \le A_f$ is the integration form of (10.2.0.8) with property $\overline{\Pi}_1(0, \zeta) = \zeta$,

For the problem associated with two complementary martensite variants, it is natural to impose the following relation,

$$\gamma_{+}^{o}(\zeta) = -\gamma_{-}^{o}(\zeta), \qquad (10.2.0.12)$$

by a consideration of self-accommodated process. It is easy to prove that (10.2.0.12) is equivalent to the following relation,

$$\gamma_{+}^{R1}(\tau, T) = -\gamma_{-}^{\overline{R1}}(-\tau, T),$$
 (10.2.0.13)

by the solutions (10.2.0.5), (10.2.0.9), and the fact of

$$\Pi_1(\tau, T) = \overline{\Pi}_1(-\tau, T).$$
 (10.2.0.14)

Example 1

For $A \leftrightarrow M_+$ process in R1, one considers a situation that the boundary condition for γ_+ is constant and equal to the transformation strain, ie.,

$$\gamma_{+}|_{\tau=0} = \gamma^{*}.$$
 (10.2.0.15)

Assume also that

$$\frac{dT}{d\tau} = f_1(\tau) = A\tau + B,$$
 (10.2.0.16)

which implies that

$$\Pi_1(\tau, T) = T - \frac{1}{2}A\tau^2 - B\tau.$$
 (10.2.0.17)

Here, A and B are positive quantities. Solution (10.2.0.5) now gives

$$\gamma_+^{R1}(\tau, T) = \frac{\tau}{\mu_M} + \gamma^*,$$
 (10.2.0.18)

where.

$$\frac{1}{\mu_M} = \frac{A}{B} \gamma^* + \frac{1}{\mu_A}. \tag{10.2.0.19}$$

Then (10.2.0.6) becomes

$$\eta_{+}^{o} = \eta_{A}^{o} - \frac{\gamma_{+}^{*}}{R}. \tag{10.2.0.20}$$

Solving (10.2.0.19) and (10.2.0.20) gives

$$B = \frac{\gamma^*}{\eta_A^o - \eta_+^o} \text{ and } A = \frac{\mu_A - \mu_M}{\mu_A \mu_M (\eta_A^o - \eta_+^o)}.$$
 (10.2.0.21)

Thus, we formally obtain the same results as expressed in $(2.2.2.3)_2$ and (2.2.2.5).

10.3 Determination of Strain in $A \leftrightarrow M$. Process

In R1, combining (10.1.0.2) and (10.1.0.13) gives

$$\frac{\partial}{\partial T}(\gamma_A - \gamma_{-}) + \frac{1}{f_2(\tau, T)} \frac{\partial}{\partial \tau}(\gamma_A - \gamma_{-}) - \frac{g_2(\tau, T)}{f_2^2(\tau, T)}(\gamma_A - \gamma_{-}) = 0, \qquad (10.3.0.1)$$

where,

$$g_2(\tau, T) = \frac{\partial}{\partial \tau} f_2(\tau, T). \tag{10.3.0.2}$$

The characteristic equation of (10.3.0.1) is

$$\frac{dT}{d\tau} = f_2(\tau, T), \qquad (10.3.0.3)$$

which is assumed integrable. Integration of (10.3.0.3) is taken to have the form

$$\Pi_2(\tau, T) = \zeta, \qquad (10.3.0.4)$$

with property $\Pi_2(0,\zeta)=\zeta$, $M_f \le \zeta \le A_f$. Boundary condition for solving this problem is given by (10.2.0.11) and $\gamma_A\big|_{\tau=0}=\gamma_A^o(\zeta)=0$. Consequently, the solution of (10.3.0.1) under the above boundary condition is found as

$$\gamma_{-}^{R1}(\tau, T) = \frac{\tau}{\mu_{A}} + \gamma_{-}^{o}(\Pi_{2}(\tau, T))e^{\int_{0}^{\tau} \alpha(t, \Pi_{2}(\tau, T))dt}.$$
 (10.3.0.5)

Here,

$$\alpha(\tau, \zeta) = \frac{g_2(\tau, s(\tau, \zeta))}{f_2(\tau, s(\tau, \zeta))},$$
 (10.3.0.6)

where, $T = s(\tau, \zeta)$ is a specified neutrality curve parametrized by ζ for $M_f \le \zeta \le A_f$.

On the other hand, $\eta_{-}^{o}(\tau, T)$ can determined by (10.1.0.2), (10.1.0.10), (10.1.0.12) and (10.3.0.5),

$$\eta_{-}^{o}(\tau, T) = \eta_{A}^{o} - \frac{\gamma_{-}^{o}(\Pi_{2}(\tau, T))e^{\int_{0}^{\tau}\alpha(t, \Pi_{2}(\tau, T))dt}}{f_{2}(\tau, T)}.$$
 (10.3.0.7)

As the same manner, based on (10.1.0.5) and (10.1.0.13) for $A \leftrightarrow M_+$ process in $\overline{R1}$, we can obtain the following solutions

$$\gamma_{+}^{\overline{R1}}(\tau,T) = \frac{\tau}{\mu_{A}} + \gamma_{+}^{o}(\overline{\Pi}_{2}(\tau,T))e^{\int_{0}^{\tau} \overline{\alpha}(t,\overline{\Pi}_{2}(\tau,T))dt}, \qquad (10.3.0.8)$$

$$\eta_{+}^{o}(\tau, T) = \eta_{A}^{o} - \frac{\gamma_{+}^{o}(\overline{\Pi}_{2}(\tau, T))e^{\int_{0}^{\tau} \overline{\alpha}(t, \overline{\Pi}_{2}(\tau, T))dt}}{\overline{f}_{2}(\tau, T)}, \qquad (10.3.0.9)$$

where,

$$\frac{dT}{d\tau} = \bar{f}_2(\tau, T), \qquad (10.3.0.10)$$

$$\bar{\alpha}(\tau,\zeta) = \frac{\bar{g}_2(\tau,\bar{s}(\tau,\zeta))}{\bar{f}_2(\tau,\bar{s}(\tau,\zeta))},$$
 (10.3.0.11)

$$\bar{g}_2(\tau, T) = \frac{\partial}{\partial \tau} \bar{f}_2(\tau, T),$$
 (10.3.0.12)

and $T = \bar{s}(\tau, \zeta)$ is a specified $A \leftrightarrow M_+$ nuetrality curve in $\overline{R1}$, parameterized by ζ , $M_f \le \zeta \le A_f$. $\overline{\Pi}_2(\tau, T) = \zeta$ is the integration form of (10.3.0.10) with property

 $\overline{\Pi}_2(0,\zeta) = \zeta$.

It can also be proven that (10.2.0.12) and (10.2.0.13) are equivalent by means of (10.3.0.5), (10.3.0.8), and

$$\Pi_2(\tau, T) = \overline{\Pi}_2(-\tau, T).$$
 (10.3.0.13)

10.4 Determination of Strain in $M_{\cdot} \rightarrow M_{+}$ Process

First of all, consider the situation in R2, by (10.1.0.3) and (10.1.0.13) the following P.D.E. can be derived

$$\frac{\partial}{\partial T}(\gamma_{+}-\gamma_{-})+\frac{1}{f_{3}(\tau,T)}\frac{\partial}{\partial \tau}(\gamma_{+}-\gamma_{-})-\frac{g_{3}(\tau,T)}{f_{3}^{2}(\tau,T)}(\gamma_{+}-\gamma_{-})=0, \qquad (10.4.0.1)$$

where,

$$g_3(\tau, T) = \frac{\partial}{\partial \tau} f_3(\tau, T). \qquad (10.4.0.2)$$

The characteristic equation of (10.4.0.1) can be written as

$$\frac{dT}{d\tau} = f_3(\tau, T). \tag{10.4.0.3}$$

Since $M_- \to M_+$ is modified by $M_- \to A$, the nuetrality curves of $M_- \to M_+$ in R2 is a extension of the nuetrality curves of $M_- \to A$ in R1. Thus, we are going to continuously employ temperature parameter ζ ($M_f \le \zeta \le A_f$) to parameterize the integration curves (nuetrality curves) of (10.4.0.3) which start at M_{f+} . Based on the above consideration, the

integration form of (10.4.0.3) is written as

$$\Pi_3(\tau, T) = \zeta,$$
 (10.4.0.4)

which starts at the intersecting point $(\tau_{\zeta}, T_{\zeta})$ on M_{f+} . This point can be found by solving equations (10.4.0.4) and M_{f+} $(T = M_{f+}(\tau))$ simultaneously, which gives

$$\tau_{\zeta} = h(\zeta), T_{\zeta} = r(\zeta). \tag{10.4.0.5}$$

The boundary conditions for solving this problem are posed as

$$\gamma_{+}^{o} = \gamma_{+}^{R1}(\tau, T) \Big|_{(\tau, T) \in M_{f+}}, \gamma_{-}^{o} = \gamma_{-}^{R1}(\tau, T) \Big|_{(\tau, T) \in M_{f+}}.$$
 (10.4.0.6)

Along a specified $M_- \to M_+$ nuetrality curve $T = s(\tau, \zeta)$ that starts at $(\tau_{\zeta}, T_{\zeta})$ and goes down to a lower area, boundary conditions (10.4.0.6) could be rewritten as

$$\gamma_{+}^{o} = B_{+}(\zeta), \ \gamma_{-}^{o} = B_{-}(\zeta).$$
 (10.4.0.7)

Therefore, the solution of equation (10.4.0.1) under the above boundary condition is found to be

$$\gamma_{+}^{R2}(\tau, T) - \gamma_{-}^{R2}(\tau, T) = (B_{+}(\Pi_{3}(\tau, T)) - B_{-}(\Pi_{3}(\tau, T)))e^{\int_{h(\Pi_{3}(\tau, T))}^{t} \psi(t, \Pi_{3}(\tau, T))dt}, \quad (10.4.0.8)$$

where,

$$\Psi(\tau, \zeta) = \frac{g_3(\tau, s(\tau, \zeta))}{f_3(\tau, s(\tau, \zeta))}.$$
 (10.4.0.9)

Solution (10.4.0.8) implies that

$$\gamma_{+}^{R2}(\tau, T) = \gamma_{1}(\tau, T) + B_{+}(\Pi_{3}(\tau, T))e^{\int_{A(\Pi_{3}(\tau, T))}^{\tau} \psi(t, \Pi_{3}(\tau, T))dt}, \qquad (10.4.0.10)$$

$$\gamma_{-}^{R2}(\tau, T) = \gamma_{1}(\tau, T) + B_{-}(\Pi_{3}(\tau, T))e^{\int_{h(\Pi_{3}(\tau, T))}^{t} \psi(t, \Pi_{3}(\tau, T))dt}.$$
(10.4.0.11)

Here, $\gamma_1(\tau, T)$ is any function that obeys boundary condition

$$\gamma_1(\tau, T)\Big|_{(\tau, T) \in M_{f*}} = 0,$$
 (10.4.0.12)

which is explicit by (10.4.0.10), (10.4.0.11) and (10.4.0.6) if one assumes that the strains of the two variant martensite satisfy $(\gamma_+(\tau, T), \gamma_-(\tau, T)) \in C^0$. By (10.1.0.3), (10.1.0.11), (10.1.0.12) and (10.4.0.8), the following relation between the entropies is obtained,

$$\eta_{+}^{o} - \eta_{-}^{o} = -\frac{B_{+}(\Pi_{3}(\tau, T)) - B_{-}(\Pi_{3}(\tau, T))}{f_{3}(\tau, T)} e^{\int_{M(\Pi_{3}(\tau, T))}^{\tau} \Psi(t, \Pi_{3}(\tau, T)) dt}.$$
 (10.4.0.13)

For more about the above specification, a particularly natural assumption is that

$$\gamma_1(\tau, T) \equiv 0.$$
 (10.4.0.14)

Then, solutions (10.4.0.10) and (10.4.0.11) become

$$\gamma_{+}^{R2}(\tau, T) = B_{+}(\Pi_{3}(\tau, T))e^{\int_{h(\Pi_{3}(\tau, T))}^{\tau} \psi(t, \Pi_{3}(\tau, T))dt}, \qquad (10.4.0.15)$$

$$\gamma_{-}^{R2}(\tau, T) = B_{-}(\Pi_{3}(\tau, T))e^{\int_{h(\Pi_{3}(\tau, T))}^{\tau} \Psi(t, \Pi_{3}(\tau, T))dt}, \qquad (10.4.0.16)$$

which would be deciphered as the natural extension of solutions (10.2.0.5) and (10.3.0.5) in R1 into R2, if one notes (10.4.0.6) and (10.4.0.7).

For region R3, the only difference from that in region R2 is that the boundary conditions are now given along T-axis, which are expressed as $(10.2.0.4)_2$ and (10.2.0.11) for $\xi \leq M_f$. Thus, relations, from (10.4.0.1) to (10.4.0.4), still suit the present condition, but, (10.4.0.4) has the property

$$\Pi_3(0, \zeta) = \zeta \text{ for } \zeta \le M_f.$$
 (10.4.0.17)

Therefore, the difference between the strains in R3 is given by

$$\gamma_{+}^{R3}(\tau, T) - \gamma_{-}^{R3}(\tau, T) = (\gamma_{+}^{o}(\Pi_{3}(\tau, T)) - \gamma_{-}^{o}(\Pi_{3}(\tau, T)))e^{\int_{0}^{\tau} \psi(\iota, \Pi_{3}(\tau, T))d\iota}$$
 (10.4.0.18)

Comparing (10.4.0.8) and (10.4.0.18) will conclude that the two solutions are identical with each other along the boundary M_{f_-} between R2 and R3 if one notes that $\gamma_+^o(\zeta)$ and $\gamma_-^o(\zeta)$ are continuous along the *T*-axis with C^0 smooth.

Solution (10.4.0.18) implies that

$$\gamma_{+}^{R3}(\tau, T) = \gamma_{2}(\tau, T) + \gamma_{+}^{o}(\Pi_{3}(\tau, T))e^{\int_{0}^{t} \psi(t, \Pi_{3}(\tau, T))dt}, \qquad (10.4.0.19)$$

$$\gamma_{-}^{R3}(\tau, T) = \gamma_{2}(\tau, T) + \gamma_{-}^{o}(\Pi_{3}(\tau, T))e^{\int_{0}^{\tau} \psi(t, \Pi_{3}(\tau, T))dt}$$
(10.4.0.20)

Here, $\gamma_2(\tau, T)$ is any function in R3. And, on the other hand we have

$$\eta_{+}^{o} - \eta_{-}^{o} = -\frac{\gamma_{+}^{o}(\Pi_{3}(\tau, T)) - \gamma_{-}^{o}(\Pi_{3}(\tau, T))}{f_{3}(\tau, T)} e^{\int_{0}^{\tau} \psi(t, \Pi_{3}(\tau, T))dt} , \qquad (10.4.0.21)$$

in R3.

If one assumes that the strains are C^0 along M_{f_-} , then, $\gamma_2(\tau, T)$ satisfies

$$\gamma_2(\tau, T)\Big|_{(\tau, T) \in M_f} = \gamma_1(\tau, T)\Big|_{(\tau, T) \in M_f},$$
 (10.4.0.22)

by (10.2.0.5), (10.3.0.5), (10.4.0.6) and (10.4.0.7). Thus, we define an arbitrary C^{\bullet} function, named $\gamma(\tau, T)$, in R2 \cup R3, upon which, $\gamma_1(\tau, T)$ in (10.4.0.10) and (10.4.0.11) as well as $\gamma_2(\tau, T)$ in (10.4.0.19) and (10.4.0.20) can be replaced by $\gamma(\tau, T)$ now. In $\overline{R2}$ and $\overline{R3}$ similar solutions can be obtained as we have illustrated above without any difficulty.